2018

Determining the Effects of Hailstone Impact on Flat Cold-Reduced Steel Roof Sheeting

Yufei Wu
University of Wollongong

Determining the Effects of Hailstone Impact on Flat Cold-Reduced Steel Roof Sheeting

YUFEI WU

This thesis submitted in the fulfilment of the requirements for the Award of the Degree of

Master of Philosophy

From the

University of Wollongong

Acknowledgement

Firstly, I would like to express my sincere gratitude to my supervisor A/Prof. Lip Teh for the continuous support of my study and related research, for his patience, motivation, and immense knowledge. Without his help, I cannot finish this thesis smoothly. He helped me develop the critical thinking, which is valuable in all the time of research and the rest of my life. I could not have imagined having a better advisor and mentor for my whole study time.

I would also like to thank my co-supervisor Prof. Timothy McCarthy. His great advice helped me a lot in my research, and his suggestion on dent analysis enlighten me in the later research.

I would like to express special thanks to Dr David Hastie for his kindness to lend the high speed camera used to measure the impact velocity of hailstones in the experiment. I also would like to thank all the support provided by Prof. Paul Cooper of the Sustainable Building Research Centre (SBRC).

I would like to thank Dr. Mehmet Eren Uz who gave me a lot of help on the hail rig equipment operation. I would like to thank the help and assistance of Alan Grant, John Barron and Craig McLauchlan, who helped me a lot in designing the experimental equipment, and gave me a lot of help during the experiment. I also would like to thank Richard Berndt, Ritchie Mclean, Cameron Neilson, John Webb, Ian Frew and other UOW technical staff in laboratories and workshops.

Thanks are also extended to Trevor Clayton of Bluescope Limited for supplying the steel roof sheeting materials.

Very special and faithful thanks to my mother and father, my parents-in-law and all my relatives and friends for their invaluable emotional and financial support. Finally, special thanks and appreciations to my wife Dian Jiao, for her patience and support.

This research has been conducted with the support of the Australian Government Research Training Program Scholarship.

Table of Contents

List of Figures

List of Tables

NOMENCLATURE

A	Area of contact
A_0	Originial area before ice ball impact
A_f	Deformed area of contact after ice ball impact
ΔA	The increase in the dented area due to the hail impact
D	Dent depth
d_e	Estimated dent depth using the proposed empirical equation
d_t	Experimental dent depth
E_{impact}	Impact energy
E_p	Plastic deformation energy
E_r	Rebound energy of the projectile
E_v	Flexural vibration energy
F_d	Denting force
k	Constant of proportionality
l	Spacing between the barrens that used for fixing the steel sheets
m	Mass of projectile
m'	Plate mass per unit area
P	Impact force of projectile
p	Momentum of projectile
R	Radius of hailstones
r	Radius of deformed area

S	Stiffness
S'	Effective plate stiffness
T	Impact time
t	Sheet thickness
v	Impact velocity of projectile
V_d	Error of the measured impact velocity
W_d	Denting energy
W_k	Kinetic energy
α, β, e, f	Constant of proportionality
Φ	Correction factor for velocity measurement using high speed camera
σ_y	Yield stress
η	Elastic ratio

Abstract

Hail damage is responsible for significant economic losses in Australia, and the damage will likely be greater in the future due to increased incidence of severe hailstorms. One of the major costs comes from damaged roofs. Compared to the conventional asphalt shingle roofing and concrete tiled roofing, steel roofing is becoming popular due to its long service life, low maintenance cost, and better resistance to natural disasters. However, there is a lack of knowledge regarding the dent resistance of steel sheet to natural hailstone impact as a function of its yield stress and thickness.

In the literature, either steel projectiles or ice balls are used as the artificial hailstones in the hail impact tests. However, there has been no study to correlate the indentation caused by a steel ball to that caused by a natural hailstone. On the other hand, the ice balls used by previous researchers shattered on impacting steel sheeting at velocities close to the terminal velocities of the natural hailstones, while some natural hailstones remain intact after impacting steel roof sheeting at their terminal velocities. When a hailstone remains intact on impact, more energy is available to damage the steel sheet.

In this thesis, a new method to make water based artificial hailstones that remain intact after impacting flat steel roof sheeting at terminal velocities has been successfully developed with a combination of 88% water and 12% PVA (Polyvinyl alcohol). The indentation results of the present artificial hailstones have been validated against those of pure clear ice balls that happened to remain intact after impact at similar velocities. Five sheet thicknesses (0.35 mm, 0.42 mm, 0.55 mm, 0.75 mm and 1.00 mm) and two sheet steel grades (G300 and G550) are tested under the impact of five sizes of artificial hailstones (25 mm, 33 mm, 38 mm, 45 mm and 50.8 mm) at three designated impact velocities (20 m/s, 30 m/s, 40 m/s). Each sheeting is screwed to timber battens spaced at 600 mm from each other, and the projectile is aimed perpendicularly at the middle between the two battens.

The dent depths caused by the PVA ice balls that remained intact after impact are significantly greater than those caused by the PVA ice balls that disintegrated upon impact. For the case involving intact artificial hailstones, the dent depth varies linearly with the square root of the impact energy, and is inversely proportional to the square roots of the sheet thickness and the

yield stress. The findings (based on experimental observations and theoretical derivations) regarding the effects of the sheet thickness and the yield stress are believed to be original.

Additional experimental findings are that the rebound energy of hailstones impacting steel roof sheeting is negligible (less than 1% of the impact energy), and that most energy loss of the impact energy is in the form of flexural vibration of the flat steel sheeting. Provided that denting takes place, the energy lost to flexural vibration is a function of the elastic flexural stiffness of the steel sheeting, and varies linearly with the impact energy.

An empirical equation is proposed in this thesis to determine the proportion of impact energy that is lost to flexural vibration of the steel sheeting, based on the sheet thickness and the spacing between the battens. Once the flexural vibration energy and therefore the net impact energy is determined, the dent depth can be estimated from the sheet thickness and the yield stress under the assumption of a (partly) spherical dent.

Chapter 1 Introduction

1.1 Background

Hailstorms cause millions of dollars of economic losses every year in Australia (Eichner 2017). Figure 1.1 shows that hail events account for nearly 35% of the total normalised loss among all weather-related disasters between 1967 and 2006 in Australia (Crompton & McAneney 2008). In 1999, the most severe hailstorm affected Sydney, leading to a total $1.7 billion (in 1999 dollar) insurance loss, which is the largest ever insurance loss due to a natural disaster in Australia. This remarkable hailstorm caused damage to over 20,000 building roofs and affected over 13,000 people. The Australian Building Codes Board predicted that the hail-days per year along the eastern coastline will increase by 4 to 6 days by 2070, which means more economic losses due to hailstorms in the future (Australian Building Codes Board 2010).

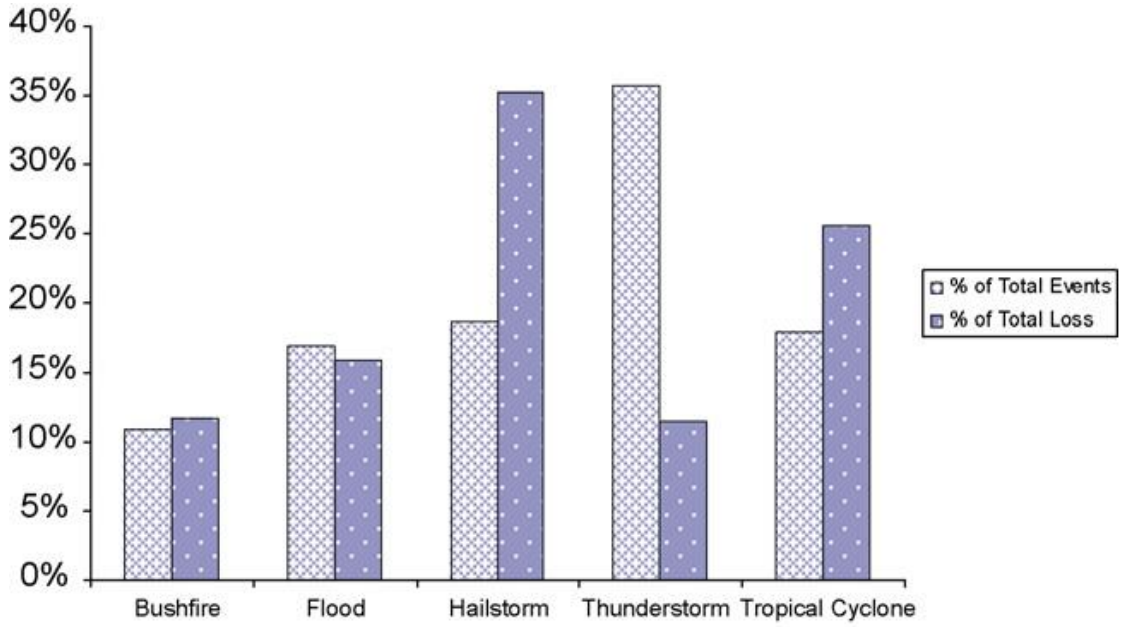

Figure 1.1: Total normalised loss for different disasters from 1967-2006 in Australia (Crompton & McAneney 2008)

According to the online declaration and reports given by Insurance Council of Australia (Insurance Council of Australia 2015, 2017), most insurance loss comes from damaged cars and roofs because both of them are directly subjected to hail impact. Figure 1.2 compares the average claim costs of the main building components due to hailstorms in the United States of America. It can be seen that the claim for roofing damage is much larger than for any other

parts of the building. In hail-affected areas, conventional roofing materials easily get damaged or even penetrated under the impact of large hailstones. Once the roof is damaged, it can cause water leakage and expose the indoor facilities to hailstone impact and the rainfall, which could lead to more economic losses.

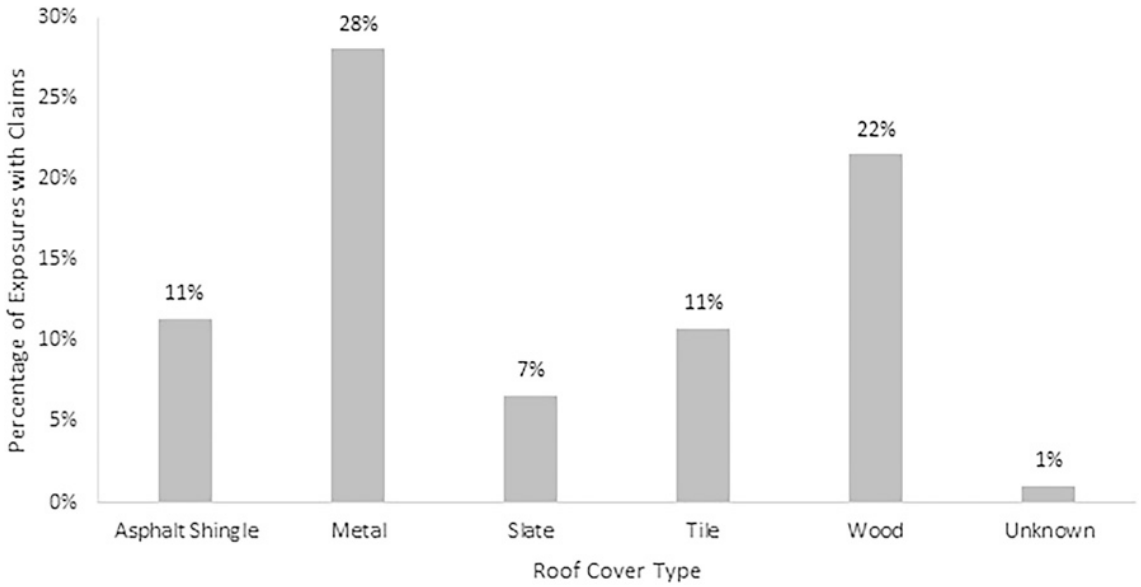

Figure 1.2: Average claim costs associated with major building component groups (Brown et al. 2015)

Compared to the conventional asphalt shingle roofing and concrete tiled roofing, steel roofing is becoming popular due to its long service life, low maintenance cost, and better resistance to natural disasters (Petty 2013). Australian Building Code Board (2010) has reported that only the hailstones with diameters larger than 25 mm cause permanent indentations on steel roofing, and the hailstones with diameters larger than 65 mm, which are rare, are likely to cause steel roof sheeting to crack. However, the permanent indentations can be accompanied by cosmetic damage on steel roofing, and more importantly the damage could cause corrosion due to ponding of rainwater, which shortens the service life of steel roofing. It is reported that historically hailstorms with hailstones diameter greater than 20 mm happened in 32% of thunderstorms between September and March in NSW (Australian Building Codes Board 2010).

While hailstorms can result in significant economic losses, there is no specific building code or standard developed in Australia to define the hail resistance of roofing material. The most widely used international standards for determining hail resistance are UL 2218 (Underwriters Laboratories 1996) and FM 4473 (ANSI 2011), which utilise steel balls and pure ice balls,

respectively, to simulate hailstone impact. However, the artificial hailstones in both standards cannot represent natural hailstones very well.

1.2 Problem Definition

Cold-formed steel roof sheeting has been widely employed on large structures where about 60% of the total cost of the steelworks is the cost of cladding (Pimpasakdi et al. 2004). Though steel roofing cannot be easily fractured under the impact of hailstones, permanent denting can be formed after severe hailstorms. Steel roofing could be corroded if water is retained in large dents (ponding), and the cost of roofing replacement is quite large. Therefore, preventing or reducing the dent sizes on steel roofing in a cost effective manner is a major issue for the roofing industry.

Research on the minimum thickness of different grades of steel sheeting to resist the impact of hailstones has been based on the following conditions: no damage from hailstones equal to or smaller than 20 mm, and no penetration from hailstones up to 100 mm (Sharafi et al. 2013). However, the impact of hailstones with diameters between 20 to 100 mm has not been fully defined, and such hailstones are quite common during a hailstorm. Hailstones with diameters between 20 and 100 mm are likely to cause permanent indentation on steel roofing, there is therefore a need to determine the relationships between dent sizes and the properties of steel sheeting under the impact of hailstones within this range.

The current international standards, UL 2218 and FM 4473, classify the dent resistance of steel roofing material based on the same criterion, which specifies that the test specimen shall show no evidence of visible cracking or breakage under the impact of artificial hailstone (Underwriters Laboratories 1996; ANSI 2011). Steel roof sheeting can still be rated as highly resistant in hail impact tests even if large dents are formed. However, large dents can shorten its service life, and there have been no studies focused on the relationship between dent sizes and steel sheet properties.

In the industry, the most popular method to make artificial hailstones is to use hollow steel balls that are designed to have the same weight as the hailstones of the same diameter. However, no correlation has been developed between the impact of hailstones and the impact of steel balls. Using ice balls is another common way to simulate natural hailstones. However, most of the ice balls used in the tests shattered on impact, whereas natural hailstones often remain intact

and therefore incur more damage as no energy is lost to breaking up the projectile (Luong 2014; Moore & Wilson 1978; Paterson & Sankaran 1994; Ramsay 2015).

1.3 Aim

The aim of the thesis is to determine the relationships between the properties of flat steel roof sheeting, the impact velocity and mass of the hailstone, and the damage (dent size) caused by the hailstone that remains intact at impact velocity around the terminal velocity of the natural hailstone. A very important goal associated with this aim is to develop a new method of making water based artificial hailstones that remain intact at high-velocity impact.

1.4 Objectives

The following objectives are designed to achieve the proposed aim of the thesis:

1) Review previous methods of making water based artificial hailstones and their outcomes.
2) Develop an effective way to make water based artificial hailstones that remain intact after impacting steel roof sheeting at velocities up to the terminal velocities of the corresponding natural hailstones.
3) Review the published relationships between the steel sheet properties, the impact velocity and mass of the hailstone, and the dent size.
4) Conduct an experimental testing program to study the relationships mentioned in the preceding objective.
5) Develop an equation to estimate the dent size caused by an intact natural hailstone impacting a flat steel roof sheeting perpendicularly at a velocity around the terminal velocity, based on the impact velocity and mass of the hailstone and the thickness, batten spacing and yield stress of the steel sheet.

1.5 Scope

All specimens are flat cold-reduced steel sheets having thicknesses ranging from 0.35 to 1.0 mm, subjected to perpendicular impacts from water based artificial hailstones travelling at 20 m/s, 30 m/s and 40 m/s. Only spherical hailstones are used, with diameters ranging from 25 to 50.8 mm. Each sheeting is screwed to timber battens spaced at 600 mm.

1.6 Thesis outlines

The outlines of each chapter are listed below:

Chapter 1 outlines the economic losses of hail damage and the desirability of reducing hail damage on steel roof sheeting in a cost-effective manner. This chapter also sets the aim and objectives of the thesis.

Chapter 2 presents a review of the published research findings on natural hailstone properties, the artificial hailstones used by researchers around the world, the published methods of making water based artificial hailstones and their outcomes, the industry standards for determining the hail impact resistance of roofing materials, the effects of steel roofing properties on its hail impact resistance, and the alternative uses of impact energy and momentum in determining the dent size or dent resistance.

Chapter 3 describes the various methods of making water based artificial hailstones attempted in the present work and their preliminary test results. It identifies the method that is most effective in producing water based artificial hailstones that remain intact after impacting flat steel roofing sheets at velocities around the terminal velocities of the corresponding natural hailstones. It sets the sizes of the artificial hailstones to be used in the present work and their target velocities. The chapter also describes the methods for measuring the impact velocity and the dent depth.

Chapter 4 presents the validation tests of the artificial hailstones used in the present experimental program. It discusses the relative accuracy of the manual and the digital methods of measuring the dent depths, and determines the method to be used in analysing the experimental results. The chapter also presents the differences in the incurred dent depth between water based artificial hailstones that remain intact and those that shatter or fracture upon impact. It discusses the energy losses during a hail impact and identifies the major energy loss. Based on the experimental results, it analyses the relationship between the impact energy and the flexural vibration energy, and that between the former and the dent depth. The test results are plotted to identify the relationship between the dent depth on one hand and the sheet thickness and yield stress on the other.

Chapter 5 proposes an empirical equation for determining the dent depth caused by a hailstone impacting a steel roofing sheet perpendicularly at a velocity around the terminal velocity of the natural hailstone. The assumptions used to derive the empirical equation are stated. The dent depth is a function of the impact energy, the sheet thickness, the batten spacing and the yield stress.

Chapter 6 summarises the findings of the present work, addressing the aim and objectives of this thesis. This chapter also provides recommendations for future research.

Chapter 2 Literature Review

This chapter provides a review of the literature on the topic of hail impact on steel roof sheeting. It reviews the methods of making artificial hailstones in past research and the industry standards related to hail impact. It also reviews the relationships between hailstone properties, steel sheet properties, and dent sizes proposed in the literature.

2.1 Introductory Remarks

The projectiles used in the hail impact experiment are critical because they determine the friction, coefficient of restitution, the kinetic energy on impact and the energy absorbed by the steel sheet. It is ideal that the projectile (artificial hailstone) has similar properties to natural hailstones. Sections 2.2 and 2.3 describe the natural hailstone formation and previous methods of making artificial hailstones.

Since there is no Australian standard or building code related to hail impact on roofing materials, international standards are used to classify the roofing materials. Section 2.4 summarises the most popular international standards for testing hail resistance.

Section 2.5 reviews the effects of some key properties of steel sheeting such as yield stress, thickness and stiffness on its hail resistance as published in the literature. Section 2.6 reviews other influencing factors on dent sizes and the methods of determining dent resistance.

2.2 Hailstones

2.2.1 Hailstone formation

A natural hailstone is a form of precipitation developed in thunderstorms, and only ice balls greater than 5 mm are defined as hailstones (Dunlop 2008). A hailstone begins with a snow pellet, an ice crystal, little water drops or even a dirt particle. These small particles are the embryos of natural hailstones (Hile 2009; Oard 2015). Small hailstones are formed when the embryos are taken into thunderclouds by the warm updraft and accrete when supercooled water is attached to them within clouds. These small hailstones can be transported to a different temperature zone to form clear and opaque layers (see Figure 2.1). The layered structure suggests that hailstones normally undergo two types of growth, dry growth and wet growth.

During dry growth, a hailstone is taken to a very high altitude, where the air temperature is well below zero degree Celsius, making the water drops within the clouds immediately freeze once attached to the embryo. Under this situation, air will be trapped in it, and an opaque layer forms. During wet growth, the water content in the air is relatively high, and air temperature is close to zero degrees. Therefore, the water drops attached to a hailstone during the wet growth will not freeze immediately. Instead, they will undergo slow freezing and expel all impurities and air, forming a clear layer outside. The number of layers of a hailstone indicates the number of dry growth to wet growth it experienced (Dunlop 2008; Michaud et al. 2014). The hailstones will fall from the cloud if the updraft cannot carry them. The stronger the updraft is, the larger the hailstones will form (Dunlop 2008; Hile 2009; Oard 2015).

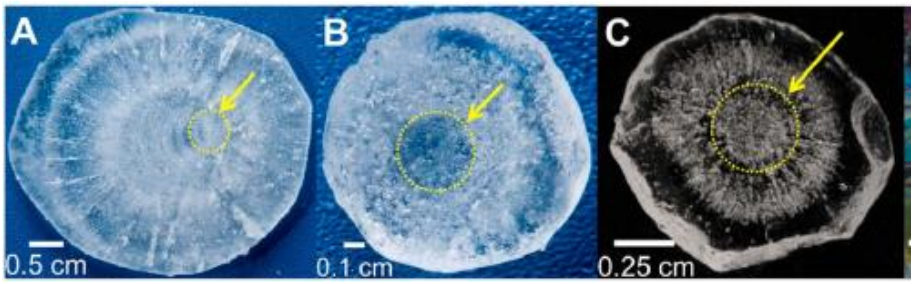

Figure 2.1: Cross sections of typical hailstones. Yellow arrow and dotted cycle denote the embryo (Michaud et al. 2014)

2.2.2 Hailstone properties

The density of hailstones ranges from 500 to 901 kg/m^3 (Knight & Heymsfield 1983). The more air a hailstone has, the lower density it will have. Some studies suggested the density of hailstones has a narrow range, which is between 820 to 870 kg/m^3 (Prodi 1970; Sharafi et al. 2013). The most common density of hailstones used in computer simulation and laboratory tests is around 846 kg/m^3 (Kim & Kedward 1999; Lavoie et al. 2011; Marco et al. 2005). Overall, the density of hailstones is lower than the density of ice due to the entrapped air in the opaque layers.

Hailstones will reach their terminal velocities when the drag force equals their weight, both of which are related to their size. The terminal velocity of a hailstone, therefore, can be estimated from its size (Cheng 2009). The relationship between hailstone sizes and terminal velocities developed by Laurie (1960) is widely used in hail impact research. Table 2.1 gives the approximate impact energy and terminal velocity of hailstones based on their sizes. Andrew

and Robert (2014) verified the data in Table 2.1 by comparing them against the terminal velocities of 2295 natural hailstones, and found good agreements.

Table 2.1: Hailstone terminal velocity and impact energy (Laurie 1960)

Diameter (mm)	Terminal Velocity (m/s)	Approximate Impact Energy (J)
25	22.3	<1.4
32	25.0	5.4
38	27.4	10.9
45	29.6	19.0
51	32.0	29.8
64	35.7	71.9
70	37.8	109.8
76	39.6	162.7

Some natural hailstones bounce off the roof and remain intact after impact (Youtube 2015, 2017). Allaby and Garratt (2014) believed the clear outside layer of hailstones is the reason why natural hailstones can bounce off without breaking up when hitting the ground or other materials. The hailstones with clear outside layer are usually stronger than soft hail that has a lower density and cloudy appearance. The average compressive stress of clear ice without air bubbles and cracks is similar to natural hailstones (Giammanco & Brown 2014). It is noteworthy that the artificial hailstones that remained intact in the laboratory tests on composite and solar panels were all stated to be clear ice balls without air and cracking (Luong 2014; Moore & Wilson 1978).

Experimental results have indicated that the artificial hailstones that remained intact upon impact caused more damage or larger dent depth compared to those that shattered (Luong 2014; Moore & Wilson 1978). When the artificial hailstone shatters on impact, significant energy is lost and less energy is available to cause plastic deformation of the impacted material.

2.3 Existing Projectiles and Artificial Hailstones

Some researchers studied the hail resistance of roofing materials under real hailstorms (Niemeier & Reynolds 1978), but it was extremely difficult to correlate the damage with the size of the impacting hailstone. Natural hailstones are also difficult to collect for use in a

laboratory test because the location of a hailstorm is not easy to predict and a hailstorm normally lasts for a very short time. On the other hand, it is problematic to make artificial hailstones that approach the properties of natural hailstones due to the complex hailstones formation process as described in Section 2.2.1.

Different shapes of hailstones will form before falling to the ground, such as ragged edges, ice spikes or cone-shaped (Oard 2015). From the collected data, most of the hailstones with diameters larger than 20 mm tend to be spheroidal or disk-shaped (Giammanco & Brown 2014). Although most large natural hailstones are not perfectly spherical (Giammanco et al. 2014; Knight 1986), most projectiles including artificial hailstones used in the hail impact experiments were spherical balls (Flüeler et al. 2008; Kim & Kedward 1999; Kim et al. 2003; Lavoie et al. 2011; Paterson & Sankaran 1994).

The most widely used method to simulate hailstones is using steel balls, especially in industrial testing, due to its convenience (BlueScope 2013; Nomura et al. 1984; Shi et al. 1991; USS Corporation 2005; Vreede et al. 1995). The steel balls were controlled to fall from certain distances to achieve similar kinetic energy to that of the same sizes of natural hailstones based on the relationship developed by Laurie (1960). However, the coefficient of restitution of a steel ball is likely to be different from that of a hailstone, and no clear correlation can be developed between their indentation effects on impacted roofing materials. Crenshaw and Koontz (2001) argued that a test specimen hit by a steel ball had a different damage condition compared to the same material under the impact of an ice ball. Compared to a steel ball, an ice ball is believed to be more realistic to simulate natural hailstones because they were also made of water (Crenshaw & Koontz 2001). In most recent hail impact research, ice balls were commonly used as artificial hailstones (Luong 2014; Prato et al. 2015; Sun et al. 2015).

However, ice balls have various mechanical properties depending on the freezing method, temperature, and pressure. Even ice balls made with the same method can have different properties from each other due to human errors. In the experimental program of Luong (2014), all the ice balls were made with the same method, yet only a few ice balls remained intact after impact on a composite material, which had an inner layer of plain weave fiberglass, with an outer layer of a carbon fibre weave of [45º/-45º] orientation. The remaining ice balls were shattered or broken in the tests. In most cases, the researchers simply froze tap water in a sphere

mould to make ice balls (Greenfeld 1969; Kim et al. 2003; Paterson & Sankaran 1994). However, such ice balls were weaker than natural hailstones as they all shattered on impact.

Some other researchers tried different methods to make ice balls more similar to natural hailstones. Moore and Wilson (1978) questioned the validity of using simple ice balls to simulate natural hailstones. In their experiment, a combination of heat and pressure was applied to make a large ice cube, which was then cut to fit into a specially designed sphere mould. The formed ice balls were put in a fridge under minus 8 degrees Celsius for at least eight hours. Unfortunately, their ice balls shattered when impacting the test glass panel, although some of them (three out of nine) bounced off when shot on a rubber surface.

Render and Pan (1995) used distilled water in lieu of tap water to make ice balls because the dirt or particles in tap water could decrease the strength of the resulting ice ball. They also tried another method by putting the flaked ice produced by an ice machine in a 12.7 mm sphere mould under a certain pressure then freezing the mould at minus 14 degrees Celsius. However, ice balls made with either of their two methods did not perform better than ice balls made with the monolithic method, which is simply to freeze tap water in the moulds. A similar method to compressing flaked ice was attempted by Lavoie et al. (2011), who compressed snow into ice ball moulds to make artificial hailstones. However, they did not mention the integrity of their artificial hailstones after impact.

In order to simulate the layered structure of hailstones, Kim et al. (2003) made artificial hailstones with the ‘flat-wise layered’ freezing method, which freezes tap water layer by layer. The flat-wise layered structure of the artificial hailstones made by Kim et al. (2003) is illustrated in Figure 2.2. However, the flat-wise layered structure is different from the ‘onion layered structure’ that natural hailstones have. Natural hailstones form layers from inside out, while the ‘flat-wise layered’ method makes a layered ice ball from the bottom to the top. The test results of Kim et al. (2003) indicated that there was no material difference between the ice balls made with the flat-wise layered freezing method and those made with the monolithic method, all of them shattered on impact.

Tippmann (2011) repeated the experiment of Kim et al. (2003), and found that the pre-existing flaws or issues with ice integrity could cause inconsistencies of the test results. However, no adjustment was taken to improve the quality of the ice balls, which all shattered on impact.

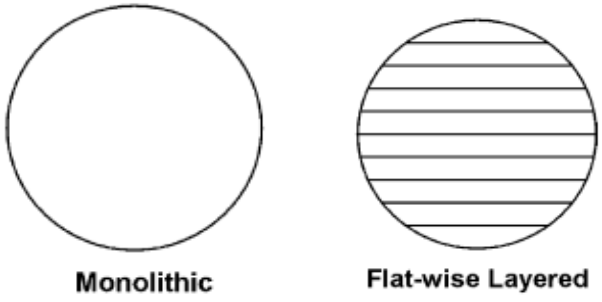

(a) (b)

Figure 2.2: Simulated hailstones: (a) Monolithic, (b) Flat-wise layered (Kim et al. 2003)

To achieve stronger ice balls, Flüeler et al. (2008) used demineralized water to produce crack-free and pore-free ice spheres. A freezer plate was put at the bottom of the mould to let ice grow from the bottom to the top, thus reducing the likelihood of trapped air. In theory, ice is stronger if there is less impurity inside it. Flüeler et al. (2008) also made polyamide balls of the same sizes as their ice balls to compare their performance in impact testing. Their ice balls were found to be brittle and shattered when shot on the testing material. Such an ice ball needed the kinetic energy of 15 to 20 times that of the same sized polyamide ball to cause the same extent of damage. No correlation was developed between these two types of artificial hailstones.

Kim et al. (2008) developed another method to make artificial hailstones by adding cotton fibres to reinforce the ice balls. It was found that the cotton ice balls penetrated the lightweight composite test specimen made from woven carbon-fibre/toughened epoxy. Swift (2013) verified the method of Kim et al. (2008) through compressive and tensile tests. The cotton reinforced ice balls were found to have an increase of 781% in tensile strength and an increase of 49% in compression strength compared to the ice balls made with tap water. However, it can be seen from Figure 2.3 that an impact test specimen had a high chance of coming into contact with the cotton material rather than the ice itself, resulting in potentially very different energy transfer mechanism between the projectile and the impacted panel compared to natural hailstones.

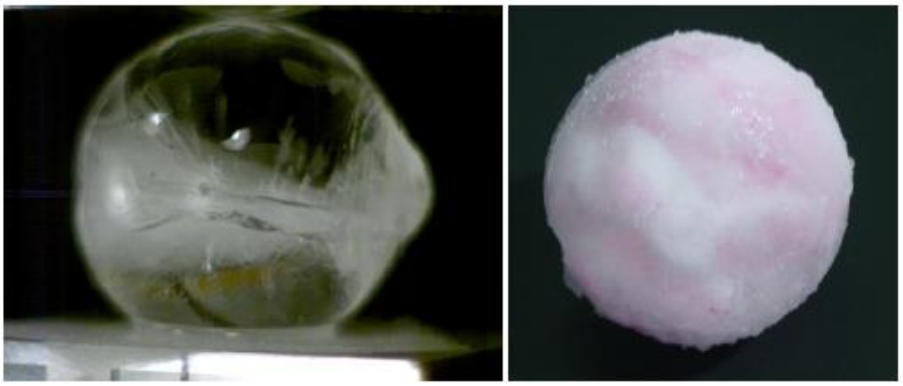

(a) (b)

Figure 2.3: Artificial hailstones made by Swift (2013): (a) clear ice ball; (b) cotton ice ball

Luong (2014) boiled de-ionized water and filled it in an aluminium-spit mould using a syringe. He explained that boiling water could help reduce the air in the water to prevent voids forming in the ice ball, and the de-ionized water could mitigate the effects of minerals present in water. Five millilitres of water was taken out of the two-inch ice ball mould to leave space for ice expansion so that cracking could be avoided. It was found that some of the resulting ice balls remained intact after impact on the composite test panel made of plain weave fibreglass and a carbon fibre, but most others did not. It is therefore unlikely that this method of artificial hailstone production will be successful for impact testing on steel panels.

The researchers at the Institute for Business and Home Safety (IBHS 2013, 2015a) used a combination of 80% seltzer water and 20% tap water to make artificial hailstones because natural hailstones have lower density compared to pure ice due to the presence of trapped air. More than 9,000 such ice balls were made and shot at different roofing materials. However, it appears from the uploaded video that most of the ice balls shattered on impact (IBHS 2014).

The researchers at IBHS (IBHS 2017) are combining 3D scanning and 3D printing techniques to reproduce artificial hailstones. They have made a number of computer models of natural hailstone with 3D scanning, and 3D printed them with plastic. However, no water based artificial hailstones have been produced.

Table 2.2 summarises the existing methods of making water based artificial hailstones and their outcomes. It shows that none of them have been successful in producing water based artificial hailstones that remain intact after impacting steel sheeting at velocities close to the terminal

velocities of natural hailstones. There is therefore a need for an effective method to make such artificial hailstones in order to obtain realistic hail impact test results.

Table 2.2: Summary of artificial hailstone making methods in past research

Researchers	Artificial Hailstones	Impacted Material	Projectile Integrity
Johnson and Schaffnit (1973) Nomura et al (1984) Fleming et al. (1997) Shi et al. (1997) McCormick et al. (1998)	Steel indenter	Steel sheet	Intact
Vreede et al. (1995) USS Corporation (2005)	Steel ball	Steel and Aluminum sheet	Intact
Flüeler et al. (2008)	Polyamide ball and ice ball made from demineralized water	Clay tiles	Intact
Greenfeld (1969)	Ice ball made from tap water	Asphalt Shingles Metal sheet Slate, asbestos and tile	Not Mentioned
Kim and Kedward (1999) Kim et al. (2003) Juntikka and Olsson (2009)	Ice ball made from tap water	Ply panel and Woven carbon-fibre/toughened epoxy composite sheet	Shattered
Chang and Khetan (1984)	Ice ball made from tap water	Steel, Aluminum Chopped-glass-fibre composite panels	Shattered

Table 2.2 (cont'd)

Paterson & Sankaran (1994)	Ice ball made from tap water	Steel sheet	Shattered
Moore and Wilson (1978)	Ice ball made from tap water combined with certain heat and pressure	Glass sheet	Shattered
		Rubber	Partly intact
Render and Pan (1995)	Ice ball made from distilled water Ice ball made from flaked ice	Steel flat sheet	Not Mentioned
Lavoie et al. (2011)	Ice ball made from flaked ice	Aluminum steel sheet	Shattered
Kim et al. (2003) Tippmann (2011)	Ice ball made from flat-wise layer freezing method	Woven carbon-fibre/toughened epoxy composite sheet	Shattered
Kim et al. (2008)	Cotton fibre ice ball	Woven carbon-fibre/toughened epoxy composite sheet	Intact, the sheet was penetrated
Luong (2014)	Double boiled de-ironized water	Plain weave fibreglass and carbon fibre sheet	Partly intact
IBHS (2014)	Ice ball made from 80% seltzer water and 20% tap water	Steel roofing sheet	Shattered

2.4 Standards for Hail Resistance

The most widely used specifications for determining hail impact resistance are:

- ASTM D-3746 Standard Test Method for Impact Resistance of Bituminous Roofing Systems (ASTM 2008)
- FM 4473 Test Standard for Impact Resistance Testing of Rigid Roofing Materials by Impacting with Freezer Ice Ball (ANSI 2011)
- UL 2218 Impact Resistance of Prepared Roof Coverings (Underwriters Laboratories 1996)

In ASTM D-3746 (ASTM 2008) and UL 2218 (Underwriters Laboratories 1996) , steel missiles (a cylinder with sphere head) and steel balls are used in the drop weight test, where they are dropped from a certain height to achieve the required impact energy. In FM 4473 (ANSI 2011), ice balls are shot using a gas gun at designated velocities. The ice balls are made of distilled water and frozen for at least 48 hours and should be free of cracking and air.

Table 2.3: Kinetic energy of projectiles as given in ASTM D-3746, FM 4473, and UL 2218

Standard	**Artificial Hailstone**	**Diameter (mm)**	**Mass (gram)**	**Distance (mm)**	**Energy (Joule)**
ASTM D-3746	Steel cylinder	50	2770	1355	22
FM 4473	Ice ball	31.8	15.3	<1500	5.5
		38.1	26.5	<1500	11.6
		44.5	42.1	<1500	20.9
		50.8	62.9	<1500	35.5
UL 2218	Steel ball	31.8	127	3700	4.6
		38.1	218	4600	9.8
		44.5	358	5200	18.3
		50.8	521	6100	31.2

Table 2.3 shows the comparison of the three different standards. Both FM 4473 and UL 2218 apply four different sizes of projectiles to test the roofing material, while ASTM D-3746 only uses one size of the steel cylinder. Hail impact resistance of roofing materials is divided into

four classes in FM 4473 and ASTM D-3746, but there is only one criterion in ASTM D-3746. In all three standards, a tested specimen passes the criterion if there is no visible cracking or breakage caused by the impact of artificial hailstones (ANSI 2011; ASTM 2008; Underwriters Laboratories 1996).

There are some other specifications related to hail resistance, such as ASTM:E822-92 (ASTM 2009), which is used to regulate hailstone damage on solar collector covers, and ASTM:E1038-98 (ASTM 2004), which is used to determine the hail resistance of photovoltaic modules. In these standards, ice balls are used to simulate hailstones. In ASTM:F320-10 (ASTM 2010), which is used to study hail damage in aerospace engineering, cotton ice ball is used.

In all the aforementioned standards, there is no information provided to clarify the importance of the integrity of the artificial hailstones, although research has shown that intact ice balls cause more severe damage (Allaby & Garratt 2014; Luong 2014; Moore & Wilson 1978).

2.5 Effects of Steel Roofing Properties on Dynamic Dent Resistance

According to the data on insurance claims, shown in Figure 2.4, metal roofing accounts for a small percentage of all roofing types (Brown et al. 2015). However, compared to shingled and tiled roofing, coated steel roofing such as Colorbond and Zincalume has better resistance to hail impact, and lasts for a longer time. It was believed that hailstones could not cause functional damage to common steel roofing unless they are 2.5 inches (65 mm) or greater in diameter (Petty 2013). However, if relatively thin steel sheeting is used, impacts from smaller hailstones can still cause large dents during a hailstorm. Even though the dents will not affect the functions of the steel roofing, rainwater could be drawn into the dents and cause corrosion if the painting is damaged, thereby shortening the service life of the steel roofing (Bluescope 2013; USS Corporation 2005).

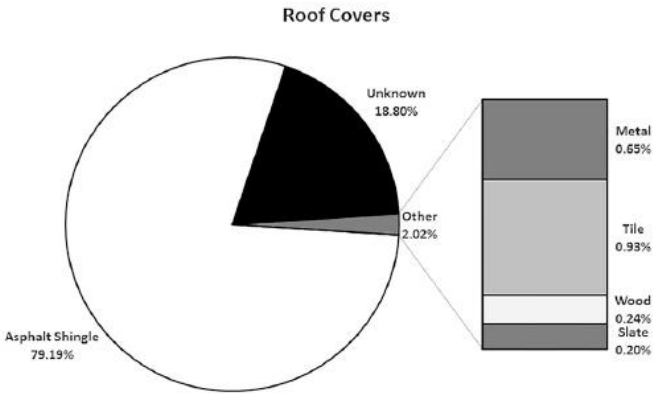

Figure 2.4: Distribution of roof cover materials (Brown et al. 2015)

The dent resistance of a steel roofing is a function of the yield stress, the sheet thickness, the panel geometry (DiCello and George 1974) and the boundary conditions (Ekstrand & Asnafi 1998; Krupitzer & Harris 1992; Shi et al. 1997). Understanding the relationship between each variable and the dent resistance facilitates efficient designs of hail-proof steel roof sheeting. However, in practice the two most important factors are the yield stress and the sheet thickness of the steel roofing.

In the automobile industry research, quasi-static testing with displacement control is usually used to define the dent resistance of a steel panel (DiCello & George 1974; Ekstrand & Asnafi 1998; Hongzhou et al. 2009; Johnson & Schaffnit 1973; Raghavan & Arwashan 1997; Shi et al. 1997; Yutori et al. 1980). However, the dynamic dent resistance is different from the static dent resistance. Under dynamic impact, the steel panel will experience a stress wave rather than stress only (DiCello & George 1974). A dynamic impact primarily involves in-plane stresses due to the panel inertia, while a static one involves a combination of bending and in-plane stresses. Therefore, the dynamic impact can only result in denting, while a static load can cause a combination of global panel deformation (h_g), bending deformation (h_b) and a dent (h_d) (Figure 2.5). In dynamic impact, the kinetic energy or momentum of the object plays an important role, while in static denting, the applied force does (Holmberg & Thilderkvist 2002; Veldhuizen et al. 1995).

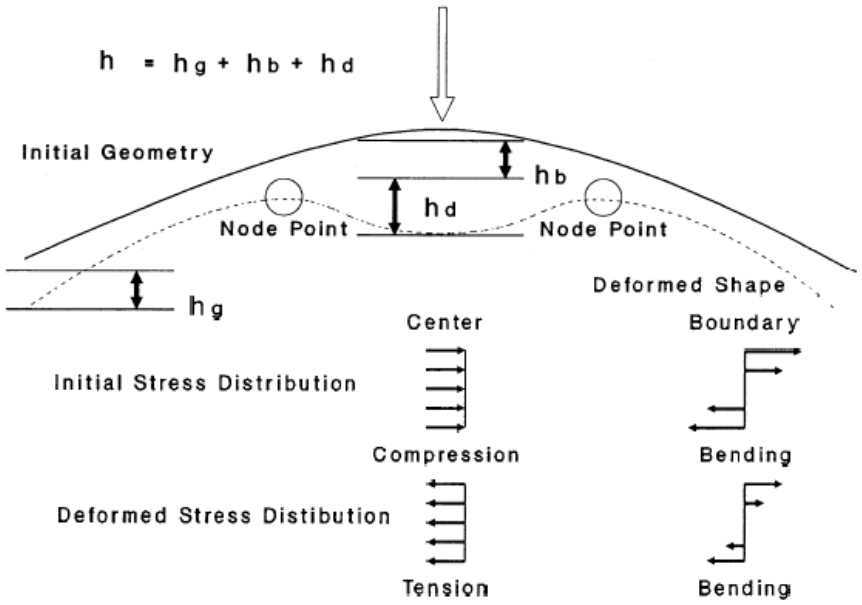

Figure 2.5: Quasi-static panel dent deflection modes (Seel 1991)

The dynamic dent resistance D_r of a material was defined by Johnson & Schaffnit (1973) as the ratio of the impact energy E_{impact} to the dent depth D

$$D_r = \frac{E_{impact}}{D} \qquad \text{Equation 2-1}$$

2.5.1 Yield stress and sheet thickness

The yield stress and the thickness of steel sheeting have a direct effect on the dent resistance (Ekstrand & Asnafi 1998; Hongzhou et al. 2009; Krupitzer & Harris 1992; Nomura et al. 1984; Zhang et al. 2006). However, the specific relationship between each of these two factors and the dent resistance has not been accurately established, especially for dynamic impact.

Johnson and Schaffnit (1973) suggested that the effect of yield stress was difficult to determine because strain hardening and ageing could affect the yield stress of the test material. After taking the effect of strain rate into consideration, they found that the dynamic dent resistance is linearly proportional to the yield stress but varies with the square of the sheet thickness by comparing the impact energies required to produce dents of a particular size.

DiCello and George (1974) proposed an equation to determine the energy W_d required to form a visible dent, defined as being 0.1 mm deep, under quasi-static loading:

$$W_d = \alpha \frac{{\sigma_y}^2 t^4}{S}$$ Equation 2-2

where *S* is the panel stiffness, and α is the constant of proportionality.

Yutori et al. (1980) proposed an equation to calculate the force required to produce a visible dent, defined as being 0.1 mm deep:

$$F_d = \beta \sigma_y t^n$$ Equation 2-3

where *n* ranges from 2.3 to 2.4 for the curved panel he studied experimentally and β is the constant of proportionality.

However, Holmberg and Thilderkvist (2002) argued that the effect of the yield stress on the static dent resistance is greater than that of the thickness based on the test results of Yutori et al. (1980). Through finite element simulation, Marzbanrad (2007) found that Equation 2-3 is accurate for steel sheet thicknesses between 0.6 and 1.0 mm with β = 1.43 and *n* = 2.05.

Compared to quasi-static denting, it requires larger energy to form the same dent size under dynamic impact due to energy losses in the form of vibration, sound and heat. Nomura et al. (1984) did a drop-weight experiment, in which a 12.7-mm steel denter of 37.8 N weight was dropped from heights ranging from 300 mm to 2200 mm to achieve different impact velocities. Their test results suggested that the dent depth varied linearly with the impact energy, and decreased with increased yield stress and/or increased thickness of the flat panel.

The relationship in Figure 2.6 suggests that the dent depth is not linearly proportional to the square of the sheet thickness in dynamic impact test, which is inconsistent with the finding of Johnson and Schaffnit (1973). The notation “300R” in the figure denotes the radius of curvature of the steel sheet, being 300 mm.

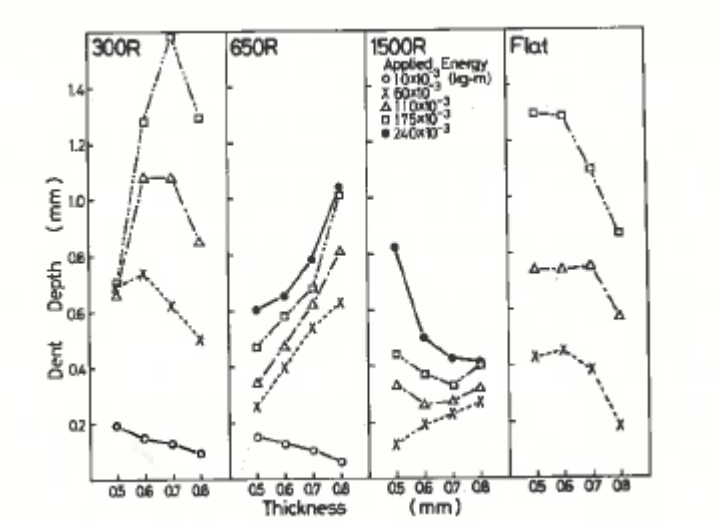

Figure 2.6: Relationship between dent depth and sheet thickness (Nomura et al. 1984)

Shi et al. (1991) did a similar drop weight test and proposed the following equations:

$$F_d = e{\sigma_y}^{0.718}t^{0.5} \qquad \text{Equation 2-4}$$

$$W_d = f{\sigma_y}^{0.915}t^{0.322} \qquad \text{Equation 2-5}$$

where e = 17.78 and f = 0.005, the yield stress σ_y is in MPa, and the sheet thickness t is in mm. The denting force F_d and the denting energy W_d are defined as the force and the energy at the onset of plastic deformation, respectively.

Shi et al. (1997) suggested that a bake-hardenable steel panel has better dent resistance even if the yield stress and the thickness are the same as those of a non-bake-hardenable steel panel. Raghavan and Arwashan (1997) verified the suggestion through finite element analysis, and found that strain hardening had a significant influence on the analysis results. For instance, neglecting the hardening effects in the 400-N load application led to a tripling of the dent depth from 0.5 mm to 1.5 mm.

2.5.2 Stiffness

The out-of-plane stiffness of the steel panel is another factor affecting the dent resistance (McCormick et al. 1998; Vadhavkar et al. 1981). For a flat panel, the stiffness is considered to be proportional to t^3 (DiCello & George 1974). From Equation 2-2, it can be concluded that for static dent resistance, the lower stiffness panel has better dent resistance. However, in other

experiments, the lower stiffness does not always contribute to higher dent resistance (Holmberg & Thilderkvist 2002; Manikandan et al. 2015). Nomura et al. (1984) found that the higher stiffness of steel panel results in better dent resistance, which is opposite to Equation 2-2.

Werner (1993) illustrated the relationship between panel stiffness and dent depth in Figure 2.7. There appears to be an optimum panel stiffness for static dent resistance, which is supported by the test results of Worswick et al. (1997) as shown in Figure 2.8.

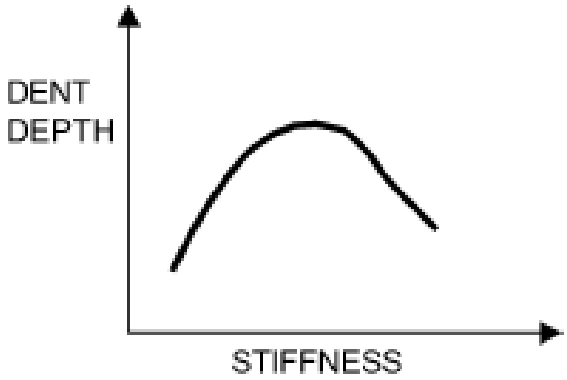

Figure 2.7: Relationship between stiffness and dent depth for static loading (Werner 1993)

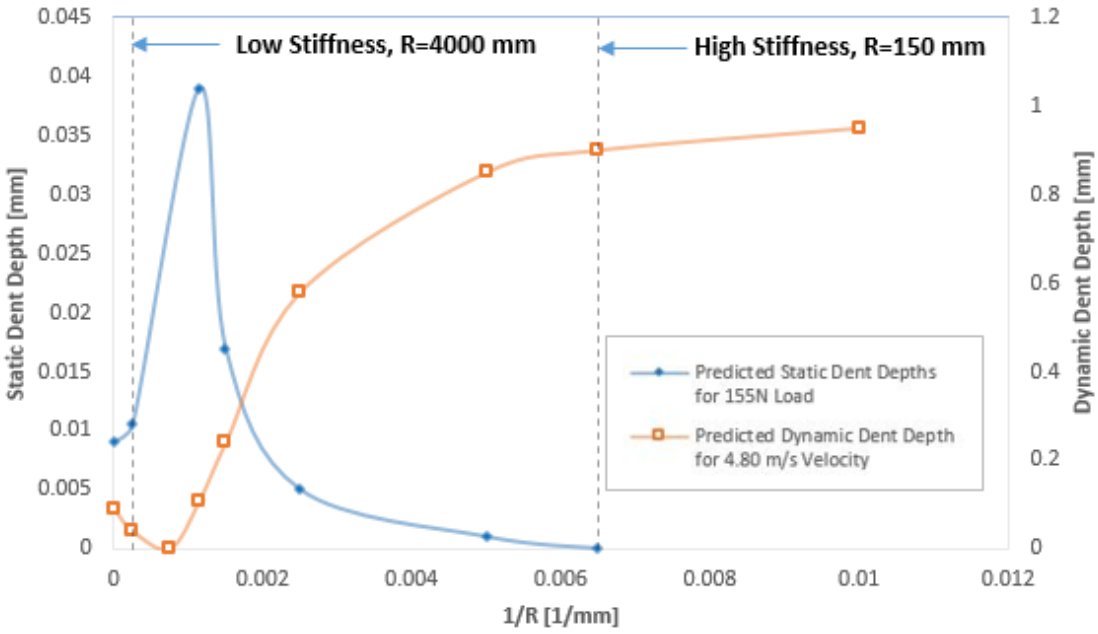

Figure 2.8: Relationship between dent depth and curvature (stiffness) for static and dynamic impact (Worswick et al. 1997)

It can also be seen from Figure 2.8 that, for dynamic denting resistance, the optimum radius of curvature appears to be well above 1,000 mm, indicating that the typical corrugated roofing

profiles are not favourable for dynamic denting resistance. Thomas (2001) suggested that the increased stiffness of the test panel resulted in a larger contact force during the dynamic impact, which caused more severe denting. However, in the high curvature range such as that found in corrugated steel roofing profiles, the variation of the dent depth is insignificant.

The effect of stiffness is not straightforward to determine because the panel stiffness is a function of the panel area, curvature, the material thickness, and the boundary condition (support system). Some factors influence the dent depth and the panel stiffness at the same time (Alaniz et al. 1990; DiCello & George 1974). For example, the panel stiffness will increase with an increased thickness, which independently improves the dent resistance. Ekstrand & Asnafi (1998) and Krupitzer & Harris (1992) believed that the boundary condition is another factor that has an influence on the static dent resistance as it affects the panel stiffness, and that the largest static dent resistance can be achieved by fixing all the edges. However, according to the experimental results of Kim et al. (2003), the boundary condition does not strongly affect the dynamic dent resistance even though it affects the stiffness. Olsson (2003) has also argued that the force generated during the dynamic impact is independent of the boundary condition as the impact is localised, which was verified by finite element modelling (Olsson et al. 2006).

2.6 Methods of Analysing Dent Resistance

The dent depth is the key factor in determining the dent resistance of a steel panel. A smaller dent size and depth on the steel panel under the same impact condition suggests the better dent resistance, which forms the basis of Equation 2-1. However, the equation assumes that the dent depth is linearly proportional to the impact energy, which may or may not be true even though the impact energy is a major factor that determines the dent depth. Nomura et al. (1984) found that that the dent depth increased linearly with the impact energy for flat panels only. This relationship was verified by Vreede et al. (1995), who also used a steel ball as the projectile on three different steel flat panels, which were mild steel, TiSulc steel and rephosphorized steel, respectively.

However, some researchers suggested that the peak impact load is the main factor of damage initiation (Olsson 2003). Olsson (2003) proposed an equation for estimating the plate deflection under a small mass impact, which is typical for hail and runway debris:

$$D = \frac{\int_0^T P\, dT}{8\sqrt{m'\ S'}}$$ Equation 2-6

where T is the impact time, P is the impact force, m' is the plate mass per unit area, and S' is the effective plate stiffness.

However, the test results only showed a good agreement for the impact under 5 m/s, while the terminal velocities of natural hailstones (see Table 2.1) are much larger than that. Also, a steel denter rather than artificial hailstones was used by (Olsson 2003) to simulate hail impact.

Worswick et al. (1997) found through their experiment at impact velocities up to 10 m/s that the dynamic dent depth varied almost linearly with the impact velocity, which means that it was proportional to the square root of the impact energy, and linearly proportional to the momentum. The finding of Worswick et al. (1997) is therefore consistent with the argument of (Olsson 2003). It is also consistent with the finding of Pernas-Sánchez et al. (2016) for a composite panel where the artificial hailstones shattered on impact at high velocities.

2.7 Concluding Remarks

Due to their formation process in the high altitude atmosphere, natural hailstones may remain intact upon impact on steel roofing at terminal velocities. Intact hailstones or ice balls cause more severe damage to the impacted material compared to those that shatter. However, the existing experimental programs either use steel balls, which have different impact characteristics from hailstones, or artificial hailstones that shatter upon impact on steel sheeting at terminal velocities. In order to properly investigate the dent resistance of steel sheeting against hailstones, it is therefore imperative that a method for producing artificial hailstones that do not break up after impact on steel sheeting at terminal velocities are developed.

As far as steel roof sheeting is concerned, the two major factors that contribute to the dent resistance is the yield stress and the sheet thickness. Although the curvature of the roofing profile has a very significant effect on the dent resistance (relative to a flat panel), the variation of its effects within the range of typical corrugated roofing profiles is negligible. Furthermore, the effect of boundary conditions on the dynamic dent resistance is insignificant.

Larger impact energy or momentum causes a larger dent, but their relationship to the dent size is not clear. Some studies suggested that the dent depth was linearly proportional to the impact velocity and therefore the projectile's momentum, but others found that the dent depth varied linearly with the impact energy, or the square of the impact velocity. The inconsistencies may be attributed to the different projectiles used (either steel or ice balls) in the impact tests, and/or very different ranges of impact velocities, reinforcing the need to conduct experimental testing using artificial hailstones that do not break up after impact on steel sheeting at terminal velocities.

Chapter 3 Methodology

3.18 Introductory Remarks

The literature review in Chapter 2 reveals the need to develop a reliable method of producing artificial hailstones that do not disintegrate upon impact on steel sheeting at their terminal velocity. The development of such a method as part of the present research is described in Section 3.2, which also includes several methods tried by the author that proved to be unsuccessful.

Section 3.3 sets the hailstone sizes and the target impact velocities, and describes the techniques used in the present work to determine the impact velocity of the projectile. It also describes the equipment and method of shooting an artificial hailstone. Two methods used to measure the dent depth in the present work are described in Section 3.4. Two sheet steel grades (G550 and G300 manufactured to AS 1397-2011) and five thicknesses (0.35 mm, 0.42 mm, 0.55 mm, 0.75 mm, 1.00 mm) were selected as the test materials to study the effects of yield stress and sheet thickness on the dent resistance of flat steel panels.

Each sheeting was screwed to timber battens spaced at 600 mm from each other, and the projectile was aimed at the middle between the two battens. The spacing of 600 mm represents the minimum found in practice, and it is expected that, the larger the spacing, the smaller the dent as more energy is lost to elastic vibration (damping).

3.2 Methods of Making Robust Artificial Hailstones

Ice is still considered to be the most suitable material to simulate hailstone because natural hailstones mainly consist of ice as well, and ice balls are easier to make in any laboratory. Many hail impact researchers (Greenfeld 1969; Kim et al. 2003; Moore and Wilson 1978; Render and Pan 1995; Tippmann 2011; Tippmann 2011; Kim et al. 2008; Swift 2013; Luong 2014; IBHS 2013, 2015a) attempted to improve the strength of their ice balls rather than using other materials to simulate artificial hailstones, without much success as summarised in Table 2.2. However, in order to make the strongest ice ball, it is desirable to understand the properties of ice first.

The graphs in Figure 3.1 illustrates the behaviour of ice under different loading scenarios. The first graph suggests that ice is ductile under low strain rate, and becomes brittle as the strain rate goes higher (Sodhi 2001). When an ice ball impacts steel sheeting at the terminal velocity, the strain rate can be extremely high, which makes the ice ball break or shatter.

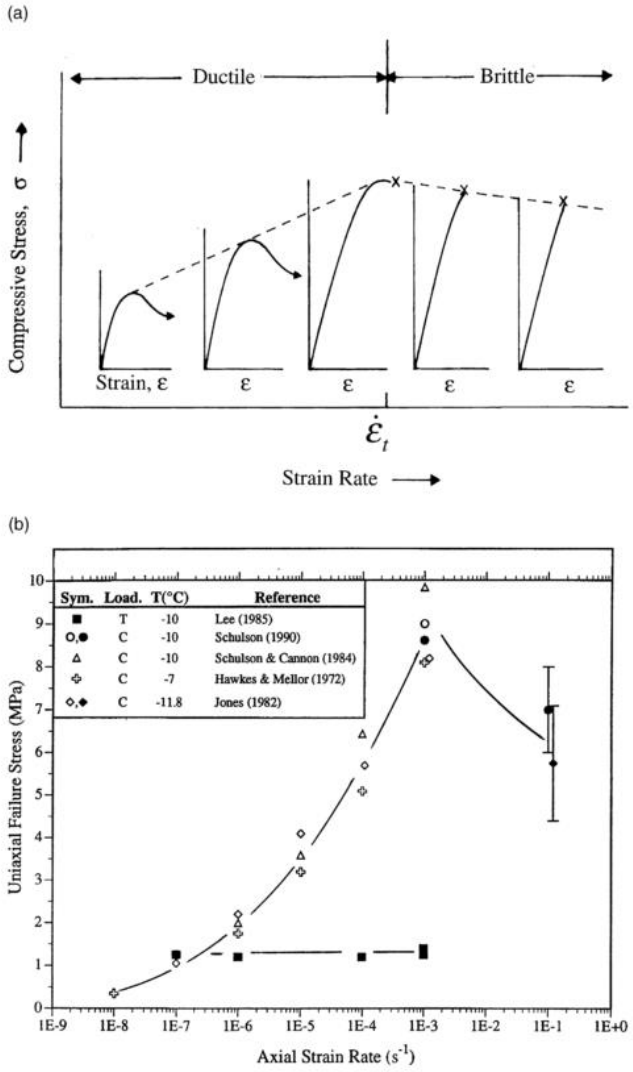

Figure 3.1: Mechanical properties of ice under different loading rates: (a) Compressive behaviour; (b) Uniaxial Failure Stress (Schulson 2001)

Through comparison between the graph in Figure 3.1(b) and Table 3.1, it can be seen that there is not much difference between the compressive strength of ice balls at high strain rate and that of natural hailstones. However, Schulson (1999) suggested that the resistance of ice to a ballistic impact is dependent on the tensile strength rather than the compressive strength. Therefore, in a hail impact test, the tensile strength of the ice ball could be the main factor for its integrity.

Table 3.1: Characteristic natural hailstone properties collected by IBHS (Giammanco & Brown 2014)

Case	Date	Location	Sample Size	Max Diameter (cm)	Mean Diameter (cm)	Max Compressive Stress (mPa)	Mean Compressive Stress (mPa)
1A-2012	5-27-12	Ravenna, NE	5	1.93	1.35	1.33	0.88
2A-2012	5-28-12	Lindsay, OK	32	4.75	2.77	2.21	0.89
3A-2012	5-29-12	Kingfisher, OK	20	7.75	2.31	3.71	1.24
3B-2012	5-29-12	Greenfield, OK	17	3.05	1.93	4.32	1.31
4A-2012	6-1-12	Channing, TX	45	3.12	1.80	4.20	0.85
5A-2012	6-2-12	Eads, CO	17	3.33	1.63	0.76	0.39
*6A-2012	6-6-12	Cheyenne, WY	36	3.23	1.44	0.54	0.22
7A-2012	6-7-12	LaGrange, WY	8	3.76	3.12	0.64	0.38
*7B-2012	6-7-12	LaGrange, WY	59	5.41	3.02	2.77	0.57
*1A-2013	5-17-13	Hyannis, NE	85	3.30	1.41	4.57	0.81
2A-2013	5-18-13	Paradise, KS	6	1.82	0.96	0.41	0.40
*3A-2013	5-19-13	Wichita, KS	112	3.20	1.47	4.24	0.61
3B-2013	5-19-13	Arkansas City, KS	16	3.43	1.51	1.51	0.64
*3C-2013	5-19-13	Blackwell/Newkirk, OK	23	2.51	1.11	1.51	0.55
*3D-2013	5-19-13	Cedar Vale, OK	71	3.99	2.08	1.12	0.29
3E-2013	5-19-13	Burbank, OK	18	2.21	1.11	1.80	0.95
*4A-2013	5-20-13	Antioch, OK	212	4.80	0.81	3.34	0.56
5A-2013	5-30-13	Blanchard, OK	15	3.98	2.08	1.58	0.59
*5B-2013	5-30-13	Ratliff City, OK	29	10.69	2.61	3.88	0.70
6A-2013	6-1-13	Mason, TX	29	2.99	1.60	7.46	1.64
6B-2013	6-1-13	London, TX	30	3.60	1.88	6.46	1.43
7A-2013	6-2-13	Elmwood, OK	36	3.71	1.88	2.86	0.51

**multiple measurement locations within the swath of hailfall from the same parent updraft*

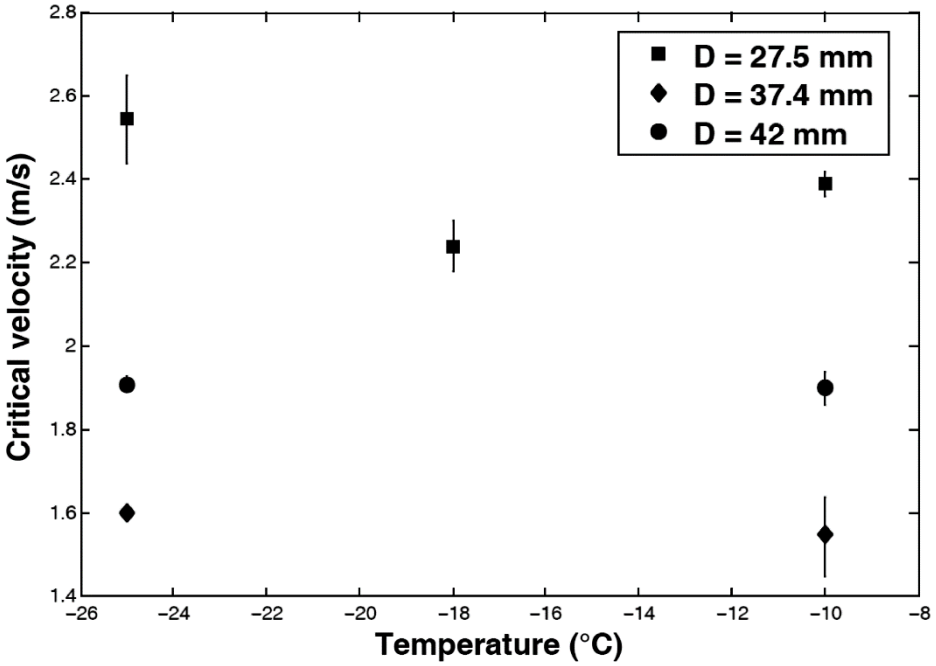

Figure 3.2: Critical impact velocity for ice fragmentation (Guégan et al. 2011)

Guégan et al. (2011) dropped ice balls on glass to find the critical velocity of ice ball fragmentation. From the results presented in Figure 3.2, it can be seen that the freezing temperatures did not influence the strength of the ice balls. However, the graph shows that the maximum velocity to avoid the ice ball fragmenting is only 2.6 m/s, which is far less than the terminal velocities of natural hailstones listed in Table 2.1.

In the present work, the artificial hailstones made with the following first three methods were verified in preliminary impact tests at velocities around 20 m/s on a 0.55-mm thick G300 steel sheet. The artificial hailstones made with the fourth (successful) method were tested at impact velocities close to 30 m/s.

Method 1. Layered-Structure Ice Ball (two techniques)

As reviewed in Chapter 2, a characteristic of natural hailstones is their layered structure. Kim et al. (2003) and Tippmann (2011) believed that the layered structure could be the reason why a natural hailstone remained intact after hitting solid objects at terminal velocity. However, they had used the flat-wise freezing method illustrated in Figure 2.2 in their experiment, which resulted in a different structure from the 'onion layered' structure typical of natural hailstones shown in Figure 2.1.

In order to replicate the onion-layered structure in the present work, artificial hailstones were made by the 'dip method' using demineralized water and dry ice (solid carbon dioxide). Natural hailstones accrete when water attaches itself on the embryo and then freeze. In the present work, an artificial embryo was made from either a water drop or a small sand particle. The embryo was dipped into demineralized water, and was then quickly transferred into dry ice to freeze the attached water. The detailed procedure is given in Appendix A.

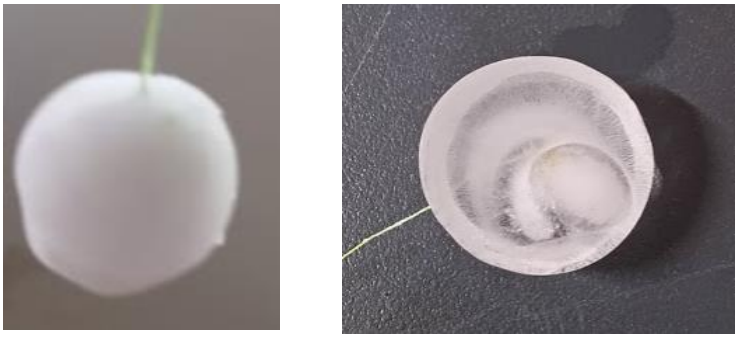

(a) (b)

Figure 3.3: Artificial hailstones made with the dry ice dipping method: a) Artificial hailstones; b) Cross section of artificial hailstones

It can be seen from Figure 3.3 that the onion-layered structure is reasonably replicated compared to Figure 2.1. Also, the density of this type of artificial hailstones is close to that of the natural hailstone, ranging from 720 to 810 kg/m^3.

However, there are disadvantages in using this method. Firstly, the shape of the artificial hailstone is difficult to control, most of the resulting ice lumps are irregular oval rather than spherical. Most importantly, the resulting artificial hailstones shattered in the preliminary impact tests. One main reason is that a significant amount of carbon dioxide was trapped in the outer layer of the artificial hailstone, increasing the grain size and thus weakening the ice (Schulson 1999).

A small modification was taken to improve the artificial hailstone. Allaby and Garratt (2014) suggested the clear outer layer of a natural hailstone to be the reason why hailstone can bounce off after impact. In the modified method, a small artificial hailstone was made with the dry ice dipping method first, and placed into a ping-pong ball with a hole at the top. The ping-pong ball was then filled with distilled water that had been boiled twice before being frozen. However, only two out of twelve such "hailstones" successfully replicated the onion-layered structure of natural hailstones, and none of them was perfectly spherical (see Figure 3.4). Most importantly, only one survived the preliminary impact tests.

(a) (b)

Figure 3.4: Artificial hailstones made with the dry ice dipping method combined with ping-pong ball freezing: a) Artificial hailstones b) Cross section of artificial hailstones

Method 2: Pure Clear Ice Ball (two techniques)

Luong (2014) claimed that some of the ice balls he made remained intact after impact at a velocity of 25.5 m/s on fibreglass composite panels. The ice balls were said to be free of cracking and air. The method of making the ice balls by first boiling deionized water was therefore replicated in the present work, except that 3D printed plastic mould instead of

aluminium mould was used. However, it was found that the resulting ice balls were not perfectly free of cracking and air, and shattered in the preliminary impact tests.

Another technique of making perfectly clear ice balls was employed using the ‘slow freezing method’, which allows water to freeze from the bottom to the top. The resulting ice balls were apparently free from cracking and air (see Figure 3.5). The detailed procedure is given in Appendix A. However, such ice balls did not survive the preliminary impact tests.

Figure 3.5: Pure ice ball free of air and cracking

Method 3: Microfibre Ice Ball

One possible way to make an ice ball remaining intact after high velocity impact on steel sheeting is to increase its tensile strength. During the Second World War, a material named pykrete, made of 14% sawdust and 86% water by weight was first developed to improve the impact resistance of ice landing ground for military aircrafts. It has been suggested that the tensile strength of pykrete can be more than twice that of pure ice (Gold 2004). However, pykrete is very different from ice. It can be seen from Figure 3.6 that the pykrete slab is more like a wooden slab than an ice one.

Figure 3.6: Pykrete slab

However, this material led to an idea in the present work on how to reinforce ice. ASTM:F320-10 (ASTM 2010) suggests using cotton fibre to reinforce ice. Kim et al. (2008) used this method in their hail impact test on fibreglass composite panels, but they did not mention whether the cotton ice ball remained intact in their experiment.

In the present work, Polypropylene fibre was used instead of cotton fibre to reinforce ice balls as the former has a higher tensile strength. Some of the resulting artificial hailstones did not shatter in the preliminary impact tests as they were held together by the microfibre, but nevertheless fractured as shown in Figure 3.7. At higher impact velocities (e.g. 40 m/s), they shattered like normal ice balls.

Figure 3.7: Microfibre ice ball after impact

Method 4: PVA (Polyvinyl acetate) Ice Ball

Based on the results obtained using the microfibre reinforcement, it was believed that if the fibre could be dissolved into water, the artificial hailstone could be uniformly reinforced. After several trials, it has been found that Liquid PVA (Polyvinyl acetate), a water-soluble glue, is perfect as the additive. It can fully dissolve in water so that the artificial hailstones can have uniform properties. Demineralized water is used to avoid impurities. In the present work, demineralized water was produced from the water purification equipment (Direct-Q UV-R water purification system) shown in Figure 3.8.

Figure 3.8: Water purification system used to produce demineralized water

Figure 3.9: Intact artificial hailstone made with 12% PVA after the impact test

Artificial hailstones made with different percentages of PVA were tested at an impact velocity of 30 m/s, which is commonly used for testing roofing materials (Revolution Roofing, 2017). Three different types of artificial hailstones were made and tested being 5% PVA with 1% microfibre, 11% PVA and 12% PVA. Table 3.2 shows the impact test results. The artificial hailstones made with 11% PVA only remained intact when their sizes are relatively large (see Appendix B). Only the artificial hailstones made with 12% PVA completely passed the preliminary impact tests, and as such they would be used in the present experimental program. Figure 3.9 shows such an artificial hailstone after the impact test. As shown in Table B.3 of Appendix B, the average density was 0.996 g/cm3, which is considered to be reasonably close to the constant density of 0.9 g/cm^3 assumed for natural hailstones (Chisholm & English 1973). Validation of the present artificial hailstones is provided in Section 4.2.

Table 3.2: Impact outcomes of various PVA contents (and microfibre)

Impact outcome	5% PVA with 1% microfibre	11% PVA	12% PVA
Intact	1	5	7
Minor Fragmentation	5	1	0
Break	4	3	0

The step-by-step procedure of making artificial hailstones with 12% PVA is as follows:

1. Use a clean beaker to get a certain amount of demineralized water from water purification system (e.g. one litre).
2. Boil the demineralized water twice or three times to expel the air.
3. Weigh the desired amount of liquid PVA (e.g. 12 grams) and the desired amount of boiled demineralised water (e.g. 100 grams), then pour the boiled water into liquid PVA carefully.
4. Mix them thoroughly by stirring the solution for 15 to 20 minutes.
5. Clean all the sphere moulds with tap water first, and then use paper towel combined with Isopropyl Alcohol to wipe the inside of the mould. Let the mould dry before using (the Isopropyl Alcohol is volatile, so the mould will dry very quick).
6. Use a syringe to inject the solution into the prepared sphere moulds until full.
7. Take out 6 to 8% of the solution from each mould to leave some space for ice expansion.
8. Put the moulds into a freezer at minus 12 degrees Celsius and freeze them for at least 48 hours.
9. After 48 hours, take the mould out of the fridge and remove the artificial hailstone. If the mould sticks together, just leave it at room temperature for a few minutes before trying to remove the artificial hailstone again.
10. Discard the ice ball with visible cracking (could result from thermal shock), and put the rest in a bag and store them in the fridge until testing time.

3.3 Impact Velocity

3.3.1 Sizes and target velocities of artificial hailstones

The kinetic energy (or impact energy) and momentum of hailstones are the main external factors that account for the dent depth in steel roofing. The kinetic energy and momentum of a projectile are:

$$W_k = \frac{1}{2}mv^2 \qquad \text{Equation 3-1}$$

$$p = mv \qquad \text{Equation 3-2}$$

where W_k is the kinetic energy, p is the momentum, m is the projectile's mass, and v is the projectile's velocity.

The mass of a hailstone is a function of its size (and density). The nominal diameters of the artificial hailstones used in the present experiment are 25 mm, 33 mm, 38 mm, 45 mm and 50.8 mm, consistent with the sizes commonly used in the industry standards (ANSI 2011; Underwriters Laboratories 1996). It may be noted that only hailstones with diameters larger than 25 mm tend to cause permanent indentations on metal roofs (Australian Building Codes Board 2010). In addition, hailstone impact with diameters smaller than 20 mm has been well studied and simulated (Sharafi et al. 2013). Hailstones greater than 2 inches (50.8 mm) rarely happen in Australia (Paterson & Sankaran 1994).

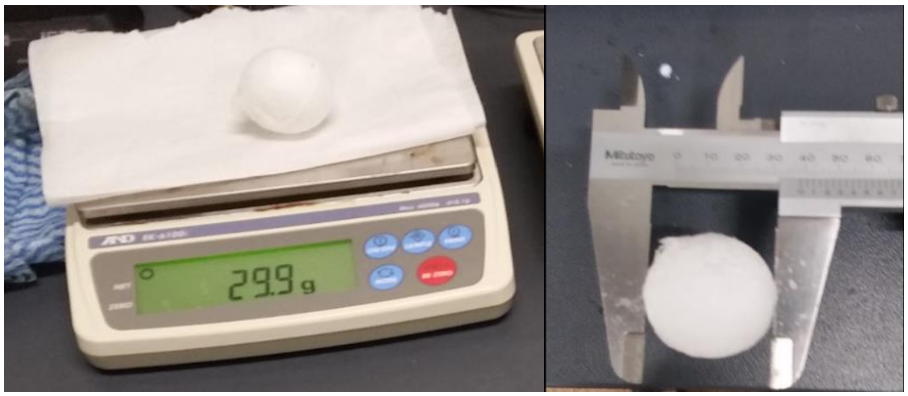

Figure 3.10：Digital scale and Vernier calliper

In the present work, the different sizes of artificial hailstones were obtained using plastic sphere moulds of the corresponding sizes. The mass and the diameter of each artificial hailstone were measured using a digital scale and a Vernier calliper, as shown in Figure 3.10.

The terminal velocities of hailstones of various sizes provided by Laurie (1960) and shown in Table 2.1 have been verified by Andrew and Robert (2014). Although the corresponding terminal velocities of the present artificial hailstones range from 22 m/s to 32 m/s, a higher target velocity of 40 m/s is included in order to study the effects of impact energy and/or momentum on dent sizes. It may also be noted that a natural hailstone may travel at a velocity higher than its terminal velocity under strong wind although it may not impact the roof perpendicularly. The target impact velocities in the present work are 20 m/s, 30 m/s and 40 m/s for every size of the artificial hailstones.

3.3.2. Measurement of impact velocity

In the present work, a gas gun was used to shoot the artificial hailstone against steel sheeting to simulate hail impact. Figure 3.11 shows the hail launcher utilised in the experiment, which comprises an air compressor to supply the compressed air used to eject the projectile (Figure 3.11: b), a steel chamber to receive and store the compressed air before shooting (painted blue in Figure 3.11: c), a steel barrel to direct the released air and guide the projectile, and a foam sabot to ensure the stored pressure is fully transferred to the projectile after release (Figure 3.11: d). The target velocity was attained by setting the appropriate shooting pressure at the air receiver.

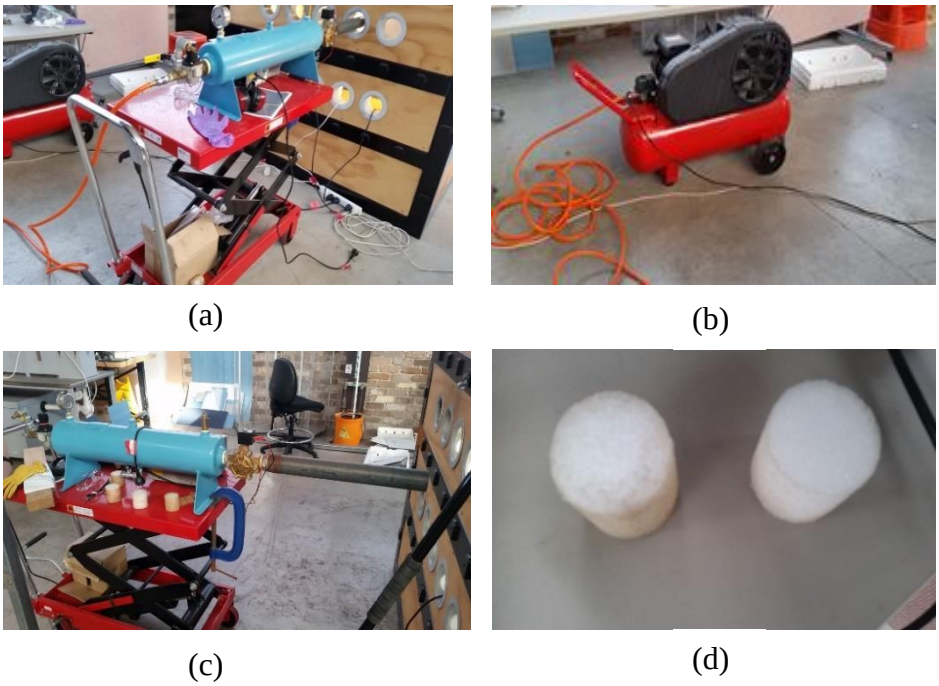

(a) (b)

(c) (d)

Figure 3.11: Gas gun used to shoot artificial hailstones: (a) Hail Launcher; (b) Air compressor; (c) Steel chamber and barrel (d) Foam sabots

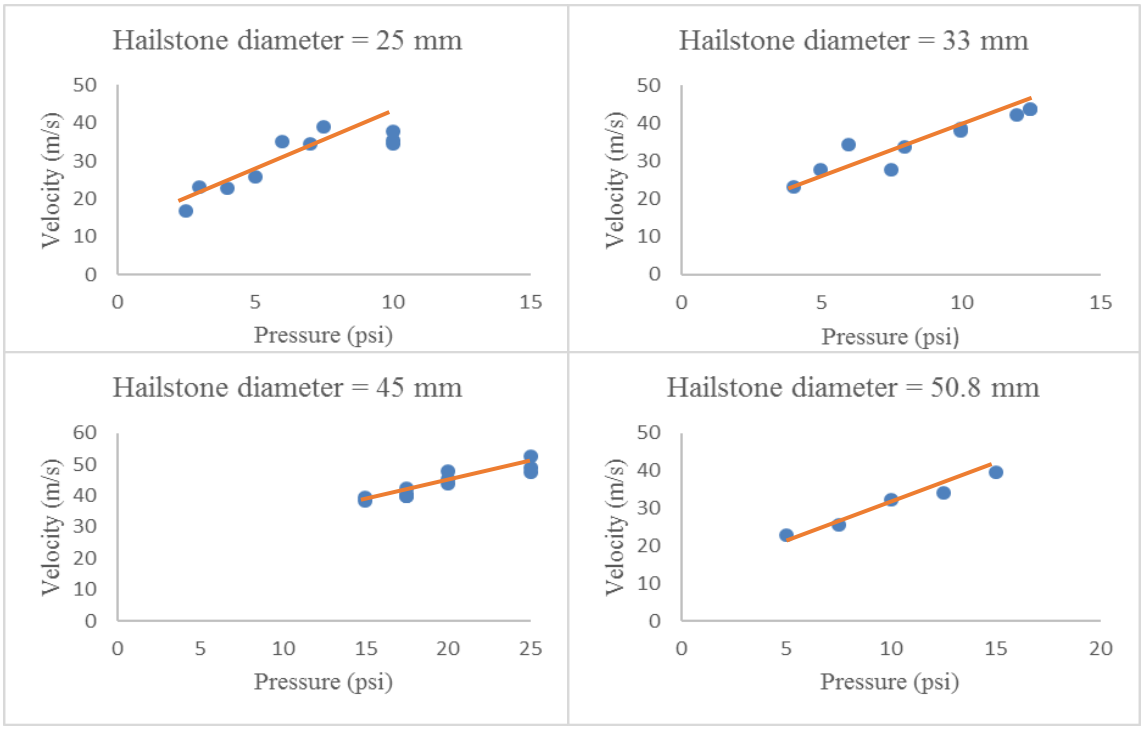

Figure 3.12: Relationship between air pressure and impact velocity of artificial hailstones

Table 3.3: Approximate air pressures for target velocities

Hailstone Size (mm)	Designed velocity (m/s)	Pressure (psi)
50	40	15
	30	10
	20	4
45	40	14
	30	9
	20	4
38	40	12.5
	30	7.5
	20	3
33	40	10
	30	6
	20	3
25	40	10
	30	6
	20	3

Figure 3.12 plots the relationships between the pressure set at the air receiver and the measured impact velocity, obtained from a series of trials, for the four sizes of artificial hailstones. It can be seen that, for a given size of hailstone, the impact velocity varies almost linearly with the shooting pressure. Table 3.3 provides an approximate guide to setting the air pressures for the target impact velocities.

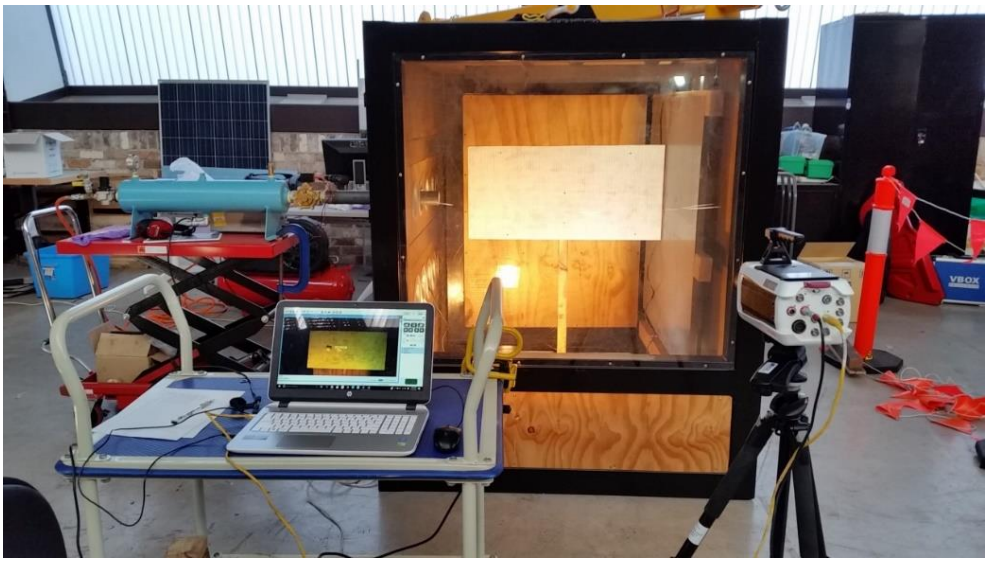

Figure3.13: Hail impact experiment set-up

The impact velocity of each artificial hailstone was measured using a high-speed camera and a whiteboard with a ruler in the background. The length of the whiteboard is 90 cm, and the ruler's scale is 1 cm. The whiteboard was located next and perpendicular to the impacted steel sheeting so that both the impact velocity and the rebound velocity could be determined, as shown in Figure 3.13.

The high-speed camera also provided a means to ascertain whether an artificial hailstone remains intact or not immediately after impact.

The image definition is mainly dependent on the frame rate set in the camera. A higher frame rate is desirable for determining the position of the projectile in each frame. In order to achieve high frame rates, two DC lights were used to illuminate the whiteboard from two different positions, one DC light was hung in front of the whiteboard, and another at the top of the whiteboard in the safety unit (shown in Figure 3.13). Through trials to balance the recording time and the image definition, the frame rate was set to 2500 per second, which allowed an accurate determination of the projectile's position (see Figure 3.14).

The whiteboard was located as close as possible to the gas gun, but there was still some distance between the board and the trajectory of the projectile. Using the high speed camera data directly would overestimate the projectile's velocity because of parallax. To solve this problem, a ruler was attached to the barrel of the gas gun and extended to the steel sheeting. A picture was then taken using the high speed camera to determine the deviation between this ruler and that on the whiteboard, from which a correction factor, $\varphi = 0.95$, was introduced when the impact velocity was calculated based on the measurements obtained from the whiteboard.

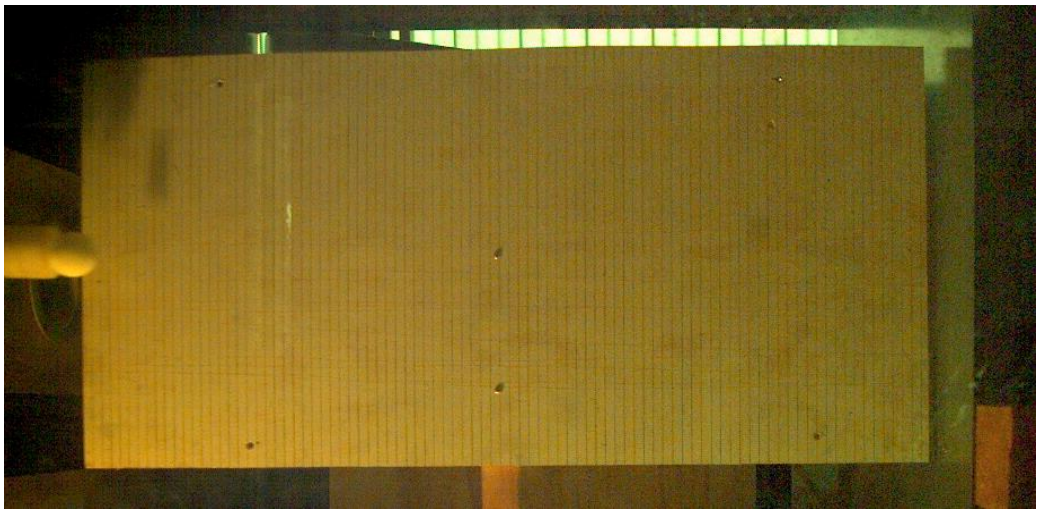

(a)

(b)

Figure 3.14: Images of an artificial hailstone at 2500 frames per second: (a) just leaving the barrel; (b) just before impact

It should be noted that, due to the relatively short distance between the barrel end and the steel sheeting, it has been found that there was a negligible decrease (less than 1%) in the velocity of

an artificial hailstone between the two positions shown in Figure 3.14. This fact means that the impact velocity of an artificial hailstone in the present work can be calculated based on its positions as illustrated in the figure.

For the shot hailstone in Figure 3.14, there are 82 images captured by the camera between the two instances shown in (a) and (b). The distance between the two locations of the artificial hailstones given in Figure 3.14 (a) and (b) can be determined from the number of scales between them, which was 87 cm. The impact velocity is then equal to:

$$V = \frac{(\frac{87\ cm}{100\ cm/m})}{(82+1)\ frame} \times 2500 \frac{frame}{s} \times 0.95 = 24.9\ m/s$$

As the whiteboard ruler's scale is 1 cm, the maximum absolute error in determining the velocity is

$$V_d = \frac{\frac{2 \times 0.5\ cm}{100\ cm/m}}{(82+1)\ frame} \times 2500 \frac{frame}{s} \times 0.95 = 0.29\ m/s$$

The maximum relative error is equal to 1.14%, which is believed to be acceptable.

3.4 Dent Depth Measurement

In the present work, dent sizes were measured using two methods, the manual method and the 3D scanning method. The former used a depth gauge and two reference plates to measure the dent depth, as shown in Figure 3.15, and a Vernier calliper to measure the dent diameter. By its nature, the manual method was prone to human errors, sometimes to a significant extent as discussed in Chapter 4.

The 3D scanning method has been widely used to accurately determine the shape and size of an object. Figure 3.16 shows the setup of the 3D scanning method in the present work. The tested steel sheeting was cut into smaller panels having three to six dents, which was then placed on a desk to be scanned at high accuracy. An example of the scanned image is shown in Figure 3.17. Each dent had three reference points and was scanned three or four times from different directions. The scan result is saved in a file having the extension name ".STL".

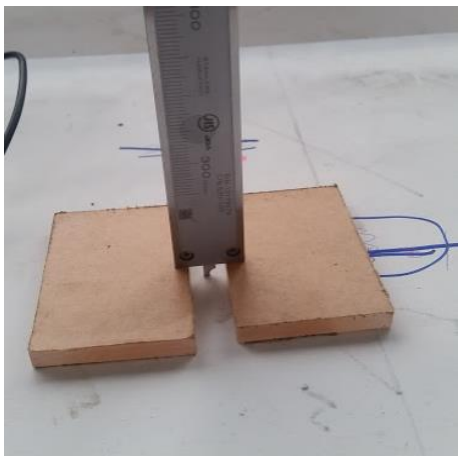

Figure 3.15: Dent depth measurement using a depth gauge

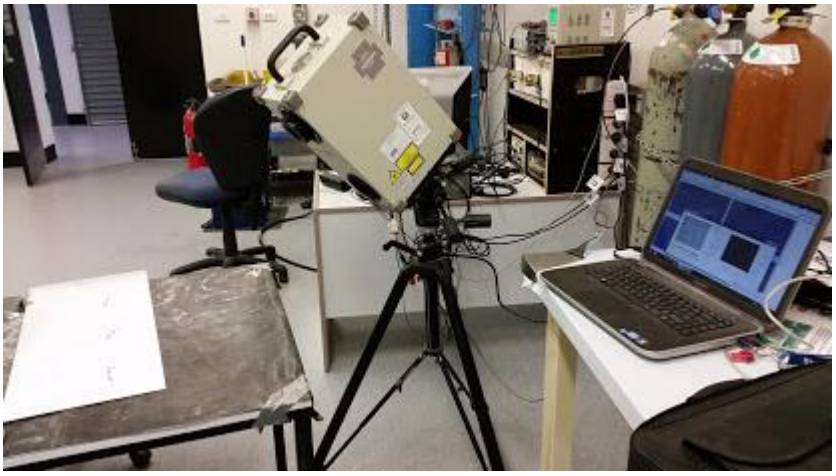

Figure 3.16: Set up of 3D scanning

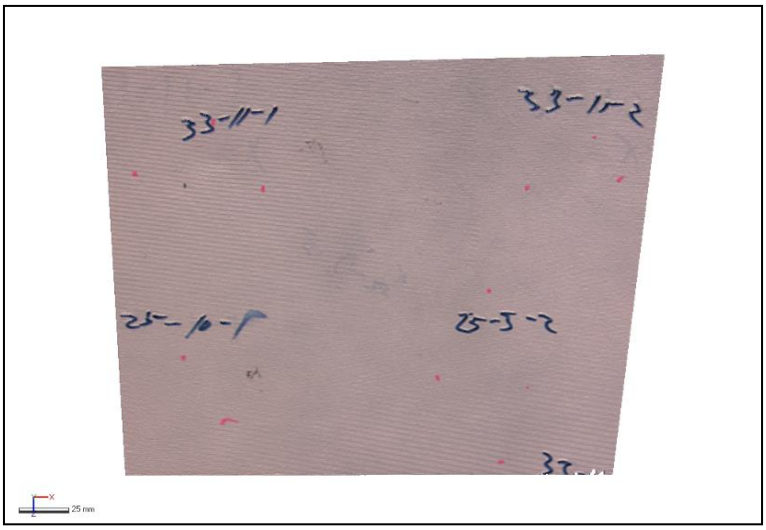

Figure 3.17: Image of a scanned steel panel

In the present work, the software ‘Geomagic Control’ (3D System 2014) was used to process the scanned file to determine the dent depth and diameter. The steps of analysing the dents are suggested as follow:

1) Create a ‘reference plate’. Since the scanned data are actually meshes of millions of points, it is difficult to determine the ‘dent depth’ by selecting two points on the mesh. Therefore, a reference plate was created to help calculate the distance between the lowest point and the surface, which is the maximum dent depth. The reference plate is a flat sheet without any dents, drawn using SolidWorks. The reference plate in the present work is set to be 0.02 mm thick, which is the minimum thickness required for the ‘3D compare’ software (see Step 3). Since most dent sizes are larger than 1 mm, the incurred error is negligible.
2) Align the scanned sheet with the reference plate using ‘Transform Alignment-Points’ function in ‘Geomagic Control’, as shown in Figure 3.18.

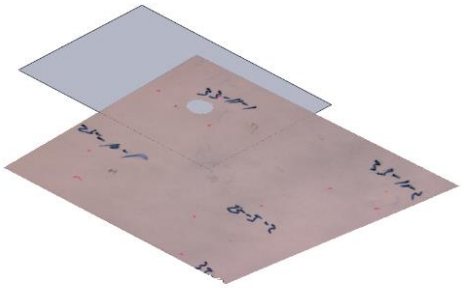

Figure 3.18: Alignment of the two plates

3) Use ‘3D Compare’ to output the maximum dent depth. The software shows the deformations due to hail impact, and the maximum dent depth can be obtained from a table (Figure 3.19). This step is repeated for the two or three other scans of the same dent in order to verify the result.
4) Sometimes, two dents could be too close to each other (Figure 3.20), and using ‘3D Compare’ can only get the maximum dent depth of the deepest dent. ‘2D Compare’ gives the dent depth along a cut section (Figure 3.21). In the present work, twenty plates spaced at 0.5 mm are employed to cut the centre of a dent in order to obtain the maximum dent depth.
5) Use ‘2D Compare’ to output the diameter of a dent (see Figure 3.22).

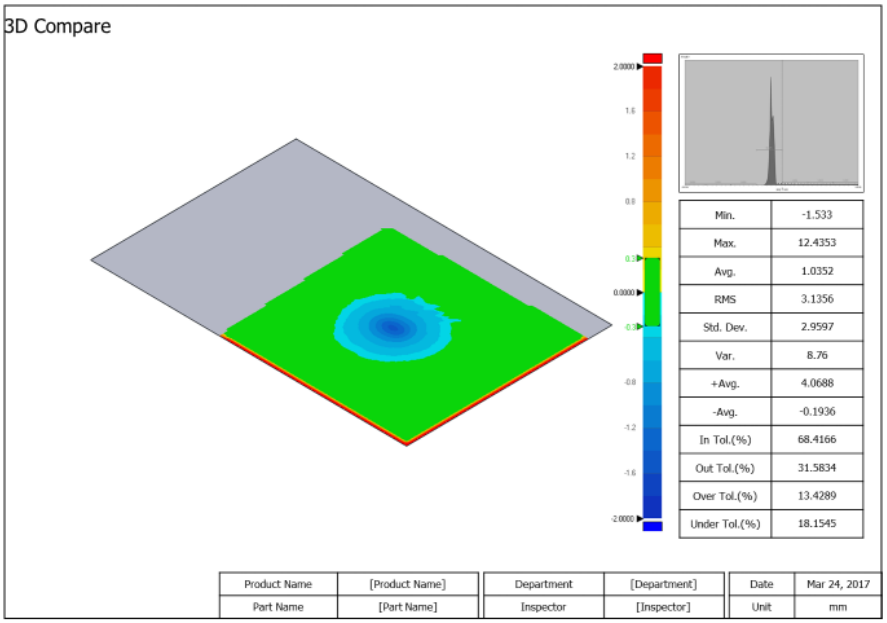

Figure 3.19: '3D Compare' with maximum dent depth

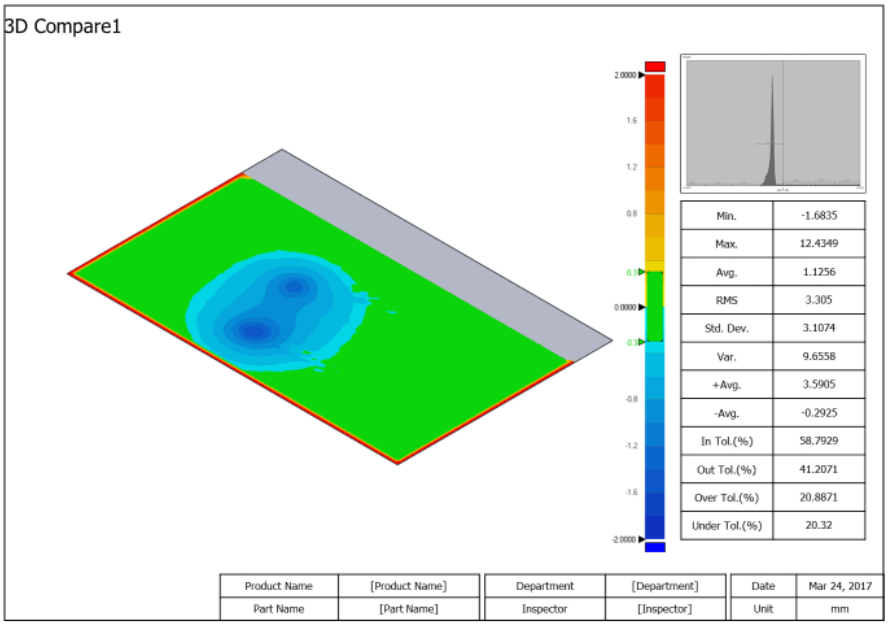

Figure 3.20: Dents too close to each other

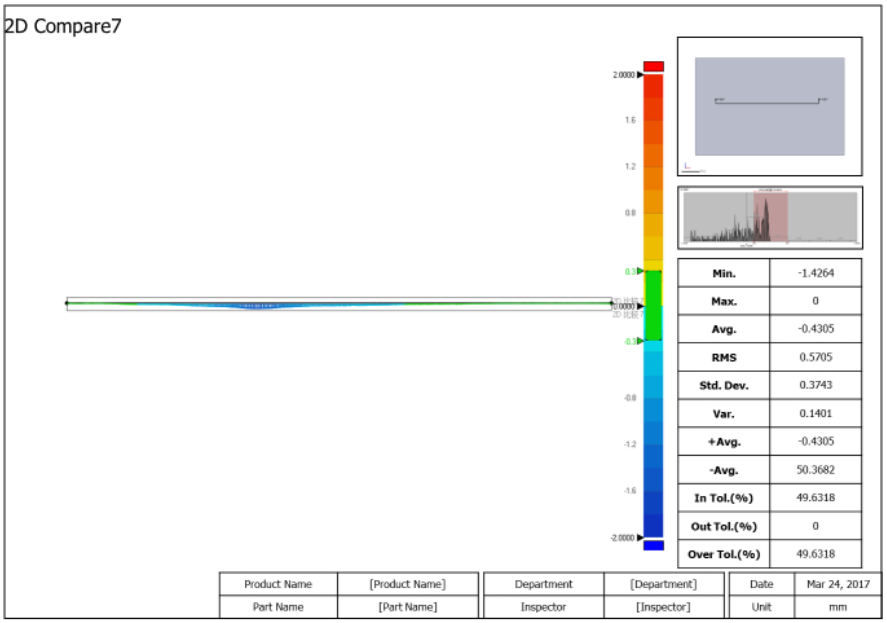

Figure 3.21: Measurement of the dent depth using '2D Compare'

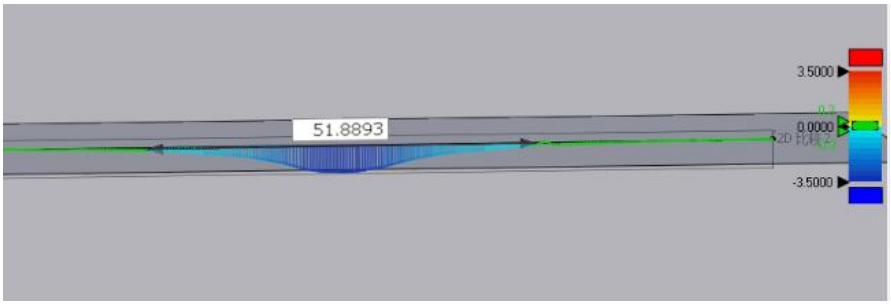

Figure 3.22: Measurement of the dent diameter using '2D Compare'

3.5 Concluding remarks

Four types of water based artificial hailstones, being the layered-structure ice ball, the pure clear ice ball, the microfibre ice ball and the PVA ice ball were made (with a total of six different techniques) in the present work and tried at impact velocities around 20 m/s on 0.55 mm thick G300 steel sheeting. Only the PVA ice ball made of 12% water-soluble PVA glue passed the preliminary impact tests (at impact velocities around 30 m/s).

It is believed that the PVA ice ball, which was first created in the present work, represents the first ever water based artificial hailstone that is capable of remaining intact after impacting steel sheeting at the terminal velocity. Its average density was reasonably close to that assumed for natural hailstones. Validation of such artificial hailstones is given in Section 4.2

Consistent with the standard industry practice, the nominal diameters of the artificial hailstones used in the present experiment were 25 mm, 33 mm, 38 mm, 45 mm and 50.8 mm. The target impact velocities for each size are 20 m/s, 30 m/s and 40 m/s, which cover the corresponding terminal velocity.

In the present work, a gas gun was used to shoot the artificial hailstone perpendicularly against steel sheeting. The steel sheeting was screwed to timber battens spaced at 600 mm from each other and was shot at the middle between the battens. The impact velocity (and the rebound velocity) of each artificial hailstone was measured using a high-speed camera and a whiteboard with a ruler in the background. A correction factor of 0.95 was applied to account for parallax.

The dent depth due to a hailstone impact was measured by two methods, being the manual method using a depth gauge and the digital 3D scanning method. A comparison between the two methods is given in Section 4.3.

Chapter 4 Experimental Results and Discussions

4.1 Introductory Remarks

This chapter provides the results of the hail impact tests conducted as part of the thesis, and discusses various aspects including the validity of using the present artificial hailstones, being the PVA ice balls produced using Method 4 described in Section 3.2. It also includes a comparison between the dent sizes determined using a depth gauge and those obtained by 3D scanning. It analyses the effects of the yield stress and thickness of the steel sheeting on the dent depths.

As mention in Section 3.1, there were two grades of cold-reduced steel sheets used in the hail impact tests, being G550 and G300 (Standards Australia 2011). All the tested panels were screwed to timber battens spaced at 600 mm from each other. For G550 steel sheets, four thicknesses were tested, being 0.35 mm, 0.42 mm, 0.55 mm and 1.00 mm. For G300 steel sheets, there were three thicknesses: 0.55 mm, 0.75 mm, and 1.00 mm. Each type of steel sheets was tested with five sizes of artificial hailstones, with diameters of 25 mm, 33 mm, 38 mm, 45 mm and 50.8 mm, each shot at three nominal impact velocities of 20 m/s, 30 m/s, and 40 m/s. The exception was that the thickest G550 steel sheet was not impacted with 25-mm hailstones, which shattered when shot at the G300 sheet of the same thickness.

Each artificial hailstone was shot at the middle of the panel, impacting the panel in the normal direction. In order to ensure the reliability of the experimental results, each size of artificial hailstones for each sheet was tested three times for each nominal velocity (the shot hailstones were not reused), entailing a total of 45 tests on each type of sheet except for the thickest G550 sheet. There was therefore a total of 310 hail impact tests in the present work, the results of which are given in Appendix C and discussed in the following sections. Validation of the Present Artificial Hailstones

Liang (2015) and Ramsay and Liang (2015) successfully made two pure clear ice balls with a diameter of 50.8 mm, which remained intact after impact on a 0.35-mm thick G550 steel sheet at velocities of 28.0 m/s and 30.7 m/s. The resulting dent depths were found to be 3.0 mm and 4.1 mm, respectively. Their dent depths are similar to those obtained using the present artificial hailstones of the same diameter on the same type of steel sheet, shot at 29.2 m/s, and 30.7 m/s,

which were 3.08 mm and 4.15 mm, respectively. Therefore, it can be seen that the inclusion of 12% PVA in the present artificial hailstones did not result in noticeably different dent depths compared to pure ice balls that remain intact after impact.

It may be noted that the common thicknesses of steel roofing sheets are 0.42 mm and 0.55 mm, and the common steel grades are G550 and G300 (Ullrich 2014; The Roofing Centre Tasmania 2017). The pure clear ice balls of Liang (2015) and Ramsay and Liang (2015) could only remain intact when impacting thinner steel sheets, with inconsistent results. In fact, the two ice balls of Liang (2015) and Ramsay and Liang (2015) mentioned in the preceding paragraph were the only ones that remained intact in their experiment.

As can be seen in Appendix C, the present artificial hailstones survived most impact tests on sheets up to 0.55-mm thick irrespective of the steel grade. As the thickness increased to 0.75 mm (G300), almost half of the present hailstones broke on impact. For the thickest sheets, only about 15% survived the impact tests. However, it should be noted that the "failures" of the present artificial hailstones mostly occurred at impact velocities greater than the respective terminal velocities of the corresponding natural hailstones and/or on thicknesses rarely used in practice for steel roofing.

4.2 Accuracy of Dent Measurements

A comparison between the manually measured dent depths using a depth gauge and the digitally measured depths using 3D scanning can be made from the results presented in Appendix C. Most readings are the same between the two methods or are within 5% of each other. However, there are greater differences for some measurements. In order to find the reason for the differences and improve the accuracy of the measurements, sixteen dents were remeasured with the depth gauge. The second readings are given in brackets in Appendix C. The 3D scanned files of all G300 steel panels were reanalysed by another researcher.

The results show that the differences between the first and the second manual measurements are quite significant and that the second measurements are all closer to the values determined from 3D scanning. On the other hand, the dent depths determined from the second 3D scanning are almost the same as the original values. Therefore, it can be concluded that the differences in results between the two methods are mainly caused by human errors in measuring the dent depths using the depth gauge.

For the rest of this thesis, the experimental dent depths refer to those determined from 3D scanning, which is named as experimental dent depth, d_t, in the later analysis.

4.3 Observations of Impact Test Results

4.3.1 Effect of the integrity of artificial hailstones

The impact outcomes of the present artificial hailstones are classified into four categories: intact, minor fragmentation, major fragmentation and shattered, which is shown in Figure 4.1.

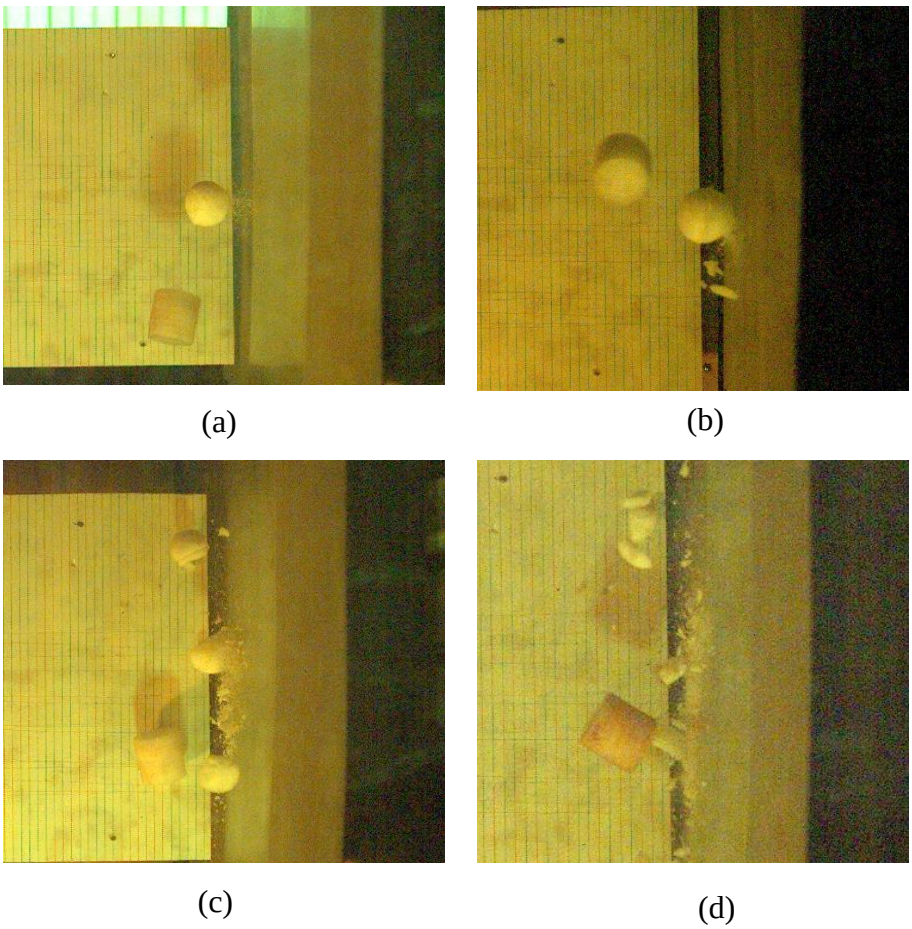

(a) (b)

(c) (d)

Figure 4.1: Integrity of artificial hailstones: (a) Intact, (b) Minor Fragment, (c) Major Fragment, (d) Shattered.

Table 4.1 shows a comparison between the dent depths caused by the artificial hailstones with different integrity. The intact projectile caused the largest dent depth, followed by those with minor fragmentation, major fragmentation, and shattered condition, in that order. The dent depth caused by the shattered artificial hailstone is less than half of that caused by the intact one, even though the former's impact energy was almost twice as large.

It is interesting to note that the dent area caused by a shattered artificial hailstone is larger than that caused by an intact one having similar impact energy, as indicated in Figure 4.2, even though the dent depths have the opposite trend. It appears that the shattered fragments resulted in an increased impact area, as can be seen in Figure 4.1(d).

Table 4.1: Dent depths caused by 25-mm hailstones of different integrity in G550_0.42 mm steel sheet

Impact Energy (Joule)	Dent Depth (mm)	Integrity
2.5	1.07	Intact
3.4	0.90	Minor Fragmentation
4.1	0.69	Major Fragmentation
4.9	0.49	Shattered

Table 4.2 further compares the dent depths caused by the shattered artificial hailstones and those caused by the intact ones that had similar impact energy. It can be seen that the intact hailstones caused dent depths that were typically 25% greater than those caused by the corresponding shattered hailstones.

Table 4.2: Comparison between the dent depths caused by the shattered and the intact artificial hailstones

	Hailstone size (mm)	Integrity	Impact energy (Joule)	Dent depth (mm)	Difference
G550_0.42 mm	38	Shattered	16.7	1.94	
	38	Intact	16.0	2.43	25%
G550_0.55 mm	38	Shattered	19.2	2.10	
	38	Intact	19.3	2.41	15%
G550_1.00 mm	50	Shattered	37.4	2.16	
	50	Intact	37.5	2.74	26%
G300_0.55 mm	33	Shattered	12.9	2.48	
	33	Intact	13.1	3.10	25%

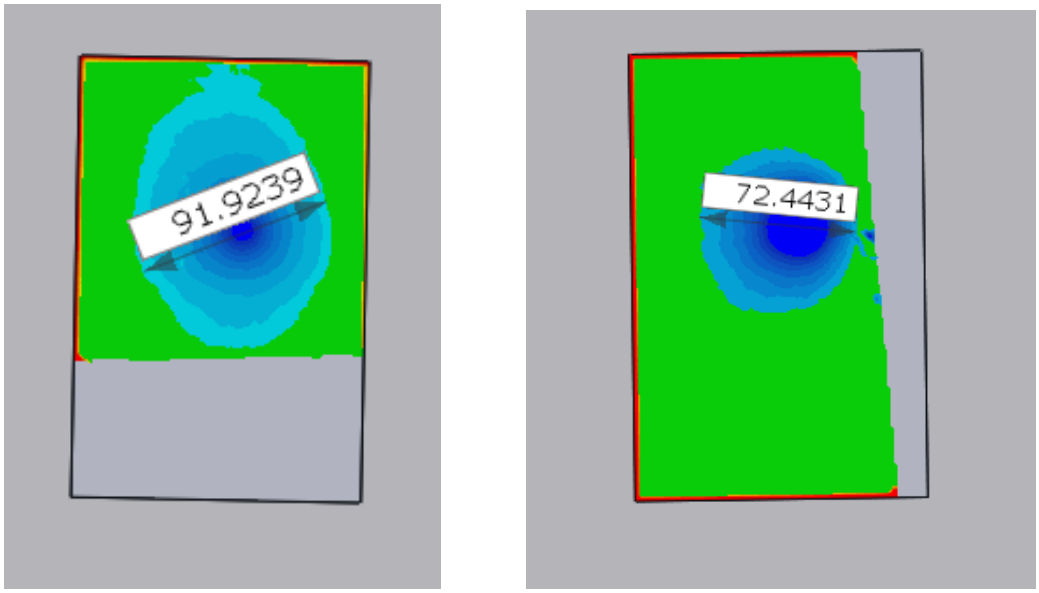

Shattered Intact

Figure 4.2: Dent diameters caused by the shattered and the intact artificial hailstone with similar impact energy (G550_1.00 mm, shattered: 50-15-1; Intact: 50-10-3)

4.3.2 The rebound energy and the flexural vibration energy

According to Patil and Higgs III (2016), the impact energy (E_{impact}) of an intact artificial hailstone is mainly converted to the plastic deformation energy of the dented sheet (E_p), the rebound energy (E_r) and the flexural vibration energy (E_v), as other forms of energy loss such as heat and sound are negligible.

Therefore, the energy conversion can be represented as:

$$E_{impact} = E_p + E_v + E_r \qquad \text{Equation 4-1}$$

In the present experiment, the rebound of each intact artificial hailstone was captured by the high speed camera, and the rebound velocity can be calculated using the method used for calculating the impact velocity. The average ratio of the rebound energy to the impact energy of the artificial hailstones tested in the present work is shown in Table 4.3 for each type of steel sheets, and it can be seen that the rebound energy is relatively small compared to the impact energy, amounting to less than 1% energy loss. The rebound energy is therefore ignored in the present analysis.

Table 4.3: The average ratio of the rebound energy to the impact energy

	Average Value of E_r / E_{impact}
G550_0.35 mm	0.76%
G550_0.42 mm	0.80%
G550_0.55 mm	0.80%
G550_1.00 mm	0.67%
G300_0.55 mm	0.35%
G300_0.75 mm	0.35%
G300_1.00 mm	0.57%

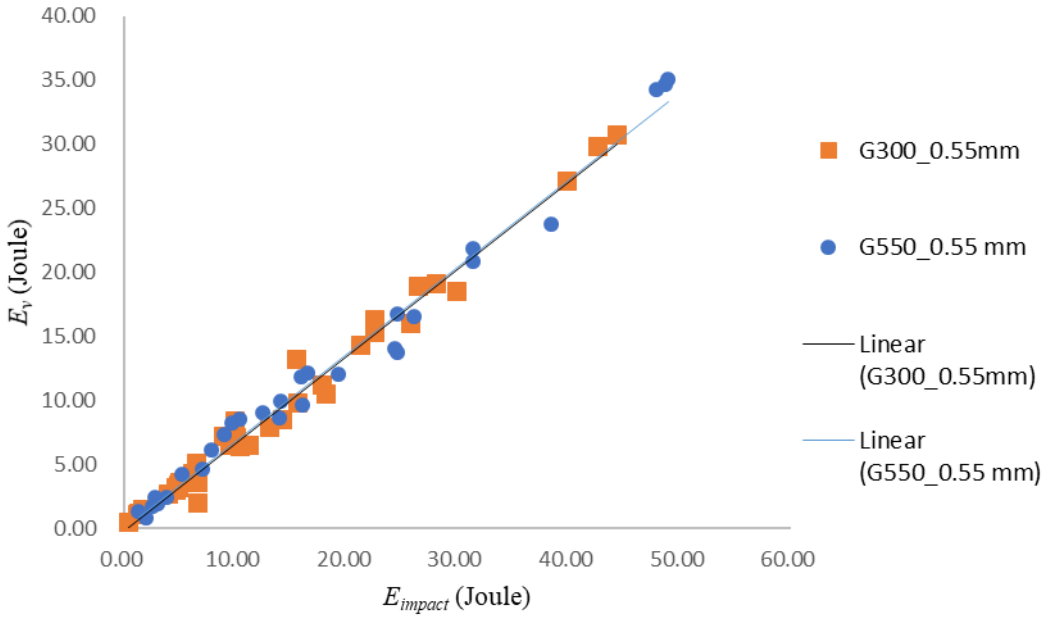

Figure 4.3: 'E_v' vs 'E_{impact}' for two grades of 0.55-mm thick steel sheets

The other form of energy loss that needs to be considered is the energy dissipated during the flexural vibration of the steel sheet since flexural vibration energy accounts for a significant part in the total energy dissipation (Farin et al. 2016; Hardy et al. 2009; Mei 1973; Venkateswara Rao et al. 1976). The energy conversion is therefore simplified as:

$$E_{impact} = E_p + E_v \qquad \text{Equation 4-2}$$

Equation 4-2 shows that once the flexural vibration energy is determined, the plastic deformation energy and therefore the dent depth can be computed from Equation 5-7 derived in Chapter 5. Future research, therefore, has to determine the amount of energy lost to vibration based on the flexural stiffness of the impacted surface.

Figure 4.3 shows the relationship between the energy dissipated in sheet vibration (E_v) and the impact energy of 0.55-mm thick G550 and G300 steel sheets. The vibration energy E_v in the graph is calculated by subtracting the plastic deformation energy E_p, determined using Equation 5-5 in Chapter 5, from the impact energy E_{impact}, which is the kinetic energy of the projectile defined by Equation 3-1.

Figure 4.3 shows that the vibration energy is linearly proportional to the impact energy, and that less than half of the impact energy is converted into the plastic deformation energy. Based on the graphs shown in Appendix D, it can be also known that the dent depth does not change linearly with the impact energy, especially when the impact energy is large. Therefore, to define the dent resistance of a material for rating purposes, testing conditions must be specified such that the energy lost to flexural vibration is negligible, or is otherwise accounted for.

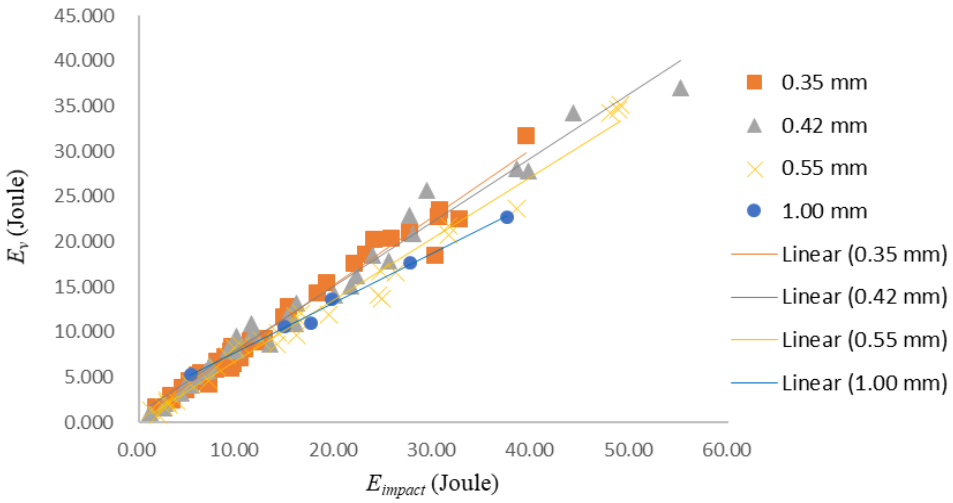

Figure 4.4: 'E_v' vs 'E_{impact}' for different thicknesses of G550 steel sheet

Figure 4.3 also shows that the significantly different yield stresses between the two sheets did not lead to a noticeable difference in the dissipated energy due to sheet vibration. Figure 4.4 shows that the proportion of impact energy dissipated in the form of sheet vibration is larger for the thinner steel sheets. For the 0.35-mm thick steel sheet more than seventy percent of the impact energy is converted into the vibration energy, while for the 1.00-mm thick steel sheet, only around fifty-five percent of the impact energy is converted into the vibration energy.

Therefore, it can be concluded that the dissipated energy due to sheet vibration changes with sheet thickness, but is independent of the yield stress of steel sheet. From these two graphs, it is also known that it is not feasible to compute the dent depth based on the momentum as this approach would not account for the different levels of energy lost between sheets of different geometry. For example, there will be much less flexural vibration energy in corrugated sheets.

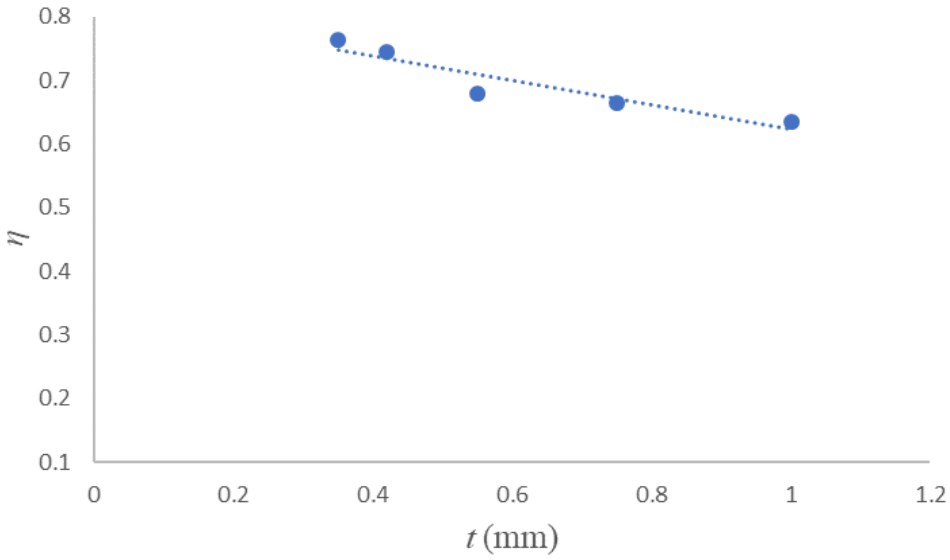

Figure 4.5: Effect of thickness on the elastic ratio, η

The energy dissipated due to the vibration of the steel sheet can be expressed as:

$$E_v = \eta E_{\text{impact}} \qquad \text{Equation 4-3}$$

where η is termed the elastic ratio in the present work. Based on the test results shown in Appendix F, the elastic ratio η is plotted against the sheet thickness t in Figure 4.5. The graph shows that the elastic ratio η changes rather linearly with the sheet thickness t.

Substituting Equation 4-3 into Equation 4-2, the relationship between the impact energy and the plastic deformation energy becomes:

$$E_{\text{p}} = (1 - \eta)\, E_{\text{impact}} \qquad \text{Equation 4-4}$$

It should be noted that Equation 4-4 is only suitable for relatively large impact energy such as that due to a hailstone travelling at the terminal velocity. When the impact energy is too low, the majority of the impact energy is converted into the sheet vibration energy, the rebound

energy, sound and heat. In any case, Equation 4-4 is supported by the test results of 0.55-mm G550 sheeting plotted in Figure 4.6. The plastic deformation energy E_p is determined from the measured dent depths using Equation 5-5 derived in Chapter 5.

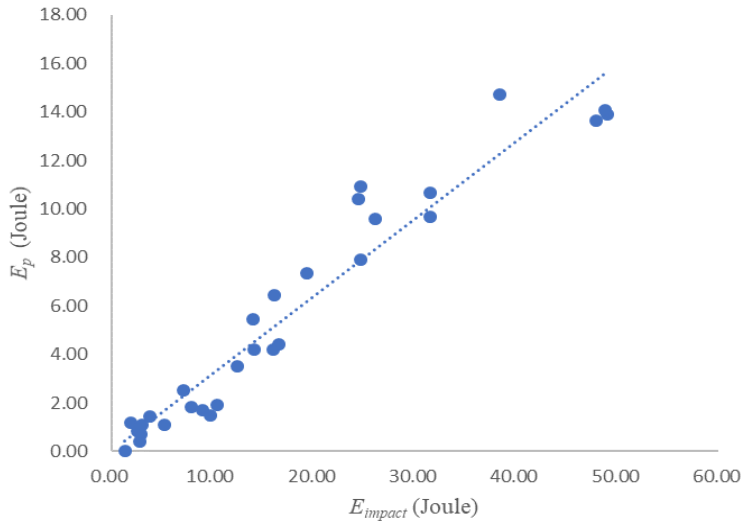

Figure 4.6: Relationship between the plastic deformation energy E_p and the impact energy E_{impact} (G550-0.55 mm steel sheet)

4.3.3 Effects of yield stress and sheet thickness on dent depth

The definition of the dynamic dent resistance D_r in Equation 2-1, proposed by Johnson and Schaffnit (1973), suggests that the relationship between the dent depth, the impact energy and the dent resistance can be represented graphically by Figure 4.7. Based on the equation, for a given impact energy and a given dent resistance (which is a function of the sheet thickness and yield stress), the dent depth can be determined from the graph.

In the present study, five different thicknesses of steel sheets of two different grades were tested to determine the effects of yield stress and sheet thickness on dent depth. Johnson and Schaffnit (1973) suggested that the dent resistance defined in Equation 2-1 was linearly proportional to the square of the sheet thickness. However, from Figure 4.8, it can be seen that the relationship determined by Johnson and Schaffnit (1973) is not applicable to the present experimental results as there is no common gradient between the different steel sheets. It should be noted that the horizontal axis does not represent the impact energy (and the 0.55-mm and 1.0-mm sheets comprised G300 and G550 grades), otherwise the steeper gradients of the thicker sheets would have made sense. In addition, it can be seen that, within a given sheet thickness, say for the

0.35 mm sheet (which was of grade G300), there is no consistent trend in the relationship between the dent depth and the square of the sheet thickness.

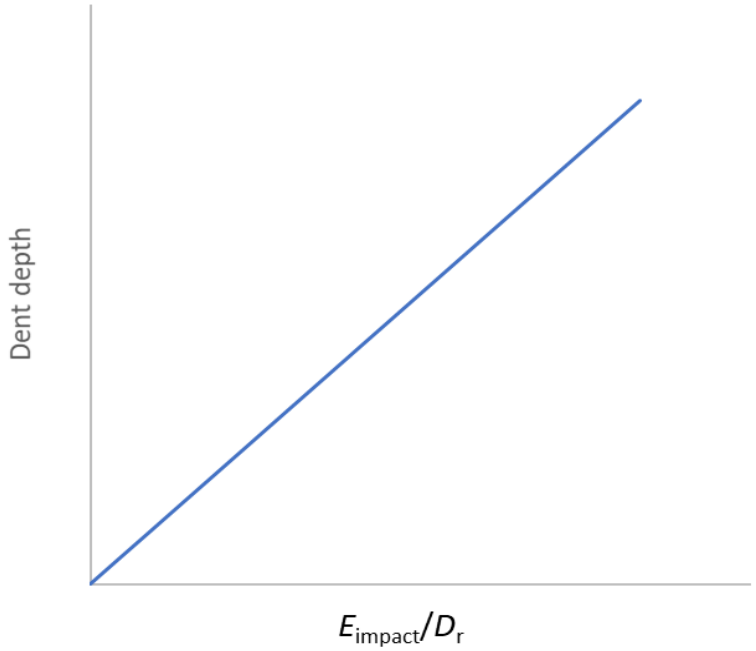

Figure 4.7: 'Dent depth *D'* vs 'E_{impact}/D_r' based on Equation 2-1 (Johnson and Schaffnit 1973)

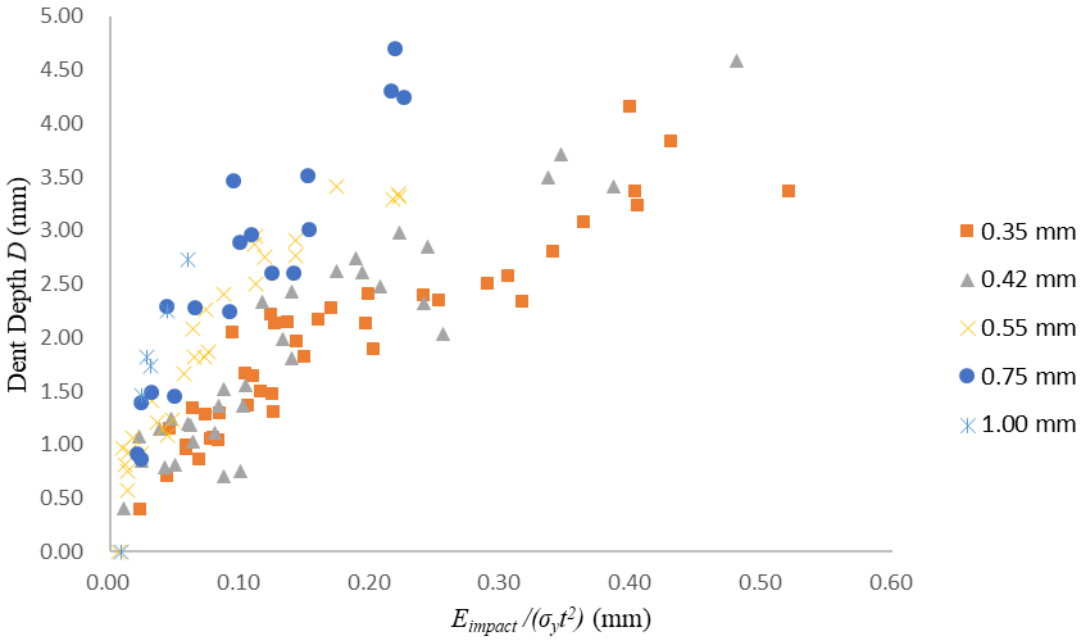

Figure 4.8: 'Dent Depth *D*' vs '$E_{impact}/(\sigma_y t^2)$'

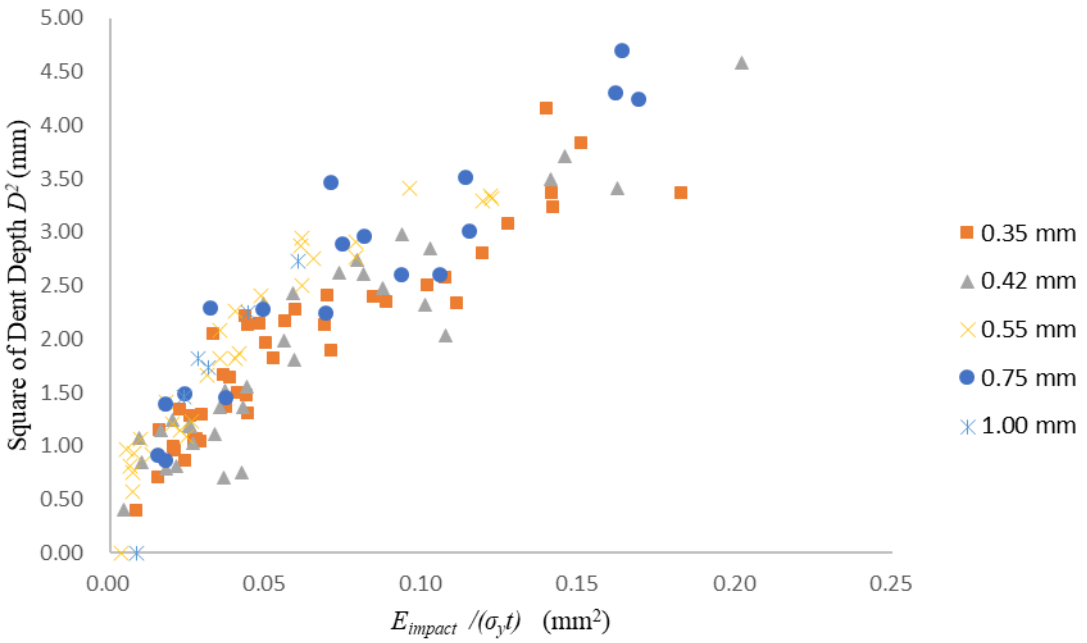

Figure 4.9: 'Square of Dent Depth D^2' vs 'E_{impact} /($\sigma_y t$)' for different thickness of steel sheets

Figure 4.9 plots the square of the dent depth D^2 against '$E_{impact}/(\sigma_y t)$' for the different steel sheets. The graph shows that there is a common gradient between the steel sheets of varying thicknesses and yield stresses, indicating that the square of the dent depth is linearly proportional to the impact energy and inversely proportional to the yield stress and the sheet thickness. In other words, the dent depth is inversely proportional to the square roots of the yield stress and the sheet thickness.

As an aside, the preceding paragraph indicates that the dent resistance defined in Equation 2-1 is not appropriate since the dent depth does not vary linearly with the impact energy. It may be noted that the present indication concerning the relationship between the dent depth and the impact energy is consistent with the finding of Worswick et al. (1997) and Pernas-Sánchez et al. (2016).

4.4 Concluding remarks

The present water based artificial hailstones, which are made with 12% PVA, have been validated against the test results of pure clear ice balls having the same diameter that happened to remain intact after impacting 0.35-mm G550 steel sheet at velocities around 30 m/s. It can be concluded that the inclusion of 12% PVA did not affect the dent depth noticeably, while

enabling the artificial hailstones to remain intact at higher impact velocities and on thicker steel sheets commonly used for steel roofing.

The manual and the digital methods of measuring the dent depth mostly gave readings within 5% of each other. However, the manual method using a depth gauge was more prone to human errors. It is recommended that dent depth measurements are performed digitally using 3D scanning in order to ensure consistent accuracy.

An artificial hailstone that remains intact after impact will cause a significantly larger dent compared to one that shatters. All other things being equal, the dent depth caused by the former is often about 25% greater than that caused by the latter. However, for some unexplained reasons, the difference can be even greater if the impact energy of the shattered artificial hailstone is higher than that of the intact one. In any case, for the purpose of developing hail-proof steel roofing, it is important to use artificial hailstones that remain intact after impact since not all natural hailstones shatter on impact.

Almost all of the impact energy of the present artificial hailstones was converted to the flexural vibration energy of the flat sheeting and the plastic deformation energy, with little amount lost to the rebound energy of the projectiles, sound and heat. Each of the flexural vibration energy and the plastic deformation energy of the dented steel sheet has an approximately linear relationship with the impact energy of the artificial hailstone. If the flexural vibration energy of an impacted sheeting can be determined based on its thickness and its span, which affect its flexural stiffness, then the plastic deformation energy and therefore the dent size can be determined for a given impact energy.

The present test results indicate that the dent depth is proportional to the square root of the impact energy, and is inversely proportional to the square roots of the yield stress and the sheet thickness.

Chapter 5 Empirical Equation for Estimating Dent Depth

5.1 Introductory Remarks

This chapter provides an empirical equation for estimating the dent depth caused by an intact hailstone on a flat steel sheet that is screwed to timber battens spaced at 600 mm from each other. The equation is intended for cases where the hailstone travels at a velocity ranging from 20 m/s to 40 m/s. In order to derive the empirical equation, a simplifying assumption is made in Section 5.2. In Section 5.3, the empirical equation is derived by relating the plastic deformation energy to the impact energy and by accounting for the effect of sheet thickness on the energy loss due to flexural vibration as described in Section 4.4.

5.2 A Theoretical Assumption for Estimating Dent Depth

As discussed in Section 4.4.2, the impact energy E_{impact} of a hailstone travelling at a velocity ranging from 20 m/s to 40 m/s and impacting a flat steel sheeting screwed to battens spaced at 600 mm from each other is mainly converted to the flexural vibration energy E_{v} and the plastic deformation energy E_{p}. The plastic deformation energy E_{p} can be determined as

$$E_p = \sigma_y t \Delta A \qquad \text{Equation 5-1}$$

where ΔA is the increase in the dented area due to the hail impact, σ_y is the yield stress of steel sheet, and t is the sheet thickness.

Figure 5.1 through Figure 5.3 show that the shapes of the dents are not perfectly round, and that the deformed area can be larger than the diameter of the artificial hailstone. Therefore, it is difficult to determine the change in the yielded area ΔA accurately.

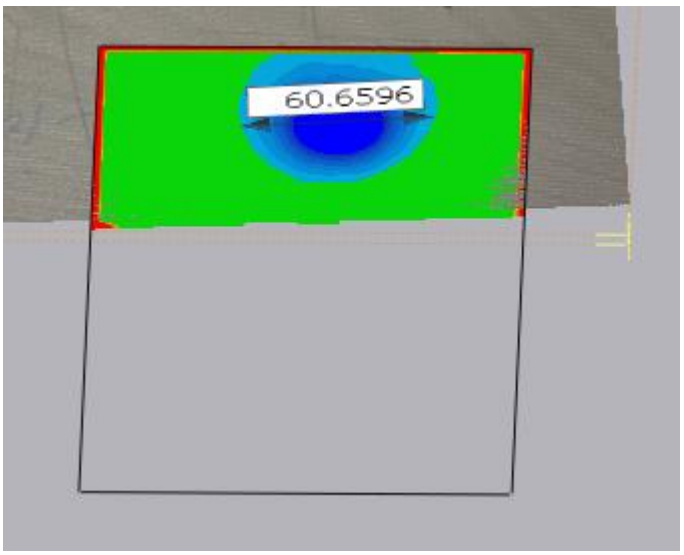

Figure 5.1: Measurement of the dent diameter (G550_0.35 mm-50-10-2)

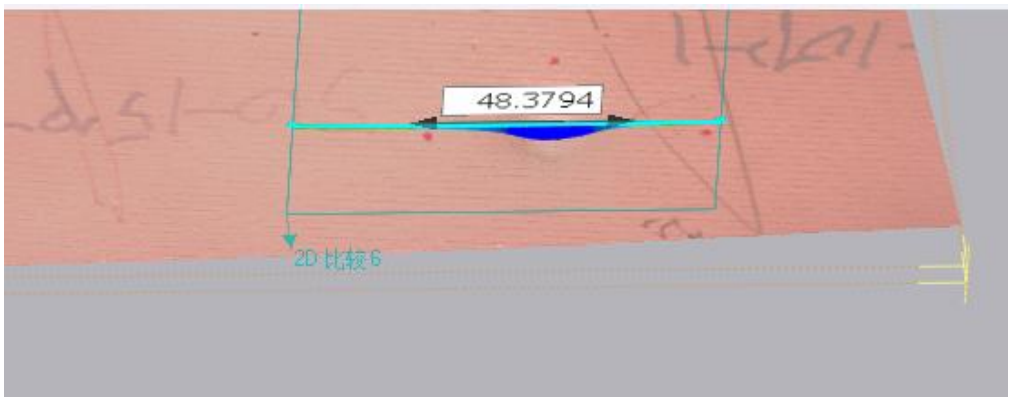

Figure 5.2: Measurement of the dent diameter (G550_0.35 mm-50-15-2)

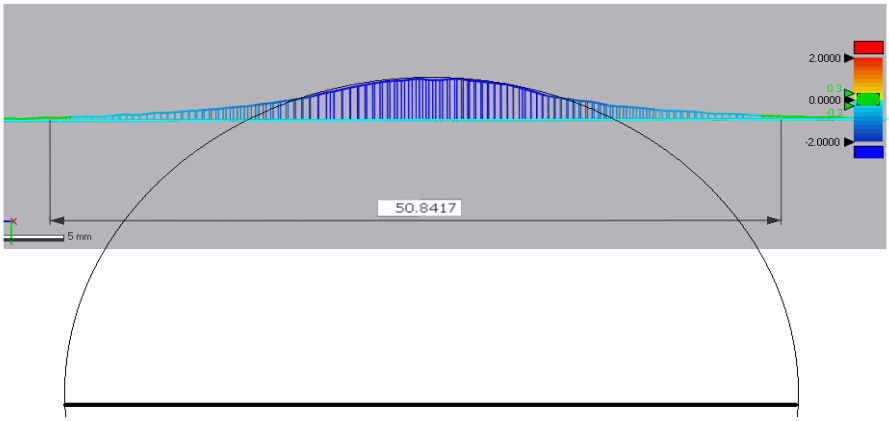

2R

Figure 5.3: Dent depth and dent diameter analysis (G550_0.35 mm-50-10-1)

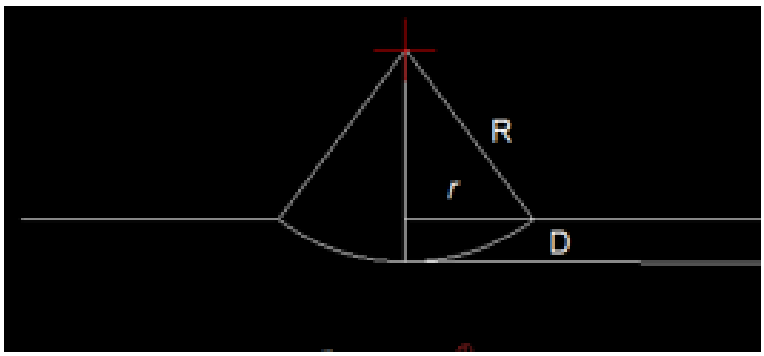

Figure 5.4: The cross section of a simplified dent

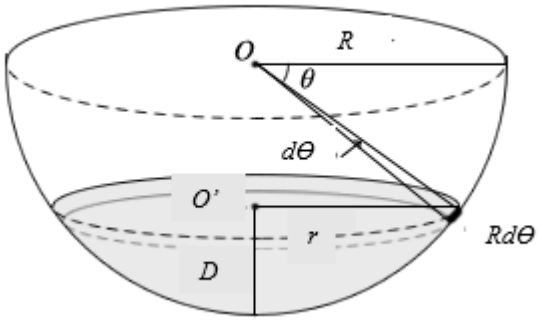

Figure 5.5: Geometric variables of a simplified dent

Since the major consideration of the present work is to predict the dent depth caused by hailstone impact and the deformation at the edge of the dent is relatively small, the dent shape is assumed to be (partly) spherical, as shown in Figure 5.4 and Figure 5.5. The radius of the dented area before the impact is denoted *r*, the radius of the artificial hailstone is *R*, and the dent depth is *D*. Under this assumption, the original dent area and the deformed area can be calculated from the diameter of the artificial hailstone and the dent depth.

The original dent area before the impact is determined as follows:

$$A_0 = \pi r^2$$

$$A_0 = \pi(R^2 - (R - D)^2)$$

$$A_0 = \pi(2RD - D^2) \qquad \text{Equation 5-2}$$

In Figure 5.5, the deformed area after the impact is shaded grey, and the area can be determined as follows:

$$A_f = \int_{\theta}^{\frac{\pi}{2}} 2\pi r R d\theta$$

$$A_f = \int_{\theta}^{\frac{\pi}{2}} 2\pi R^2 \cos\theta \, d\theta$$

$$A_f = 2\pi R^2 (1 - \sin\theta)$$

$$A_f = 2\pi RD \qquad \text{Equation 5-3}$$

The increase in the dented area is therefore:

$$\Delta A = A_f - A_0 = \pi D^2 \qquad \text{Equation 5-4}$$

which implies that the change in the dented area and therefore the plastic deformation energy is independent of the projectile's diameter.

Substituting Equation 5-4 into Equation 5-1:

$$E_p = \pi D^2 \sigma_y t \qquad \text{Equation 5-5}$$

$$D^2 = \frac{E_p}{\pi \sigma_y t} \qquad \text{Equation 5-6}$$

$$D = \sqrt{\frac{E_p}{\pi \sigma_y t}} \qquad \text{Equation 5-7}$$

Equation 5-6 (and therefore Equation 5-7) is consistent with the experimental results discussed in Section 4.4.3 and shown in Figure 4.9 since the plastic deformation energy E_p is proportional to the impact energy E_{impact}, vindicating the present assumption shown in Figure 5.4 and Figure 5.5.

5.3 Equation Derivation and Verification

The relationship between the impact energy of the projectile and the plastic deformation energy of the impacted panel was often determined using the coefficient of restitution between the projectile and the impacted panel (Goldsmith 2001; Hunter 1957; Kharaz & Gorham 2000; Koller & Kolsky 1987; Reed 1985). However, all these studies used thick plates as the test specimens, with which the projectiles had relatively high coefficients of restitution. In the

present hail impact tests, the thickest steel sheet was only 1.00 mm, much thinner than the plates used by the cited researchers. It has been shown in Section 4.4.2 that, for each of the tested panels, which was a flat steel sheet screwed to battens spaced at 600 mm from each other and shot at the middle, the impact energy of the artificial hailstone was almost wholly converted to the flexural vibration energy and the plastic deformation energy of the panel.

It has also been shown in Figure 4.5 that the elastic ratio η changes linearly with the sheet thickness (in millimetres):

$$\eta = -0.193t + 0.82 \qquad \text{Equation 5-8}$$

The elastic ratio η is of course dimensionless. Considering that the elastic flexural stiffness of a flat sheet is proportional to the cube of the sheet thickness but is inversely proportional to the cube of the spacing between its supports, the elastic ratio η can be rewritten as follows:

$$\eta = -\frac{115.8t}{l} + 0.82 \qquad \text{Equation 5-9}$$

in which l is the spacing between the battens. In deriving Equation 5-9, the fact that the spacing between the battens in the present work is 600 mm has been taken into account.

Substituting Equation 5-9 into Equation 4-4, the plastic deformation energy can be determined as follows:

$$E_p = (\frac{115.8t}{l} + 0.18)E_{impact} \qquad \text{Equation 5-10}$$

Substituting Equation 5-10 into Equation 5-7, the dent depth can be estimated as follows:

$$D = \sqrt{\frac{(\frac{115.8t}{l}+0.18)E_{impact}}{\pi\sigma_y t}} \qquad \text{Equation 5-11}$$

Table 5.1: Comparison between the experimental dent depth (d_t) and the estimated dent depth (d_e) excluding the abnormal dents and no denting

	G550				G300		
Thickness (mm)	0.35	0.42	0.55	1.00	0.55	0.75	1.00
Average professional factor	0.94	0.91	1.02	0.96	1.06	0.97	0.95
Coefficient of variation	0.15	0.17	0.14	0.06	0.13	0.15	0.11

Table 5.1 shows the professional factors of Equation 5-11 for all the tested panels. In the present work, a professional factor is a ratio of the test dent depth (d_t) to the estimated dent depth (d_e). The yield stresses used in Equation 5-11 were obtained through the standard coupon tests, as given in Appendix F. Although in general the dynamic yield stress of a given sheet steel increases with the strain rate, in the present case it is not a relevant issue since Equation 5-11 is derived empirically.

As mentioned in Section 4.1, each size of artificial hailstones for each sheet was tested three times for each nominal velocity. In most cases, the actual impact velocity was reasonably close to the target velocity, as approximated using Table 3.3. However, in some cases there were anomalies either in the resulting impact energy (too low) or in the dent size. In the present work, a reading is considered to be an anomaly if it deviates by 30% or more from the target or average value. Such anomalies are excluded from Table 5.1. However, the amount of abnormal data is very limited compared to the total test data (see Appendix C).

In any case, it can be seen in Table 5.1 that the average professional factor for each type of steel sheet is reasonably close to unity, and the coefficients of variation are not excessive except perhaps for 0.42-mm G550 sheeting.

As an aside, it may appear unintuitive to some readers that a smaller (spherical) hailstone will cause the same dent depth if the impact energy is the same as that of the larger hailstone (both remaining intact after impact), since the smaller one could be expected to cause a deeper dent. However, it should be noted that, for the same impact energy the momentum of the smaller hailstone is less than the other.

Figure 5.6 illustrates the theoretical variations of dent depths with sheet thicknesses according to Equation 5-11 for sheeting having battens spaced at various distances, impacted

in the middle region by a 32-mm hailstone travelling at the terminal velocity of 25 m/s. It shows that, for steel roofing, the dent depth always increases with decreasing sheet thickness although a thinner sheet leads to greater energy loss due to flexural vibration, as suggested by Equation 5-9. As an aside, a comparison between the results for l = 500 mm and l = 600 mm in Figure 5.6 indicates that any errors due to the inaccuracy in measuring the present batten spacing, the actual location of hail impact, and/or the number of screws used are insignificant. While this indication is yet to be tested in the laboratory, it is consistent with the finding of Kim et al. (2003) and Olsson (2003).

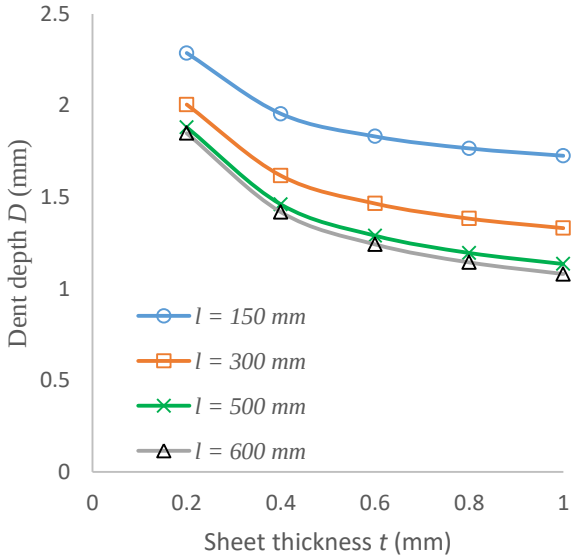

Figure 5.6: Variation of dent depth D against sheet thickness t

5.4 Concluding remarks

This chapter has shown through mathematical derivations that, for a spherical dent, the depth is directly proportional to the square root of the plastic deformation energy, and is inversely proportional to the square root of the yield stress. The dent depth is more or less inversely proportional to the square root of the sheet thickness. The derivation results are consistent with the observations of the test results discussed in Section 4.4.3.

The dent depth is not exactly inversely proportional to the square root of the sheet thickness as a thicker sheet leads to a stiffer sheeting for the same boundary condition, reducing the amount of impact energy lost to flexural vibration.

The definition of a dent resistance proposed by Johnson and Schaffnit (1973) does not appear to be appropriate as it wrongly assumes that the dent depth varies linearly with the impact energy. The present test results and theoretical derivation show that the dent depth is proportional to the square root of the impact energy. Furthermore, while Johnson and Schaffnit (1973) suggested the dent depth to be inversely proportional to the square of the sheet thickness for a given impact energy, the present test results and theoretical derivation indicate a much weaker relationship.

The equation derived in the present work determines the dent depth based on the impact energy, the sheet thickness, the yield stress and the batten spacing. The dent depth is independent of the hailstone's diameter, so a smaller hailstone will cause the same dent depth as a larger one if the impact energy is the same (the former's momentum is smaller). The derived equation is reasonably accurate for estimating the dent depths obtained in the laboratory tests, which involved G300 and G550 steel sheets screwed to timber battens spaced at 600 mm from each other and impacted perpendicularly in the middle region by hailstones having nominal diameters ranging from 25 mm to 50.8 mm travelling at nominal velocities ranging from 20 m/s to 40 m/s.

Chapter 6 Conclusions

6.1 Summary

Hailstone impact on roofing materials has been widely studied due to huge economic losses incurred by hailstorms. Owing to the formation processes of natural hailstones in the atmosphere, some of them do not disintegrate upon impact on steel roof sheeting when they fall to the earth. Such hailstones cause more severe damage compared to those that shatter on impact since energy is lost to shattering the hailstones in the latter case. In the previous research, a variety of artificial hailstones were employed to simulate natural hailstones, such as steel ball or indenter; ice balls made from tap water, distilled water, double-boiled de-ionized water, seltzer water, flaked ice, tap water under the application of certain heat and pressure, and flat-wise layer freezing method; polyamide ball and cotton fibre ice ball, as summarised in Table 2.2. As natural hailstones are mainly composed of ice, frozen water based projectiles are believed to be the most suitable artificial hailstone. However, none of the published water based artificial hailstones has been shown to remain intact after impacting steel sheeting at a velocity close to the terminal velocity of the natural hailstone.

In the literature, inconsistent relationships between the incurred dent depth and the steel sheet thickness have been proposed, most likely due to the inconsistent use of projectiles. Some researchers used steel balls or indenters, while others used ice balls that fragmented or shattered upon impacting the tested steel sheets. None of such projectiles can accurately represent the impact of natural hailstones that do not shatter nor fragment upon impact. Also, while some researchers found that the dent depth varied linearly with the impact energy, others found a different relationship. In this thesis, four different basic methods of making water based artificial hailstones were tried, resulting in the layered-structure ice ball (two techniques, the pure clear ice ball (two techniques), the microfibre ice ball, and the PVA (Polyvinyl acetate) ice ball. The preliminary test results showed that only the last one, made of 12% liquid PVA and 88% demineralised water, remained intact after impacting flat steel roof sheeting at a velocity close to or above the terminal velocity of natural hailstones. This PVA ice ball was used as the artificial hailstone in this thesis.

The nominal diameters of the artificial hailstones used in this thesis were 25 mm, 33 mm, 38 mm, 45 mm and 50.8 mm, consistent with the sizes commonly used in the industry standards.

The target velocities for each size were 20 m/s, 30 m/s and 40 m/s, which covers the terminal velocity of the corresponding natural hailstone (some of the tested velocities are lower than the terminal velocity, while others are higher than same). It was found that the larger hailstones were more able to remain intact after impacting the steel sheeting at their corresponding terminal velocities compared to the smaller ones. In the experiment, the impact (and rebound) velocity of an artificial hailstone was measured using a high speed camera, with a correction factor of 0.95 to account for parallax.

The type of water based artificial hailstone used in this thesis, being the PVA ice ball, was validated against the test results of two pure clear ice balls having a diameter of 50.8 mm made by previous researchers that happened to remain intact after impacting a 0.35-mm G550 steel sheet at velocities close to 30 m/s. The dent depths caused by the different types of water based artificial hailstones were very close to each other.

The dent depths caused by the impact of artificial hailstones in the present work were measured manually using a depth gauge and digitally using a 3D scanner. However, only the readings obtained using the latter were used in the analysis as they were found to be more reliable.

It was found that the dent depths caused by the PVA ice balls that remained intact after impact were significantly greater than those caused by the ice balls that disintegrated upon impact. This outcome is obviously due to a significant part of the impact energy being lost to disintegrating the hailstone so that less energy was available to denting the steel sheet.

The effects of the sheet thickness and yield stress on the dent depth was investigated by testing steel sheets having different thicknesses and yield stresses. Two cold-reduced sheet steel grades (G550 and G300 manufactured to AS 1397-2011) and five thicknesses (0.35 mm, 0.42 mm, 0.55 mm, 0.75 mm, 1.00 mm) were selected.

The rebound energy of intact hailstones shot perpendicularly at the sheeting was found to be typically less than 1% of the impact energy, and was therefore ignored in the analysis of the test results. More than half of the impact energy of an artificial hailstone was lost to flexural vibration of the steel sheeting, which was screwed to timber battens spaced at 600 mm from each other. Provided that denting took place, the energy lost to flexural vibration was found to be a function of the elastic flexural stiffness of the steel sheeting, and varied linearly with the

impact energy. The plastic deformation energy stored in a dent can therefore be considered to be linearly proportional to the impact energy.

By plotting the dent depths obtained in the present experiment against the corresponding impact energy, sheet thickness and yield stress, it was found that the dent depth varied linearly with the square root of the impact energy, and was inversely proportional to the square roots of the sheet thickness and the yield stress. The present finding regarding the relationship between the dent depth and the impact energy is consistent with the finding of Worswick et al. (1997) and Pernas-Sánchez et al. (2016). However, the relationships between the dent depth on one hand and the sheet thickness and the yield stress on the other, obtained in the present experimental program, are believed to be new.

The experimental observations described in the preceding paragraph support the theoretical assumption employed in this thesis in deriving the theoretical relationships between the dent depth on one hand and the impact energy, the sheet thickness and the yield stress on the other. The resulting theoretical relationships (Equation 5-7), based on the assumption that the dent shape is (partly) spherical, match the experimental findings.

An empirical equation was derived in Section 5.3 (Equation 5-9) to determine the proportion of impact energy that was lost to flexural vibration of the steel sheeting, based on the sheet thickness and the spacing between the battens. It was observed that the proportion decreases linearly with the thickness of the steel sheetings tested in the experimental program, which were screwed to timber battens spaced at 600 mm from each other. Since the sheet thickness and the batten spacing (sheeting span) have the same order of effects (but opposite) on the elastic flexural stiffness of the sheeting, the empirical expression for the elastic ratio relating the flexural vibration energy to the impact energy is dimensionless.

The present experimental and theoretical findings, which are consistent with each other, that the dent depth of a flat steel roofing sheet caused by a hailstone impact is inversely proportional to the square roots of the sheet thickness and the yield stress, are believed to be new.

6.2 Recommendations for Future Work

This thesis only covers the effects of hailstone impact on flat steel roofing sheets, and ignores the effects of global curvature and/or corrugation. Since in practice steel roofing sheets are often

curved and/or corrugated, future experimental programs on the research topic should include the effects of curvature and/or corrugation as they affect the elastic flexural stiffness of the sheeting and therefore the proportion of energy lost to flexural vibration. In addition, the empirical equation derived in this thesis for determining the aforementioned proportion should be verified against flat steel sheeting having spans other than 600 mm.

An alternative to future experimental tests is numerical simulations that have been validated against the present experimental tests. A validated numerical method is not only more economical, but is also easier to control as the hailstone can be guaranteed to impact the sheeting at a particular location.

It may also be worthwhile for future research on the topic to include hailstone impacts that are not perpendicular to the plane of the steel sheet, as natural hailstorms normally impact roofs (and walls) in this manner. However, it is believed that the present experiment represents the most severe case for a given impact energy of the hailstone (which may be due to a combination of the terminal velocity under gravity and the wind speed).

For the purpose of industry rating of steel roofing materials, it will be beneficial if an artificial hailstone that is not water based is used. However, such an artificial hailstone should be validated or calibrated against the present test results. While this thesis has found that the dent depth can be computed without any reference to the water based hailstone's diameter (due to the interaction of the diameter and the impact momentum), the finding may not be necessarily true for projectiles composed of other materials. It is desirable that the non-water based artificial hailstone causes the same dent depth in a given sheeting as the present artificial hailstone for the same impact energy and the same diameter.

Using a high speed camera to measure the impact velocity of an artificial hailstone is time-consuming and is subject to human errors. Preliminary tests by the author involving corrugated sheets (presented in Appendix G) have shown that the rebound energy of a hailstone impacting steel roof sheeting is negligible, and that a laser based chronograph is a very convenient and accurate method for measuring the impact velocity. It is recommended that the laser based chronograph be used in the future for measuring the impact velocity of a hailstone.

References

Alaniz, C., Brookes, L. and Seel, T. (1990) *Investigation of body panel stiffness as predicted by finite element analysis*. SAE technical paper, Society of Automotive Engineers.

Allaby, M. and Garratt, R. (2014) Hail, Sleet, Snow. In: *Blizzards.* Facts On File, New York, pp. 85-92.

Andrew, H. and Robert, W. (2014) Graupel and hail terminal velocities: Does a "Supercritical" Reynolds Number Apply? *Journal of the Atmospheric Sciences.* 71(9), pp. 3392-3403.

ANSI (2011) ANSI FM 4473. *Test standard for impact resistance testing of rigid roofing materials by impacting with freezer ice ball*. American Natioanl Standards Institute, Norwood, MA. ANSI.

ASTM (2008) ASTM:D3746-85. *Standard test method for impact resistance of bitumious roofing system*. West Conshohocken, PA. ASTM International.

ASTM (2009) ASTM:E822-92. *Standard practice for determining resistance of solar collector covers to hail by impact with propelled ice ball*. West Conshohocken, PA. ASTM International.

ASTM (2004) ASTM:E1038-98. *Standard test method for determining resistance of photovoltaic modules to hail by impact with propelled ice balls*. West Conshohocken, PA. ASTM International.

ASTM (2010) ASTM:F320-10. *Standard test method for hail impact resistance of aerospace transparent enclosures*. West Conshohocken, PA. ASTM International.

Australian Building Codes Board (2010) *An investigation of possible building code of Australia (BCA) adaptation measures for climate change*. Australian Building Codes Board.

BlueScope (2013) *Impact of hail damage to COLORBOND steel and ZINCALUME steel roofing*. Technical Bulletin.

BlueScope (2014) *Builder's guide to Australian steel sheet and strip standards*. Technical Bulletin.

Brown, T. M., Pogorzelski, W. H. and Giammanco, I. M. (2015) Evaluating hail damage using property insurance claims data. *Weather, Climate & Society.* 7(3), pp. 197-210.

Cheng, N.-S. (2009) Comparison of formulas for drag coefficient and settling velocity of spherical particles. *Powder Technology.* 189(3), pp. 395-398.

Chisholm, A. J., and English, M. (1973) "Alberta hailstorms," Meteorological Monographs, 14 (36).

Combescure, A., Chuzel-Marmot, Y. and Fabis, J. (2011) Experimental study of high-velocity impact and fracture of ice. *International Journal of Solids and Structures.* 48(20), pp. 2779-2790.

Crenshaw, V. and Koontz, J. D. (2001) Simulated hail damage and impact resistance test procedures for roof coverings and membranes. *RCI Interface.* 19(5), pp. 5-10.

Crompton, R. P. and McAneney, K. J. (2008) Normalised Australian insured losses from meteorological hazards: 1967–2006. *Environmental Science & Policy.* 11(5), pp. 371-378.

DiCello, J. and George, R. (1974) *Design criteria for the dent resistance of auto body panels*. SAE technical paper, Society of Automotive Engineers.

DiCostanzo, G., Matlock, D. and Foley, R. (1996) *Effect of tensile properties on dent resistance of sheet steels*. SAE technical paper, Society of Automotive Engineers.

Dunlop, S. (2008) *A Dictionary of Weather.* New York. Oxford University Press. Available from: https://books.google.com.au/books?id=27DdCC-nSCEC&pg=PT204&dq=A+dictionary+of+weather+hailstone&hl=en&sa=X&redir_esc=y#v=onepage&q=A%20dictionary%20of%20weather%20hailstone&f=false [Accessed 18th March 2016].

Eichner, J. (2017) *Natural disasters in Australia and New Zealand – Expect the unexpected.* Severe convective storms and hail - Icy cricket balls from above. Munich RE. Available from: https://www.munichre.com/site/australia-hazards/get/documents_E-166132984/mr/Australia-Hazards/documents/Downloads/MR-Australia-Hailstorms.pdf [Accessed 13th April 2017].

Ekstrand, G. and Asnafi, N. (1998) On testing of the stiffness and the dent resistance of autobody panels. *Materials & Design.* 19(4), pp. 145-156.

Farin, M., Mangeney, A., Rosny, J. d., Toussaint, R., Sainte-Marie, J. and Shapiro, N. M. (2016) Experimental validation of theoretical methods to estimate the energy radiated by elastic waves during an impact. *Journal of Sound and Vibration.* 362, pp. 176-202.

Flüeler, P., Stucki, M., Guastala, F. and Egli, T. (2008) Hail impact resistance of building materials testing, evaluation and classification. In: *11DBMC International Conference on Durability of Building Materials and Components.* Istanbul. Istanbul Technical University, Istanbul.

Giammanco, I. M. and Brown, T. M. (2014) Observations of Hailstone Characteristics in Multicell and Supercell Thunderstorms. In: *94th American Meteorological Society Annual Meeting*. Atlanta, GA.

Giammanco, I. M., Brown, T. M., Kumjian, M. R. and Heymsfield, A. J. (2014) Observations of hailstone sizes and shapes from the IBHS hail measurement program: 2012-2014. In: *American Meteorological Society 27th Conference on Severe Local Storms*. Madison, WI. American Meteorological Society.

Gold, L. W. (2004) Building ships from ice: Habbakuk and after. *Interdisciplinary Science Reviews.* 29(4), pp. 373-384.

Goldsmith, W. (2001) Results of Impact Experiments. In: *Impact, The theory and physical behaviour of colliding solids.* London, Edward Arnold Publishers. pp. 249-296.

Greenfeld, S. H. (1969) *Hail resistance of roofing products*. National Bureau of Standards, NBS 23.

Guégan, P., Othman, R., Lebreton, D., Pasco, F., Villedieu, P., Meyssonnier, J. and Wintenberger, S. (2011) Critical impact velocity for ice fragmentation. *Proceedings of the Institution of Mechanical Engineers, Part C: Journal of Mechanical Engineering Science.* 226(7), pp. 1677-1682.

Hardy, P., Ichchou, M., Jézéquel, L. and Trentin, D. (2009) A hybrid local energy formulation for plates mid-frequency flexural vibrations. *European Journal of Mechanics - A/Solids.* 28(1), pp. 121-130.

Hile, K. (2009) Clouds and Precipitation. In: *The Handy Weather Answer Book.* The United States of America, Visible Ink Press. pp. 83-117.

Holmberg, S. and Thilderkvist, P. (2002) Influence of material properties and stamping conditions on the stiffness and static dent resistance of automotive panels. *Materials & Design.* 23(8), pp. 681-691.

Hongzhou, L., Mingtu, M., Jianghai, Y. and Zhigang, L. (2009) Dent Resistance for Automobile Body Panels. *Chinese Journal of Mechanical Engineering.* 22(6).

Hunter, S. C. (1957) Energy absorbed by elastic waves during impact. *Journal of the Mechanics and Physics of Solids.* 5(3), pp. 162-171.

IBHS (2013) *IBHS Hailstorm Demonstration Results*. The Insurance Institute for Business & Home Safety.

IBHS (2015a) *Disaster Safety Review*. The Insurance Institute for Business & Home Safety.

IBHS (2015b) *Research to Operations: A Hail Detection Network*. Insurance Institute for business & Home Safety. Available from: https://disastersafety.org/hail/ibhs-hail-field-studies/. [Accessed 13th April 2016].

IBHS (2017) *3D scanner-2017 IBHS hail field study.* Available from: https://disastersafety.org/ibhs-blog/3d-scanner-2017-ibhs-hail-field-study/. [Accessed 13th April 2017].

Johnson, T. E. and Schaffnit, W. O. (1973) *Dent resistance of cold-rolled low-carbon steel sheet*. SAE Technical Paper, Society of Automotive Engineers.

Jung, D.-W. and Worswick, M. (2004) A parameter study for static and dynamic denting. *KSME International Journal.* 18(11), pp. 2009-2020.

Kassar, M., and Yu, W.W. (1991) Effect of strain rate on material properties of sheet steels. *Journal of Structural Engineer.* 118(11), pp. 3136-3150.

Kharaz, A. H. and Gorham, D. A. (2000) A study of the restitution coefficient in elastic-plastic impact. *Philosophical Magazine Letters.* 80(8), pp. 549-559.

Kim, H. and Kedward, K. T. (1999) Experimental measurement and numerical prediction of hail ice impact damage on composite panels. In: *International Committee on Composite Materials 12 Conference, Paris.* Paris, ICCM Conferences.

Kim, H., Nightingale, J. and Park, H. (2008) Impact damage resistance of composite panels impacted by cotton-filled and unfilled ice. In: *16th International Conference on Composite Materials.* Kyoto, ICCM-16.

Kim, H., Welch, D. A. and Kedward, K. T. (2003) Experimental investigation of high velocity ice impacts on woven carbon/epoxy composite panels. *Composites Part A: Applied Science and Manufacturing.* 34(1), pp. 25-41.

Knight, N. C. (1986) Hailstone shape factor and its relation to radar interpretation of hail. *Journal of Climate and Applied Meteorology.* 25(12), pp. 1956-1958.

Koller, M. G. and Kolsky, H. (1987) Waves produced by the elastic impact of spheres on thick plates. *International Journal of Solids and Structures.* 23(10), pp. 1387-1400.

Krupitzer, R. P. and Harris, R. P. (1992) *Improvements in the dent resistance of steel body panels*. SAE Technical Paper, Society of Automotive Engineers.

Laurie, J. (1960) *Hail and its Effects on Buildings.* Council for Scientific and Industrial Research.

Lavoie, M.-A., Nejad Ensan, M. and Gakwaya, A. (2011) Development of an efficient numerical model for hail impact simulation based on experimental data obtained from pressure sensitive film. *Mechanics Research Communications.* 38(1), pp. 72-76.

Liang, M. (2015) *Experimental investigation, development and optimisation of steel roof sheeting against the effect of hail impact.* Bachelor Thesis, Bachelor of Engineering, University of Wollongong.

Luong, S. D. (2014) *Hail Ice Impact of Lightweight Composite Sandwich Panels.* Master thesis, Master of Science in Structural Engineering, University of California, San Diego. UC San Diego Electronic Theses and Dissertations.

Manikandan, G., Verma, R. K., Lansbergen, M., Raj, A. and Deshpande, D. (2015) Effect of Yield Strength, Pre-strain, and Curvature on Stiffness and Static Dent Resistance of Formed Panel. *Advances in Material Forming and Joining*: Springer. pp. 47-59.

Marco, A., L., C. L.-M., Fabio, I. and Marco, M. (2005) A survey of numerical models for hail impact analysis using explicit finite element codes. *International Journal of Impact Engineering.* 31(8), pp. 929-944.

Marzbanrad, J. (2007) Thickness and material yield strength effects of thin sheets on dent resistance. *Wseas Transactions on Applied and Theoretical Mechanics.* 2(6), pp. 127-131.

McCormick, M., Fekete, J., Meuleman, D. and Shi, M. (1998) *Effect of steel strengthening mechanisms on dent resistance of automotive body panels*. SAE Technical Paper, Society of Automotive Engineers.

Mei, C. (1973) Finite element displacement method for large amplitude free flexural vibrations of beams and plates. *Computers & Structures.* 3(1), pp. 163-174.

Michaud, A. B., Dore, J. E., Leslie, D., Berry, W., Sands, D. C. and Priscu, J. C. (2014) Biological ice nucleation initiates hailstone formation. *Journal of Geophysical Research: Atmospheres.* 119(21), pp. 12,186-12,197.

Moore, D. M. and Wilson, A. (1978) *Photovoltaic solar panel resistance to simulated hail*. California Institute of Technology Pasadena, California. Available from: https://www2.jpl.nasa.gov/adv_tech/photovol/ppr_75-80/PV%20Panel%20Resistance%20to%20Hail_5101-62_JPL1978.pdf. [Accessed 15th April 2016].

Niemeier, B. A. and Reynolds, C. E. B. (1978) *Hailstone Response of Body Panels-Real and Simulated*. SAE Technical Paper, Society of Automotive Engineers.

Nomura, S., Yutori, Y., Iwaya, J., Miyahara, M. and Kokubo, I. (1984) A study of the dynamic dent resistance. In: *13th. Biennial Congress International Deep Drawing Research Group-Efficiency in Sheet Mental Forming*. Melbourn. pp. 394-402.

Oard, M. (2015) Dangerous Thunderstorm. In: *The new weather book.* New Leaf Publishing Group. pp. 40-52.

Olsson, R. (2003) Closed form prediction of peak load and delamination onset under small mass impact. *Composite Structures.* 59(3), pp. 341-349.

Olsson, R., Donadon, M. V. and Falzon, B. G. (2006) Delamination threshold load for dynamic impact on plates. *International Journal of Solids and Structures.* 43(10), pp. 3124-3141.

Pan, C. L., Wu, S., and Yu, W. W. (2000) Strain rate and aging effect on the mechanical properties of sheet steels. *Thin-Walled Structures*. 39, pp 429-444.

Paterson, D. A. and Sankaran, R. (1994) Hail impact on building envelopes. *Journal of Wind Engineering and Industrial Aerodynamics.* 53(1), pp. 229-246.

Patil, D. and Higgs III, C. F. (2016) Critical plate thickness for energy dissipation during sphere-plate elastoplastic impact involving flexural vibrations. *Journal of Tribology*. 139(4).

Pernas-Sánchez, J., Artero-Guerrero, J. A., Varas, D. and López-Puente, J. (2016) Experimental analysis of ice sphere impacts on unidirectional carbon/epoxy laminates, *International Journal of Impact Engineering.* 96, pp. 1-10.

Petty, S. E. (2013) Hail damage and general hail-strike damage assessment methodology. In: *Forensic Engineering: Damage Assessments for Residential and Commercial Structures.* Florida. CRC Press, pp. 23-69.

Pimpasakdi, S., Albermani, F. and Kitipornchai, S. (2004) Interactive analysis and design of cold-formed steel cladding system. *Journal of Constructional Steel Research.* 60(10), pp. 1409-1423.

Prato, A., Anghileri, M., Milanese, A. and Castelletti, L. M. (2015) Soft body impact against aeronautical structures. *International Journal of Engineering Research and Technology*. 3(10), pp. 886-892.

Prodi, F. (1970) Measurements of local density in artificial and natural hailstones. *Journal of Applied Meteorology*. 9(6), pp. 903-910.

Raghavan, K. and Arwashan, N. (1997) *Analysis of quasi-static denting behaviour of automotive sheet steels.* SAE technical paper, Society of Automotive Engineers.

Ramsay, H. (2015) *Experimental investigation, development and optimisation of steel roof sheeting against the effect of hail impact.* Bachelor Thesis, Bachelor of Engineering, University of Wollongong.

Reed, J. (1985) Energy losses due to elastic wave propagation during an elastic impact. *Journal of Physics D: Applied Physics.* 18(12), pp. 2329.

Render, P. and Pan, H. (1995) Experimental studies into hail impact characteristics. *Journal of Propulsion and Power.* 11(6), pp. 1224-1230.

Revolution roofing (2017) *Revolution roofing specifier's manual.* Revolution roofing. Available From: http://www.revolutionroofing.com.au/_literature_136294/REV_SPEC. [Accessed April 2017].

Rusinek, A., Cheriguene, R., Bäumer, A., and Larour, P (2008) Dynamic behaviour of high strength sheet steel in dynamic tension: Experimental and numerical analyses. *The Journal of Strain Analysis for Engineering Design.* pp. 37-53.

Schulson, E. M. (1999) The structure and mechanical behaviour of ice. *JOM.* 51(2), pp. 21-27.

Schulson, E. M. (2001) Brittle failure of ice. *Engineering Fracture Mechanics.* 68(17–18), pp. 1839-1887.

3D Systems (2014) *Geomagic Control brochure*. 3D Systems. Available from: https://www.thinglab.com.au/downloads/geomagic-control-2014-brochure.pdf [Accessed November 2016]

Seel, T. N. (1991*) Bake Hardening steel application study - key factors of dent resistance improvement*. SAE Technical Paper, Society of Automotive Engineers.

Sharafi, P., Teh, L. H. and Hadi, M. N. (2013) Theory based sensitivity analysis and damage detection of steel roof sheeting for hailstone impact. *Topics in Dynamics of Civil Structures.* 4, pp. 243-252.

Shi, M. F., Brindza, J., Michel, P., Bucklin, P., Belanger, P. and Prencipe, J. (1997) *Static and dynamic dent resistance performance of automotive steel body panels*. SAE technical paper, Society of Automotive Engineers.

Shi, M. F., Meuleman, D. J., Alaniz, C. L. and Zurdosky, S. J. (1991) *An evaluation of the dynamic dent resistance of automotive steels*. SAE Technical Paper, Society of Automotive Engineers.

Sodhi, D. S. (2001) Crushing failure during ice–structure interaction. *Engineering Fracture Mechanics.* 68(17–18), pp. 1889-1921.

Standards Australia (2011) AS 1397-2011. *Continuous hot-dip metallic coated steel sheet and strip - Coatings of zinc and zinc alloyed with aluminium and magnesium*. Standards Australia, NSW.

Steeline (2017) *Steeline Metal Roof Battens*. Steeline. Available from: http://www.steel.com.au/products/building-and-construction/products/framing/top-hat-sections/steeline-roof-batten-st44 [Accessed December 2017]

Stratco (2017) *CGI Corrugated Design Guide*. Stracto. Available from: https://s0.yellowpages.com.au/a1ae5f6e-2c2f-4ce3-9ebb-6bdc97b7e4a2/stratco-archerfield-4108-document.pdf [Accessed December 2017]

Sun, J., Lam, N., Zhang, L., Ruan, D. and Gad, E. (2015) Contact forces generated by hailstone impact. *International Journal of Impact Engineering.* 84, pp. 145-158.

Swift, J. M. (2013) *Simulated hail ice mechanical properties and failure mechanisms at quasi-static strain rates.* Master Thesis, Master of Science in Aeronautics and Astronautics, University of Washington. Available from: https://digital.lib.washington.edu/researchworks/handle/1773/22847. [Accessed 15th April 2016].

The Roofing Centre Tasmania. (2017) *Roofing and walling.* Available from: http://www.roofingcentretas.com.au/products/roofing. [Accessed 15th April 2017]

Thomas, D. (2001) *The numerical prediction of panel dent resistance incorporating panel forming strains.* Master Thesis, Master of Applied Science in Mechanical Engineering, University of Waterloo. Uwspace, Waterloo's Institutional Repository.

Tippmann, J. D. (2011) *Development of a strain rate sensitive ice material model for hail ice impact simulation.* Master Thesis. Master of Science in Structural Engineering, University of California, San Diego. UC San Diego Electronic Theses and Dissertations.

Ullrich (2014) *Sheet, plate and rollformed metal products*. Available from: http://www.ullrich.com.au/pdfs/Brochure_pdfs/Sheet-Plate-Rolled-Metal.pdf. [Accessed 25th August 2016].

Underwriters Laboratories (1996) UL:2218. *Impact resistance of prepared roof coverings.* Standard UL 2218.

United States Steel Corporation (2005) *Hail damage on coated sheet steel roofing*. The United States. Steel Technical Bulletin-Construction.

Vadhavkar, A., Fecek, M., Shah, V. and Swenson, W. (1981) *Panel optimisation program (pop)*. SAE Technical Paper, Society of Automotive Engineers.

Veldhuizen, B. v., Kranendonk, W., Ruifrok, R. and BV, H. C. The relation between the curvature of horizontal automotive panels, the panel stiffness and the static dent resistance. In: *Materials & body Testing: Proceedings of the international body engineering conference*. Detroit, Michigan. pp. 62-70.

Venkateswara Rao, G., Raju, I. S. and Kanaka Raju, K. (1976) A finite element formulation for large amplitude flexural vibrations of thin rectangular plates. *Computers & Structures.* 6(3), pp. 163-167.

Vreede, P. T., Tamis, P. J., Roelofsen, M. E. and BV, H. G. (1995) The Influence of Material Properties and Geometry on Dynamic Dent Resistance: Experiments and Simulations. In:

Material & Body Testing: Proceedings of the International Body Engineering Conference. IBEC, Detroit, Michigan. pp, 79-86.

Warner, M. (1993) Finite element simulation of steel body panel performance for quasi-static dent resistance. In: *Proceedings of International Business and Economy Conference*. Automotive Body Materials-IBEC'9.

Worswick, M. J., Finn, M. J. and Thorburn, H. J. (1997) *A numerical study of the geometric and material parameters affecting static and dynamic denting*. Internal Report KR-97/025, Alcan International Limited, Kingston Research and Development Centre.

Youtube (2014) *PBS' This Old House - Hail*. Directed by IBHS. Available from: https://www.youtube.com/watch?v=oy_YWMKXOYs. [Accessed 18th April 2016]

Youtube (2015) *Boston hail storm in slow motion*. Available from: https://www.youtube.com/watch?v=Im5uizDM6B0. [Accessed 15th August 2016].

Youtube (2017) *Massive hail-storm in Kellyville, NSW, Australia*. Available from: https://www.youtube.com/watch?v=ntscfd49OjA. [Accessed 19th February 2017].

Yutori, Y., Nomura, S., Kokubo, I. and Ishigaki, H. (1980) Studies on the static dent resistance. In: Avril (eds.) *Memoires Scientifiques Revue. Metallurgie*. 74, pp. 561-569.

Zhang, Y., Lai, X., Zhu, P. and Wang, W. (2006) Lightweight design of automobile component using high strength steel based on dent resistance. *Materials & Design.* 27(1), pp. 64-68.

Appendix A. Trial methods of making artificial hailstones

Method 1a. Layered-Structure Ice Ball:

1) Prepare a box of dry ice (carbon dioxide).
2) Take a string and dip it into distilled water, then move it along with a water drop at the end to the dry ice box for thirty seconds. The frozen water drop is the 'embryo' of the artificial hailstone. An alternative is to pick a sand or a tiny stone, and attach it to the string to simulate the embryo.
3) Dip the embryo into distilled water then transfer it into the dry ice box for thirty seconds until the water outside the embryo is frozen. Several ice balls may be grown at the same time in the dry box, as shown in Figure A1.
4) Repeat Step 3 until the ice ball grows to the intended size.
5) Cut the string and store the ice ball in a freezer.

Figure A.1: Ice balls in the dry ice box

Method 1b. Layered-Structure Ice Ball (clear outside layer):

1）Cut a small hole in a ping-pong ball without removing the cut parts.

2）Use Method 1a to make a small artificial hailstone that fits into the hole of the ping-pong ball.

3）Insert the artificial hailstone into the ping-pong ball then fill it with distilled water.

4）Use an adhesive tape to stick the cut parts back to the ping-pong ball.

5）Put the ping-pong ball into a freezer for 48 hours.

6）Take the ping-pong ball out of the freezer and carefully peeled off the ping-pong ball.

7）Store the ice ball in the freezer for later use.

Method 2a. Clear ice ball (Luong 2014):

1. Clean the entire surface of both halves of the 3D printed ice mould (see Figure A2) with isopropyl alcohol.
2. Carefully apply petroleum jelly around the circumference of the hemispherical cavity of either half of the mould to facilitate a complete seal, but make sure not to get any in the hemispherical cavity.
3. Boil deionized water for at least 5 minutes to expel the air.
4. Put the two halves together and secure them using the screws.
5. Use a syringe to fill the mould with deionized water until it overflows.
6. Remove excess water off the top surface of the mould.
7. Withdraw a pre-determined amount of water through the fill hole so that the mass of water in the mould is the same as the desired mass of the artificial hailstone.

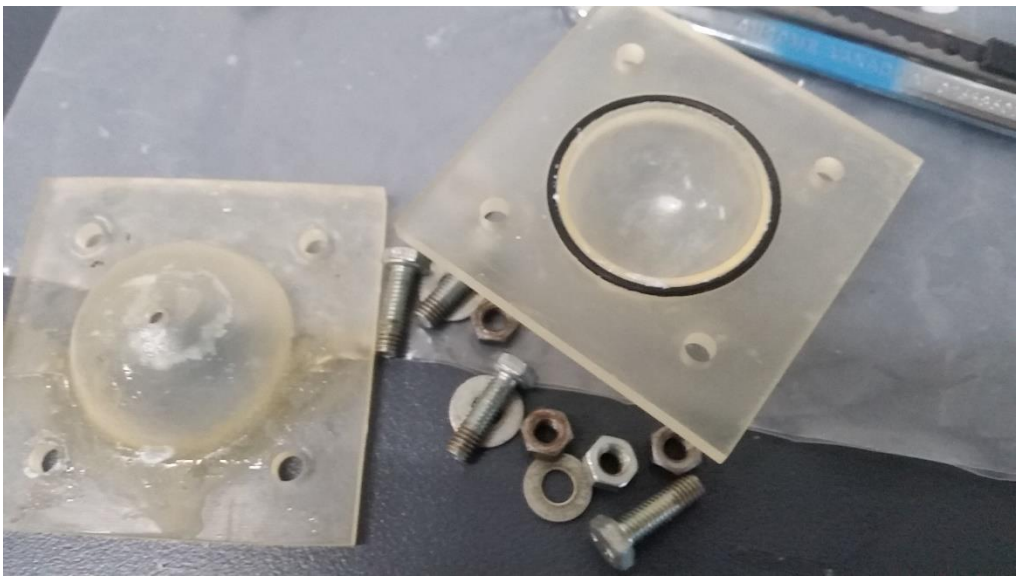

Figure A.2: 3D printed sphere mould (two halves)

8. Immediately place mould in a freezer (below minus 5 degrees Celsius) for at least 6 hours.
9. Carefully open the mould with a screwdriver, and then pull off the top half of the mould with both hands.
10. Take the half of the mould with the ice ball still frozen in the cavity and place the outside of the mould under a small stream of running water for 5 to 10 seconds (or however long is necessary to release the ice ball) without wetting the ice ball.
11. Remove the ice ball and quickly transfer to a sealed plastic bag and place it in the freezer for storage.

Method 2b. Pure ice ball (revised):

1. Fill half of a cooler box with demineralised water.
2. Fill the mould with demineralized water.
3. Place the mould into the water in the cooler box with the filler hole facing the bottom of the box. If the mould with water does not float, place a hollow cylinder below it as a support.
4. Put the cooler box in a freezer carefully, avoiding any vibration in case the mould sinks to the bottom. Figure A3 shows an ice block with the mould embedded inside.
5. Freeze for at least three days.
6. Take the cooler box out and leave it at room temperature until the ice block can be taken out.
7. Use hammer and chisel to break the ice block carefully, avoiding any damage to the mould.
8. Take the mould out of the crushed ice.
9. Take the ice ball out of the mould.
10. Use finger to remove any trapped air bubbles near the filler hole (if exist).

Figure A.3: Ice block containing the mould filled with water

Method 3. Ice ball with polypropylene (PP) fibre:

1) Weigh the desired amount of polypropylene fibre (see Figure A4), which is 5% by weight of the artificial hailstone, and shred it into smaller pieces.

2) Boil distilled water twice to expel the air.

3) Place the prepared fibre into the sphere mould.

4) Inject the boiled water into the mould.

5) Place the mould into a freezer for two days.

Figure A.4: Polypropylene (PP) fibre

Appendix B. Trial tests results of artificial hailstones with polyvinyl acetate (PVA) additive and polypropylene (PP) fibre

Table B.1: Results for 5% PVA additive with 1% PP fibre

Mass (g)	Nominal Diameter (mm)	Density (g/cm^3)	Impact Velocity (m/s)	Rebound velocity (m/s)	Impact outcome
19.7	33	1.02	42.4	1.8	Break, but hold by the fibres
18.9	33	1.07	38.0	2	Minor fragmentation
20.1	33	1.02	43.8	N.A.	Break
19.7	33	1.03	27.6	1.9	Minor fragmentation
19.1	33	1.01	27.8	1.2	Minor fragmentation
29.8	38	0.97	42.3	3.6	Minor fragmentation
9.1	25	0.94	39	N.A.	Break
8.6	25	1.05	35.4	N.A.	Break
9.3	25	1.03	25.9	3.1	Minor fragmentation
8.0	25	1.00	16.9	1.3	Fully intact

Table B.2: Results for 11% PVA additive

Mass (g)	Nominal Diameter (mm)	Density (g/cm^3)	Impact Velocity (m/s)	Rebound velocity (m/s)	Impact outcome
20.3	33	0.99	42.3	1.3	Minor fragmentation
19.5	33	1.05	23.1	1.7	Fully intact
18.6	33	1.05	34.4	2.1	Break
30	40	0.90	26.2	1.0	Fully intact
66.4	50.8	0.95	39.7	1.9	Fully intact
65.2	50.8	0.94	34.3	0.9	Fully intact
67.1	50.8	0.96	25.5	1.8	Fully intact
8.9	50.8	1.05	34.7	N.A.	Break
8.9	50.8	1.05	35.2	N.A.	Break

Table B.3: Results for 12% PVA additive

Mass (g)	Nominal Diameter (mm)	Density (g/cm^3)	Impact Velocity (m/s)	Rebound velocity (m/s)	Impact outcome
19.6	50.8	0.94	33.9	3.1	Fully intact
29.4	40	0.93	33.4	1.4	Fully intact
62.4	50.8	0.95	32.4	1.6	Fully intact
57.2	50.8	0.97	22.7	1.8	Fully intact
10.3	25	1.04	37.7	5.5	Fully intact
8.7	25	1.05	34.4	2.8	Fully intact
9.2	25	1.09	23.2	3.7	Fully intact

Appendix C: Impact Test Results

G550_0.35 mm

Test ID	Mass (g)	Average Diameter (mm)	Density (g/cm^3)	Impact Velocity (m/s)	Rebound Velocity (m/s)	Hailstone Integrity	Dent Depth		Coefficient of Restitution	Impact Moment (g.m/s)	Impact Energy (Joule)	Energy of Plastic Deformation (Joule)
							Gauge (mm)	3D Scan (mm)				
50-15-1	65.8	51.0	0.95	31.4	1.5	Intact	3.80	3.83	0.05	2069	32.5	10.0
50-15-2	64.2	50.6	0.95	30.7	0.5	Intact	4.00	4.02	0.02	1968	30.2	11.7
50-15-3	66.1	50.7	0.97	34.5	0.9	Intact	2.9 (3.25)*	3.36	0.03	2283	39.4	7.7
50-10-1	64.8	50.5	0.96	26.7	1.4	Intact	2.55	2.57	0.05	1732	23.1	4.5
50-10-2	64.5	50.9	0.94	29.2	1.3	Intact	3.00	3.08	0.04	1884	27.5	6.5
50-10-3	63.8	49.4	1.01	27.4	1.9	Intact	2.50	2.34	0.07	1748	24.0	3.7
50-4-1	67.5	51.2	0.96	13.3	0.3	Intact	1.05	1.06	0.02	900	6.0	0.8
50-4-2	66.8	50.8	0.98	21.1	1.5	Intact	2.10	2.13	0.07	1407	14.8	3.1
50-4-3	65.9	50.9	0.95	21.5	1.3	Intact	1.95	1.89	0.06	1418	15.3	2.4
45-14-1	45.2	44.5	0.98	36.8	0.3	Intact	2.90	3.23	0.01	1663	30.6	7.1
45-14-2	45.1	45.1	0.94	36.8	0.0	Intact	3.10	3.36	0.00	1658	30.5	7.7
45-14-3	44.5	43.5	1.03	34.0	0.0	Intact	2.80	2.81	0.00	1513	25.7	5.4
45-10-1	46.2	45.7	0.92	28.1	0.0	Intact	2.30	2.39	0.00	1297	18.2	3.9
45-10-2	47.9	45.7	0.96	30.2	1.8	Intact	2.45	2.50	0.06	1448	21.9	4.3
45-10-3	45.9	44.7	0.98	28.9	0.6	Intact	2.25	2.34	0.02	1325	19.1	3.7
45-5-1	46	45.3	0.94	20.3	0.5	Intact	1.30	1.30	0.03	936	9.5	1.2
45-5-2	45.8	44.9	0.97	20.3	2.8	Intact	1.40	1.47	0.14	927	9.4	1.5
45-5-3	48.1	46.7	0.90	18.2	1.8	Intact	1.35	1.37	0.10	876	8.0	1.3
38-12.5-1	29.7	38.4	1.00	28.5	3.5	Intact	1.70	2.16	0.12	847	12.1	3.2
38-12.5-2	27	36.9	1.03	33.3	2.4	Intact	2.35	2.40	0.07	899	15.0	3.9
38-12.5-3	27.1	37.5	0.98	30.8	2.0	Intact	2.05	2.28	0.07	834	12.8	3.5
38-7.5-1	26.7	37.8	0.95	24.9	2.3	Intact	1.60	1.64	0.09	664	8.3	1.8

*: The value in the bracket is the second measurement

**: The abnormal dent depths due to the human error during the tests

***: No dent was formed under a hailstone impact

G550_0.35 mm (cont'd)

Test ID	Mass (g)	Average Diameter (mm)	Density (g/cm^3)	Impact Velocity (m/s)	Rebound Velocity (m/s)	Hailstone Integrity	Dent Depth		Coefficient of Restitution	Impact Moment (g.m/s)	Impact Energy (Joule)	Energy of Plastic Deformation (Joule)
							Gauge (mm)	3D Scan (mm)				
38-7.5-2	28.8	38.4	0.97	27.4	3.4	Intact	1.90	1.96	0.12	788	10.8	2.6
38-7.5-3	28.9	38.0	1.00	28.0	3.2	Intact	1.80	1.82	0.11	808	11.3	2.2
38-4-1	27	37.5	0.98	21.6	1.5	Intact	1.15	1.05	0.07	582	6.3	0.7
38-4-2	29.4	38.0	1.02	19.9	1.5	Intact	1.10	1.06	0.08	584	5.8	0.8
(38-4-3)**	26.4	37.0	0.99	19.8	3.8	Intact	1.00	0.87	0.19	522	5.2	0.5
33-11-1	18.6	32.2	1.07	33.3	3.4	Intact	2.05	2.15	0.10	620	10.3	3.1
33-11-2	16.9	31.5	1.03	29.1	2.0	Intact	2.00	1.93	0.07	491	7.1	2.8
33-11-3	19.4	33.0	1.03	31.4	2.8	Intact	1.85	2.13	0.09	609	9.6	3.1
33-6-1	19.2	34.2	0.91	30.3	1.2	Intact	1.40	1.50	0.04	580	8.8	1.5
33-6-2	19.3	34.5	0.89	31.1	4.8	Intact	1.7 (2.05)*	2.21	0.15	599	9.3	3.3
33-6-3	19.5	34.1	0.94	28.4	2.4	Intact	1.45	1.67	0.08	552	7.8	1.9
33-3-1	19.9	34.0	0.96	21.1	1.5	Intact	0.90	0.96	0.07	420	4.4	0.6
(33-3-2)**	18.9	34.2	0.90	24.2	4.0	Intact	1.05	1.28	0.16	459	5.6	1.1
33-3-3	18.9	34.0	0.92	25.9	1.5	Intact	1.40	1.29	0.06	490	6.3	1.1
25-6-1	8.9	25.5	1.02	29.5	N.A.	Major Fragment	0.60	0.85	N.A.	261	3.9	0.5
25-10-2	9.2	26.2	0.98	38.5	N.A.	Major Fragment	1.60	1.74	N.A.	354	6.8	2.1
25-10-3	9.5	25.9	1.04	38.0	N.A.	Major Fragment	1.45	1.51	N.A.	361	6.9	1.6
25-10-1	9.5	26.4	0.99	40.6	N.A.	Shatter	1.35	1.37	N.A.	387	7.9	1.3
25-6-2	9.0	26.4	0.94	31.2	2.0	Intact	1.05	1.00	0.06	282	4.4	0.7
25-6-3	9.4	25.8	1.05	32.0	2.6	Intact	1.10	1.35	0.08	301	4.8	1.2
25-3-1	10.0	26.4	1.04	26.2	4.8	Intact	1.10	1.15	0.18	261	3.4	0.9
(25-3-2)**	10.0	26.8	0.99	18.8	0.0	Intact	0.50	0.39	0.00	189	1.8	0.1
(25-3-3)**	10.2	26.7	1.03	25.3	3.0	Intact	0.70	0.70	0.12	259	3.3	0.3

*: The value in the bracket is the second measurement

**: The abnormal dent depths due to the human error during the tests

***: No dent was formed under a hailstone impact

G550_0.42 mm

Test ID	Mass (g)	Average Diameter (mm)	Density (g/cm^3)	Impact Velocity (m/s)	Rebound Velocity (m/s)	Hailstone Integrity	Dent Depth		Coefficient of Restitution	Impact Moment (g.m/s)	Impact Energy (Joule)	Energy of Plastic Deformation (Joule)
							Gauge (mm)	3D Scan (mm)				
50-15-1	61.4	48.2	1.05	37.9	2.3	Intact	3.40	3.41	0.06	2330	44.2	10.0
50-15-2	61.6	49.4	0.98	38.1	1.4	Major Fragment	3.05	3.05	0.04	2346	44.7	8.0
50-15-3	64.0	50.8	0.93	41.5	4.8	Intact	3.90	4.58	0.11	2654	55.1	18.0
50-10-1	61.9	49.2	0.99	26.7	2.3	Intact	2.50	2.61	0.08	1655	22.1	5.8
50-10-2	60.6	48.4	1.02	30.1	0.8	Intact	2.30	2.32	0.03	1826	27.5	4.6
50-10-3	65.8	51.6	0.92	34.2	4.0	Intact	3.45	3.49	0.12	2249	38.5	10.4
(50-4-1)**	66.4	51.1	0.95	18.6	0.0	Intact	0.75	0.75	0.00	1233	11.5	0.5
(50-4-2)**	63.9	50.7	0.94	17.6	0.9	Intact	0.70	0.70	0.05	1126	9.9	0.4
50-5-3	64.1	50.7	0.94	29.5	4.0	Intact	2.45	2.85	0.13	1890	27.9	7.0
45-14-1	44.7	45.0	0.94	36.2	6.1	Intact	1.95	2.04	0.17	1617	29.2	3.6
45-14-2	44.4	44.9	0.94	33.9	1.7	Intact	2.80	2.98	0.05	1504	25.5	7.6
45-14-3	47.1	46.3	0.91	41.0	2.2	Intact	3.55	3.71	0.05	1933	39.7	11.8
45-10-1	44.6	44.8	0.95	32.2	N.A.	Major Fragment	2.05	2.42	N.A.	1437	23.1	5.0
45-10-2	44.6	44.8	0.95	31.1	1.3	Intact	2.25	2.75	0.04	1386	21.5	6.5
45-9-3	46.8	46.3	0.90	31.9	2.6	Intact	1.90	2.48	0.08	1492	23.8	5.3
45-5-1	47.2	45.8	0.94	22.4	1.1	Intact	1.50	1.56	0.05	1058	11.9	2.1
45-5-2	46.5	45.9	0.92	17.7	0.0	Intact	0.90 (1.0)*	1.03	0.00	821	7.2	0.9
45-4-3	45.3	44.6	0.97	26.6	3.5	Intact	1.50	1.80	0.13	1204	16.0	2.8
38-12.5-1	27.5	37.9	0.97	34.1	1.2	Intact	2.40	2.43	0.04	937	16.0	5.1
38-12.5-2	28.1	37.8	0.99	32.8	5.2	Intact	1.80	1.98	0.16	921	15.1	3.4
38-12.5-3	27.6	38.2	0.95	38.0	4.9	Intact	2.60	2.62	0.13	1050	19.9	5.9
38-7.5-1	27.2	37.7	0.97	25.9	1.7	Intact	0.90	1.11	0.07	705	9.1	1.1
38-7.5-2	26.4	37.0	1.00	29.7	2.8	Intact	1.35	1.37	0.09	783	11.6	1.6

*: The value in the bracket is the second measurement

**: The abnormal dent depths due to the human error during the tests

***: No dent was formed under a hailstone impact

G550_0.42 mm (cont'd)

Test ID	Mass (g)	Average Diameter (mm)	Density (g/cm3)	Impact Velocity (m/s)	Rebound Velocity (m/s)	Hailstone Integrity	Dent Depth		Coefficient of Restitution	Impact Moment (g.m/s)	Impact Energy (Joule)	Energy of Plastic Deformation (Joule)
							Gauge (mm)	3D Scan (mm)				
38-7.5-3	25.7	37.9	0.90	36.0	N.A.	Shatter	1.45	1.94	N.A.	925	16.7	3.2
38-4-1	26.7	37.2	0.99	19.0	0.9	Intact	0.70	0.79	0.05	508	4.8	0.5
(38-4-2)**	26.7	37.7	0.95	20.7	0.9	Intact	0.75	0.81	0.04	553	5.7	0.6
38-3-3	24.9	37.3	0.92	28.3	0.7	Intact	1.40	1.51	0.02	704	10.0	2.0
33-11-1	19.3	33.8	0.96	37.2	1.2	Intact	2.15	2.33	0.03	718	13.4	4.7
33-11-2	19.6	33.5	1.00	36.4	N.A.	Major Fragment	1.70	1.51	N.A.	714	13.0	2.0
33-11-3	18.1	32.6	1.00	39.1	N.A.	Shatter	1.50	1.68	N.A.	705	13.8	2.4
33-6-1	19.3	33.9	0.95	26.9	0.9	Intact	1.00	1.18	0.03	520	7.0	1.2
33-6-2	19.6	33.3	1.02	29.1	1.3	Minor Fragment	0.90	0.94	0.04	570	8.3	0.8
33-6-3	19.0	32.7	1.03	31.7	2.0	Intact	1.40	1.36	0.06	602	9.5	1.6
33-3-1	19.5	33.3	1.01	23.5	2.4	Intact	1.00 (1.15)*	1.24	0.10	458	5.4	1.3
33-3-2	19.3	32.9	1.04	21.3	1.0	Intact	0.95	1.14	0.05	411	4.4	1.1
33-3-3	18.8	34.0	0.91	27.0	2.2	Intact	1.20	1.19	0.08	507	6.8	1.2
25-10-1	8.8	25.4	1.03	33.4	N.A.	Shatter	0.60	0.49	N.A.	294	4.9	0.2
25-10-2	10.0	27.0	0.97	28.7	N.A.	Major Fragment	0.70	0.69	N.A.	287	4.1	0.4
25-10-3	8.8	25.7	0.98	41.5	N.A.	Shatter	0.95	1.04	N.A.	364	7.6	0.9
25-6-1	8.7	25.3	1.02	25.1	0.0	Intact	0.85	0.85	0.00	218	2.7	0.6
25-6-2	9.2	25.8	1.02	26.2	N.A.	Major Fragment	0.60	0.58	N.A.	241	3.2	0.3
25-6-3	9.4	25.8	1.04	29.5	N.A.	Major Fragment	1.00	1.15	N.A.	276	4.1	1.1
(25-3-1)**	9.8	26.4	1.02	22.8	3.5	Intact	0.75	1.07	0.15	223	2.5	1.0
25-3-2	10.2	26.9	1.01	25.6	0.0	Minor Fragment	0.65	0.90	0.00	262	3.4	0.7
25-3-3	9.2	26.1	0.98	16.1	2.4	Intact	0.45	0.40	0.15	148	1.2	0.1

*: The value in the bracket is the second measurement

**: The abnormal dent depths due to the human error during the tests

***: No dent was formed under a hailstone impact

G550_0.55 mm

Test ID	Mass (g)	Average Diameter (mm)	Density (g/cm^3)	Impact Velocity (m/s)	Rebound Velocity (m/s)	Hailstone Integrity	Dent Depth		Coefficient of Restitution	Impact Moment (g.m/s)	Impact Energy (Joule)	Energy of Plastic Deformation (Joule)
							Gauge (mm)	3D Scan (mm)				
50-15-1	63.1	50.5	0.94	39.0	0.8	Intact	3.20	3.29	0.02	2459	47.9	13.6
50-15-2	64.8	51.1	0.93	38.9	2.0	Intact	3.30	3.32	0.05	2519	49.0	13.9
50-15-3	65.4	50.6	0.97	38.6	1.7	Intact	2.50	3.34	0.04	2526	48.8	14.1
50-10-1	62.4	50.7	0.92	34.4	N.A.	Minor fragment	2.15	2.19	N.A.	2146	36.9	6.1
50-10-2	64.1	50.8	0.93	27.6	3.0	Intact	2.65	2.87	0.11	1769	24.4	10.4
50-10-3	64.7	50.3	0.97	31.2	4.0	Intact	2.80	2.91	0.13	2019	31.5	10.7
50-4-1	65.0	51.4	0.91	17.9	0.9	Intact	1.15	1.23	0.05	1166	10.5	1.9
50-4-2	65.2	50.8	0.95	12.7	0.6	Intact	0.70	0.93	0.05	829	5.3	1.1
50-5-3	65.8	50.9	0.95	22.0	3.0	Intact	1.70	1.82	0.13	1449	16.0	4.2
45-14-1	45.6	45.0	0.96	27.8	0.4	Minor fragment	1.90	2.31	0.01	1268	17.6	6.7
45-14-2	44.6	44.7	0.96	37.6	2.8	Intact	2.55	2.77	0.07	1676	31.5	9.7
45-14-3	45.5	44.7	0.97	41.1	4.0	Intact	2.95 (3.15)*	3.41	0.10	1870	38.4	14.7
45-10-1	46.6	45.8	0.93	26.6	2.1	Intact	1.85	1.87	0.08	1240	16.5	4.4
45-10-2	45.0	45.2	0.93	33.1	1.3	Intact	2.30	2.50	0.04	1488	24.6	7.9
45-9-3	46.1	44.9	0.97	33.7	3.0	Intact	2.50	2.75	0.09	1551	26.1	9.6
45-5-1	45.2	45.1	0.94	24.0	N.A.	Major fragment	1.40	1.60	N.A.	1083	13.0	3.2
45-5-2	48.2	46.6	0.91	22.8	2.4	Intact	1.40	1.66	0.11	1097	12.5	3.5
45-4-3	45.6	44.9	0.96	24.9	1.2	Intact	1.45	1.82	0.05	1135	14.1	4.2
38-12.5-1	31.0	39.1	0.99	35.2	N.A.	Shatter	2.00	2.10	N.A.	1092	19.2	5.6
38-12.5-2	29.5	38.6	0.98	40.9	3.0	Intact	2.70	2.94	0.07	1207	24.7	10.9
38-12.5-3	26.0	37.7	0.93	38.6	4.0	Intact	2.40	2.41	0.10	1002	19.3	7.3
38-7.5-1	26.3	38.1	0.91	35.0	2.7	Intact	2.05	2.26	0.08	920	16.1	6.5
38-7.5-2	27.7	38.7	0.91	33.7	3.5	Minor fragment	1.80	2.11	0.10	932	15.7	5.6

*: The value in the bracket is the second measurement

**: The abnormal dent depths due to the human error during the tests

***: No dent was formed under a hailstone impact

G550_0.55 mm (cont'd)

Test ID	Mass (g)	Average Diameter (mm)	Density (g/cm^3)	Impact Velocity (m/s)	Rebound Velocity (m/s)	Hailstone Integrity	Dent Depth		Coefficient of Restitution	Impact Moment (g.m/s)	Impact Energy (Joule)	Energy of Plastic Deformation (Joule)
							Gauge (mm)	3D Scan (mm)				
38-7.5-3	29.1	39.0	0.94	31.1	2.0	Intact	1.75 (2.00)*	2.08	0.07	904	14.0	5.5
38-4-1	28.9	38.4	0.97	26.0	3.0	Intact	0.95	1.09	0.12	750	9.7	1.5
38-4-2	27.3	37.1	1.02	24.1	2.2	Intact	1.00	1.21	0.09	658	7.9	1.8
38-4-3	27.0	37.8	0.95	16.8	2.0	Intact	0.75	1.06	0.12	454	3.8	1.4
33-11-1	19.2	33.7	0.96	27.2	N.A.	Shatter	1.30	1.32	N.A.	522	7.1	2.2
33-11-2	19.2	34.0	0.93	37.8	N.A.	Shatter	1.55	1.56	N.A.	725	13.7	3.1
33-11-3	18.9	34.1	0.91	39.3	N.A.	Major fragment	1.55	1.70	N.A.	745	14.7	3.7
33-6-1	18.7	34.0	0.91	20.6	N.A.	Major fragment	0.85	0.96	N.A.	385	4.0	1.2
33-6-2	18.9	33.7	0.95	27.5	0.9	Intact	1.40	1.41	0.03	519	7.1	2.5
33-6-3	19.4	33.7	0.97	30.5	2.7	Intact	0.90	1.15	0.09	592	9.0	1.7
(33-3-1)**	20.0	33.7	1.00	14.0	0.9	Intact	0.45	0.97	0.06	281	2.0	1.2
33-3-2	19.6	33.9	0.96	20.7	N.A.	Shatter	0.60	0.74	N.A.	405	4.2	0.7
33-3-3	19.4	34.3	0.92	16.2	1.7	Intact	0.40	0.82	0.11	315	2.5	0.8
25-10-1	8.7	25.6	0.99	39.9	N.A.	Shatter	0.65	0.65	N.A.	347	6.9	0.5
25-10-2	8.9	25.7	1.01	26.1	N.A.	Major fragment	0.65	0.85	N.A.	233	3.0	0.9
25-10-3	9.2	26.4	0.96	40.3	N.A.	Shatter	0.85	0.72	N.A.	370	7.4	0.7
25-6-1	9.4	26.3	0.99	24.8	0.0	Intact	0.55	0.76	0.00	233	2.9	0.7
25-6-2	9.1	26.0	0.99	25.6	N.A.	Major fragment	0.55	0.71	N.A.	233	3.0	0.6
25-6-3	8.8	26.0	0.95	26.3	N.A.	Shatter	0.40	0.00	N.A.	230	3.0	0.0
25-3-1	9.2	26.5	0.94	24.9	4.0	Intact	0.40	0.58	0.16	230	2.9	0.4
25-3-2	8.8	26.4	0.91	26.4	3.5	Intact	0.95	0.94	0.13	231	3.0	1.1
(25-3-3)***	8.7	26.1	0.94	17.4	1.6	Intact	0.00	0.00	0.09	152	1.3	0.0

*: The value in the bracket is the second measurement

**: The abnormal dent depths due to the human error during the tests

***: No dent was formed under a hailstone impact

G550_1.00 mm

Test ID	Mass (g)	Average Diameter (mm)	Density (g/cm^3)	Impact Velocity (m/s)	Rebound Velocity (m/s)	Hailstone Integrity	Dent Depth		Coefficient of Restitution	Impact Moment (g.m/s)	Impact Energy (Joule)	Energy of Plastic Deformation (Joule)
							Gauge (mm)	3D Scan (mm)				
50-15-1	63.5	50.3	0.95	34.3	N.A.	Shatter	1.70 (2.00)*	2.16	N.A.	2180	37.4	9.2
50-15-2	63.1	50.2	0.95	36.0	N.A.	Shatter	1.20	1.47	N.A.	2271	40.9	4.2
50-15-3	65.7	51.8	0.90	31.5	N.A.	Minor fragment	1.85	2.40	N.A.	2072	32.7	11.4
50-10-1	64.9	50.3	0.98	32.0	1.25	Minor fragment	1.75	2.31	0.04	2079	33.3	10.5
50-10-2	62.8	49.9	0.97	29.7	3.03	Intact	1.70	2.25	0.10	1863	27.6	9.9
50-10-3	65.4	51.0	0.94	33.9	1.73	Intact	2.40	2.74	0.05	2213	37.5	14.7
50-4-1	60.1	48.7	0.99	24.1	2.20	Intact	1.25 (1.55)*	1.82	0.09	1450	17.5	6.5
50-4-2	67.0	52.1	0.91	24.2	2.38	Intact	1.05	1.73	0.10	1620	19.6	5.9
50-4-3	68.3	52.2	0.92	20.8	1.70	Intact	0.95	1.46	0.08	1422	14.8	4.2
45-14-1	46.6	45.6	0.94	37.8	N.A.	Shatter	0.95	1.61	N.A.	1762	33.3	5.1
45-14-2	45.4	45.0	0.95	38.9	N.A.	Shatter	1.50	1.53	N.A.	1764	34.3	4.6
45-14-3	45.9	45.1	0.96	37.9	N.A.	Shatter	1.10	1.55	N.A.	1739	32.9	4.7
45-10-1	46.0	45.8	0.92	33.7	N.A.	Shatter	0.65	1.09	N.A.	1549	26.1	2.4
45-10-2	46.9	44.9	0.99	25.8	N.A.	Major fragment	0.95	1.21	N.A.	1211	15.6	2.9
45-10-3	48.6	45.7	0.97	33.0	N.A.	Shatter	1.10	1.03	N.A.	1602	26.4	2.1
45-5-1	47.7	45.5	0.97	25.7	N.A.	Major fragment	0.50	0.71	N.A.	1227	15.8	1.0
45-5-2	46.4	45.3	0.95	20.4	2.69	Minor fragment	0.55	1.27	0.13	946	9.6	3.2
45-5-3	47.4	45.3	0.98	25.0	N.A.	Major fragment	0.65	0.77	N.A.	1188	14.9	1.2
38-7.5-1	29.1	38.7	0.96	27.7	N.A.	Shatter	0.50	0.51	N.A.	806	11.2	0.5
38-7.5-2	27.7	37.6	0.99	27.1	N.A.	Shatter	0.50	0.52	N.A.	750	10.1	0.5
38-7.5-3	28.8	38.8	0.94	32.7	N.A.	Shatter	0.65	0.72	N.A.	942	15.4	1.0
38-12.5-1	26.4	37.8	0.93	39.7	N.A.	Shatter	1.15	1.36	N.A.	1046	20.8	3.6
38-12.5-2	27.2	37.0	1.02	36.6	N.A.	Shatter	1.00	1.21	N.A.	996	18.2	2.9

*: The value in the bracket is the second measurement

**: The abnormal dent depths due to the human error during the tests

***: No dent was formed under a hailstone impact

G550_1.00 mm (cont'd)

Test ID	Mass (g)	Average Diameter (mm)	Density (g/cm^3)	Impact Velocity (m/s)	Rebound Velocity (m/s)	Hailstone Integrity	Dent Depth		Coefficient of Restitution	Impact Moment (g.m/s)	Impact Energy (Joule)	Energy of Plastic Deformation (Joule)
							Gauge (mm)	3D Scan (mm)				
38-12.5-3	26.9	37.4	0.98	35.4	N.A.	Shatter	1.00	1.05	N.A.	952	16.8	2.2
38-4-1	27.2	37.6	0.97	27.1	1.87	Minor fragment	0.50	0.87	0.07	736	10.0	1.5
38-4-2	26.9	37.9	0.94	24.8	2.43	Minor fragment	0.15	0.65	0.10	667	8.3	0.8
(38-4-3)***	27.4	36.9	1.04	19.7	0.95	Intact	0.00	0.00	0.05	539	5.3	0.0
33-11-1	19.7	34.8	0.89	39.6	N.A.	Major fragment	0.70	0.73	N.A.	779	15.4	1.0
33-11-2	19.5	34.5	0.91	41.6	N.A.	Shatter	0.55	0.82	N.A.	812	16.9	1.3
33-11-3	19.6	33.8	0.97	38.4	N.A.	Shatter	0.00	0.62	N.A.	752	14.4	0.8
33-6-1	19.2	33.8	0.94	32.6	3.46	Minor fragment	0.50	0.54	0.11	624	10.2	0.6
33-6-2	18.6	33.0	0.99	25.6	N.A.	Major fragment	0.00	0.00	N.A.	476	6.1	0.0
33-6-3	19.5	34.1	0.94	32.3	N.A.	Major fragment	0.50	0.46	N.A.	629	10.2	0.4
33-3-1	18.7	32.3	1.06	25.4	2.38	Minor fragment	0.00	0.44	0.09	474	6.0	0.4
33-3-2	18.9	33.1	1.00	14.3	N.A.	Major fragment	0.00	0.00	N.A.	269	1.9	0.0
33-3-3	17.7	33.2	0.92	17.4	N.A.	Major fragment	0.00	0.00	N.A.	308	2.7	0.0
25-10-1	9.8	27.2	0.93	34.9	N.A.	Shatter	0.00	0.00	N.A.	342	6.0	0.0
25-10-2	8.9	25.3	1.05	46.8	N.A.	Shatter	0.00	0.00	N.A.	417	9.7	0.0
25-10-3	10.3	27.6	0.94	31.3	N.A.	Shatter	0.00	0.00	N.A.	322	5.0	0.0
25-6-1	9.8	26.9	0.96	28.0	N.A.	Shatter	0.00	0.00	N.A.	275	3.9	0.0
38-4-2	26.9	37.9	0.94	24.8	2.43	Minor fragment	0.15	0.65	0.10	667	8.3	0.8
38-4-3	27.4	36.9	1.04	19.7	0.95	Intact	0.00	0.00	0.05	539	5.3	0.0
33-11-1	19.7	34.8	0.89	39.6	N.A.	Major fragment	0.70	0.73	N.A.	779	15.4	1.0
33-11-2	19.5	34.5	0.91	41.6	N.A.	Shatter	0.55	0.82	N.A.	812	16.9	1.3
33-11-3	19.6	33.8	0.97	38.37	N.A.	Shatter	0.00	0.62	N.A.	752	14.4	0.8

*: The value in the bracket is the second measurement

**: The abnormal dent depths due to the human error during the tests

***: No dent was formed under a hailstone impact

G300_0.55 mm

Test ID	Mass (g)	Average Diameter (mm)	Density (g/cm^3)	Impact Velocity (m/s)	Rebound Velocity (m/s)	Hailstone Integrity	Dent Depth		Coefficient of Restitution	Impact Moment (g.m/s)	Impact Energy (Joule)	Energy of Plastic Deformation (Joule)
							Gauge (mm)	3D Scan (mm)				
50-4-3	66.2	51.5	0.93	26.1	1.7	Intact	2.60 (3.25)*	3.40	0.06	1729	22.6	6.3
50-4-2	62	49.0	1.01	22.4	1.8	Intact	1.60	2.07	0.08	1388	15.5	2.3
50-4-1	59.7	47.9	1.04	18.4	1.0	Intact	1.40	1.76	0.06	1097	10.1	1.7
50-15-3	67	51.2	0.95	36.4	1.9	Intact	4.60	5.00	0.05	2439	44.4	13.6
50-15-2	64	50.2	0.97	36.5	2.0	Intact	3.90	4.85	0.06	2337	42.7	12.9
50-15-1	63.2	50.2	0.95	35.6	1.9	Intact	3.90	4.84	0.05	2247	39.9	12.8
50-10-3	61.4	50.3	0.92	31.2	1.5	Intact	4.00	4.57	0.05	1918	29.9	11.4
50-10-2	64.1	50.4	0.96	28.4	1.0	Intact	3.30	4.26	0.03	1821	25.9	9.9
50-10-1	62.1	49.8	0.96	24.2	0.4	Intact	3.05	3.76	0.01	1503	18.2	7.7
45-5-2	46.4	45.8	0.92	N. A	N. A	Intact	0.75	0.84	N. A	N. A	N. A	0.4
45-5-1	46.3	44.9	0.98	19.6	0.8	Intact	1.50	1.79	0.04	909	8.9	1.7
45-4-3	46	44.8	0.98	22.2	2.1	Intact	2.55	2.98	0.09	1019	11.3	4.9
45-14-3	46	45.2	0.95	34.0	1.3	Intact	3.45	3.75	0.04	1563	26.5	7.7
45-14-2	47.8	45.2	0.99	34.3	1.3	Intact	3.75	4.08	0.04	1640	28.1	9.1
45-14-1	48.1	45.8	0.96	40.7	2.3	Minor Fragment	4.00	4.36	0.06	1958	39.9	10.4
45-10-3	48.1	46.1	0.94	29.8	2.4	Intact	3.20	3.59	0.08	1431	21.3	7.0
45-10-2	45.6	45.0	0.96	20.5	1.6	Intact	2.00	2.38	0.08	933	9.5	3.1
45-10-1	44.8	44.0	1.00	31.8	1.9	Intact	2.90	3.67	0.06	1424	22.6	7.3
38-7.5-3	26.9	38.4	0.91	29.0	2.5	Intact	2.35	2.97	0.09	781	11.3	4.8
38-7.5-2	28	37.5	1.02	26.9	2.4	Intact	1.95	2.34	0.09	753	10.1	3.0
38-7.5-1	27	38.2	0.92	27.9	1.0	Intact	2.30	2.74	0.04	754	10.5	4.1
38-4-3	26.6	37.7	0.95	22.2	1.1	Intact	1.35	1.68	0.05	591	6.6	1.5
38-4-2	26.9	38.0	0.94	19.3	0.5	Intact	1.25	1.72	0.03	519	5.0	1.6

*: The value in the bracket is the second measurement

**: The abnormal dent depths due to the human error during the tests

***: No dent was formed under a hailstone impact

G300_0.55 mm (cont'd)

Test ID	Mass (g)	Average Diameter (mm)	Density (g/cm^3)	Impact Velocity (m/s)	Rebound Velocity (m/s)	Hailstone Integrity	Dent Depth		Coefficient of Restitution	Impact Moment (g.m/s)	Impact Energy (Joule)	Energy of Plastic Deformation (Joule)
							Gauge (mm)	3D Scan (mm)				
38-4-1	27.1	37.8	0.96	18.6	1.7	Intact	1.25	1.67	0.09	504	4.7	1.5
38-12.5-3	25.1	36.9	0.96	37.7	1.4	Intact	3.00 (3.4)*	3.50	0.04	946	17.8	6.7
38-12.5-2	27.8	38.1	0.96	33.5	1.5	Intact	1.30 (3.3)*	3.28	0.04	932	15.6	5.9
38-12.5-1	30.5	38.7	1.00	30.6	2.8	Intact	2.95	3.27	0.09	934	14.3	5.8
33-6-3	18.3	32.5	1.02	26.1	1.5	Intact	1.90	1.88	0.06	478	6.2	1.9
33-6-2	18.5	32.4	1.04	26.9	0.3	Intact	2.05	2.41	0.01	498	6.7	3.2
(33-6-1)**	19.6	32.7	1.07	26.1	0.0	Intact	2.40	2.93	0.00	512	6.7	4.7
33-3-3	18.1	32.0	1.05	23.4	0.7	Intact	1.25	1.83	0.03	423	5.0	1.8
33-3-2	19.1	32.1	1.10	20.5	1.4	Intact	1.20	1.60	0.07	391	4.0	1.4
33-3-1	17.8	31.9	1.04	22.9	1.8	Intact	1.45	1.77	0.08	408	4.7	1.7
33-11-3	16.9	31.1	1.07	39.0	N. A.	Shattered	2.20	2.48	N. A.	660	12.9	3.4
33-11-2	19.3	32.5	1.08	34.9	0.7	Minor Fragment	2.45	2.97	0.02	674	11.8	4.8
33-11-1	19.1	33.3	0.99	37.1	0.8	Intact	2.70	3.10	0.02	709	13.1	5.3
25-6-3	9.9	26.3	1.04	32.1	0.9	Intact	1.40	1.68	0.03	318	5.1	1.5
25-6-2	10.1	27.3	0.94	29.4	N. A.	Shattered	0.60	0.93	N. A.	297	4.4	0.5
25-6-1	9.2	25.5	1.06	32.8	2.4	Intact	1.35	1.74	0.07	302	5.0	1.7
25-3-4	10.2	26.3	1.07	16.1	0.4	Intact	0.50	0.72	0.02	164	1.3	0.3
25-3-3	8.6	25.2	1.02	20.2	1.5	Intact	0.90	0.73	0.07	173	1.7	0.3
(25-3-2)***	8.2	24.6	1.05	10.4	1.2	Intact	0.00	0.00	0.12	85	0.4	0.0
(25-3-1)**	9.9	26.4	1.03	16.4	0.6	Intact	0.60	0.53	0.03	163	1.3	0.2
25-10-3	9.5	26.2	1.01	32.4	N. A.	Major fragment	0.90	1.48	N. A.	308	5.0	1.2
25-10-2	9.1	25.8	1.01	39.0	N. A.	Shattered	1.65	1.59	N. A.	355	6.9	1.4

*: The value in the bracket is the second measurement

**: The abnormal dent depths due to the human error during the tests

***: No dent was formed under a hailstone impact

G300_0.75 mm

Test ID	Mass (g)	Average Diameter (mm)	Density (g/cm^3)	Impact Velocity (m/s)	Rebound Velocity (m/s)	Hailstone Integrity	Dent Depth		Coefficient of Restitution	Impact Moment (g.m/s)	Impact Energy (Joule)	Energy of Plastic Deformation (Joule)
							Gauge (mm)	3D Scan (mm)				
50-15-1	66.1	50.8	0.96	34.8	1.5	Intact	3.85 (4.05)*	4.70	0.04	2298	39.9	17.0
50-15-2	66.5	51.8	0.91	35.2	1.7	Intact	3.60	4.25	0.05	2342	41.2	13.9
50-15-3	62.4	50.6	0.92	35.6	2.6	Intact	3.60	4.30	0.07	2219	39.5	14.2
50-10-1	67.3	50.8	0.98	28.7	1.3	Intact	3.00 (3.25)*	3.51	0.04	1931	27.7	9.5
50-10-2	66.7	51.3	0.94	31.1	1.1	Minor Fragment	3.20	3.61	0.04	2077	32.3	10.0
50-10-3	63.9	52.0	0.87	29.6	2.7	Intact	2.65	3.01	0.09	1892	28.0	7.0
50-4-1	67.1	52.0	0.91	26.1	1.7	Intact	2.20	2.61	0.07	1748	22.8	5.2
50-4-2	67.3	50.4	1.01	27.6	2.0	Intact	2.25	2.60	0.07	1861	25.7	5.2
50-5-3	65.2	51.2	0.93	22.7	2.6	Intact	2.90	2.25	0.12	1480	16.8	3.9
45-14-1	45.5	44.7	0.98	38.7	0.0	Minor Fragment	3.15	3.55	0.00	1761	34.1	9.7
45-14-2	46.4	44.7	0.99	35.4	N.A.	Major Fragment	2.90	3.39	N.A.	1642	29.0	8.8
45-14-3	45.9	46.5	0.87	40.3	2.2	Minor Fragment	3.00	3.46	0.05	1850	37.3	9.2
45-10-1	44.1	45.0	0.92	N. A	N.A.	Intact, not catched	2.45	2.49	N. A	N. A	N. A	4.8
45-10-1-1	47.2	46.2	0.92	29.0	0.8	Intact	2.20	2.96	0.03	1369	19.8	6.7
(45-10-2)**	43.9	44.4	0.96	28.0	0.6	Intact	2.90	3.47	0.02	1230	17.2	9.3
45-9-3	46.1	45.9	0.91	28.1	2.4	Intact	2.45	2.89	0.08	1294	18.2	6.4
45-5-1	46.5	46.0	0.91	19.7	0.6	Intact	1.50	1.46	0.03	917	9.0	1.6
45-5-2	45.3	45.2	0.94	26.8	N.A.	Major Fragment	2.15	2.57	N.A.	1214	16.3	5.1
45-4-3	46.7	46.1	0.91	18.3	0.8	Intact	2.30	2.30	0.04	855	7.8	4.1
38-12.5-1	27.5	37.6	0.99	40.1	N.A.	Major Fragment	2.25	2.56	N.A.	1102	22.1	5.0
38-12.5-2	28.6	38.4	0.96	38.7	N.A.	Major Fragment	1.3 (1.90)*	1.85	N.A.	1107	21.4	2.6
38-12.5-3	27.0	37.9	0.95	35.2	N.A.	Major Fragment	2.30	2.76	N.A.	952	16.8	5.9
38-7.5-1	28.2	38.0	0.98	14.3	0.0	Minor Fragment	1.35	1.40	0.00	404	2.9	1.5
38-7.5-2-2	29.0	38.2	0.99	20.0	0.2	Intact	1.25	1.60	0.01	578	5.8	2.0

*: The value in the bracket is the second measurement

**: The abnormal dent depths due to the human error during the tests

***: No dent was formed under a hailstone impact

G300_0.75 mm (cont'd)

Test ID	Mass (g)	Average Diameter (mm)	Density (g/cm^3)	Impact Velocity (m/s)	Rebound Velocity (m/s)	Hailstone Integrity	Dent Depth		Coefficient of Restitution	Impact Moment (g.m/s)	Impact Energy (Joule)	Energy of Plastic Deformation (Joule)
							Gauge (mm)	3D Scan (mm)				
38-7.5-2	28.3	38.4	0.95	N. A.	N.A.	Intact, not catched	1.45	2.35	N. A.	N. A.	N. A.	4.3
38-7.5-3	26.1	38.0	0.91	30.2	1.7	Intact	2.00	2.28	0.06	787	11.9	4.0
(38-4-1)**	28.8	38.6	0.95	17.2	1.0	Intact	0.70	0.87	0.06	496	4.3	0.6
38-4-2	28.9	38.7	0.95	22.1	N.A.	Major Fragment	1.35	1.37	N.A.	637	7.0	1.4
38-3-3	28.7	38.5	0.96	19.4	2.2	Major Fragment	1.00	1.23	0.11	557	5.4	1.2
33-11-1	19.5	31.1	1.24	37.4	N.A.	Major Fragment	2.15	2.16	N.A.	730	13.6	3.6
33-11-2	18.8	33.4	0.96	39.2	N.A.	Shatter	1.60	1.86	N.A.	738	14.5	2.7
33-11-3	19.1	33.4	0.98	38.8	N.A.	Major Fragment	1.75	2.38	N.A.	739	14.3	4.3
33-6-1	18.6	33.8	0.92	30.5	N.A.	Major Fragment	1.50	1.74	N.A.	568	8.7	2.3
33-6-2	19.0	33.2	0.99	24.6	0.6	Intact	0.85	1.49	0.02	468	5.8	1.7
33-6-3	19.3	34.4	0.91	31.5	N.A.	Major Fragment	1.20	1.50	N.A.	606	9.5	1.7
33-3-1	18.7	33.2	0.98	21.4	1.1	Intact	0.50	1.39	0.05	401	4.3	1.5
33-3-2	19.2	34.9	0.86	19.6	1.0	Intact	0.15	0.91	0.05	376	3.7	0.6
33-3-3	19.2	34.5	0.89	22.8	1.4	Minor Fragment	0.90	0.87	0.06	438	5.0	0.6
25-10-1	8.9	26.3	0.94	30.2	N.A.	Major Fragment	0.45	1.27	N.A.	268	4.0	1.2
25-10-2	10.2	27.2	0.97	33.3	N.A.	Major Fragment	0.55	1.32	N.A.	340	5.7	1.3
25-10-3	10.0	26.4	1.03	39.9	N.A.	Shatter	1.15	1.20	N.A.	399	7.9	1.1
25-6-1	8.9	24.5	1.15	25.9	N.A.	Major Fragment	0.00	1.17	N.A.	230	3.0	1.1
25-6-2	9.5	26.2	1.01	26.6	N.A.	Major Fragment	0.00	1.14	N.A.	253	3.4	1.0
25-6-3	10.3	26.2	1.10	28.7	N.A.	Shatter	0.00	0.00	N.A.	297	4.3	0.0
25-3-1	9.1	25.4	1.06	20.6	0.9	Minor Fragment	0.00	0.00	0.04	188	1.9	0.0
25-3-2	9.0	25.8	1.00	14.3	0.0	Minor Fragment	0.00	0.00	0.00	128	0.9	0.00
25-3-3	10.0	26.2	1.06	24.0	0.3	Shatter	0.00	0.00	0.01	241	2.9	0.00

*: The value in the bracket is the second measurement

**: The abnormal dent depths due to the human error during the tests

***: No dent was formed under a hailstone impact

G300_1.00 mm

Test ID	Mass (g)	Average Diameter (mm)	Density (g/cm^3)	Impact Velocity (m/s)	Rebound Velocity (m/s)	Hailstone Integrity	Dent Depth		Coefficient of Restitution	Impact Moment (g.m/s)	Impact Energy (Joule)	Energy of Plastic Deformation (Joule)
							Gauge (mm)	3D Scan (mm)				
50-15-1	64.9	50.7	0.95	35.2	N.A.	Major Fragment	2.00	2.93	N.A.	2285	40.2	10.7
50-15-2	65.8	50.7	0.96	36.2	2.1	Intact	2.95 (3.30)*	3.75	0.06	2382	43.1	17.6
50-15-3	66.5	51.5	0.93	36.2	N.A.	Major Fragment	2.80	3.43	N.A.	2407	43.6	14.7
50-10-1	66.9	51.3	0.95	30.7	0.0	Major Fragment	2.55	3.12	0.00	2054	31.5	12.1
50-10-2	66.0	50.7	0.97	31.5	2.3	Intact	2.60 (2.60)*	2.80	0.07	2077	32.7	9.8
50-10-3	64.6	50.0	0.99	29.2	2.1	Intact	2.20	2.48	0.07	1889	27.6	7.6
50-4-1	62.9	50.5	0.93	23.4	N.A.	Major Fragment	1.15	1.76	N.A.	1472	17.2	3.9
50-4-2	63.5	49.9	0.98	20.9	N.A.	Major Fragment	0.80	1.28	N.A.	1327	13.9	2.1
50-4-3	63.5	49.8	0.98	17.3	1.3	Intact	0.80	0.83	0.08	1097	9.5	0.9
45-14-1	45.2	44.4	0.99	34.7	N.A.	Major Fragment	1.90	2.69	N.A.	1570	27.3	9.0
45-14-2	46.9	45.3	0.96	38.0	N. A.	Shatter	2.25	2.56	N. A.	1781	33.8	8.2
45-14-3	47.2	45.2	0.98	38.2	N. A.	Shatter	2.45	2.95	N. A.	1802	34.4	10.8
45-10-1	47.0	44.8	1.00	31.0	N.A.	Major Fragment	1.65	2.07	N.A.	1459	22.6	5.3
45-10-2	48.7	44.8	1.04	35.3	N. A.	Shatter	1.55	1.80	N. A.	1718	30.3	4.0
45-10-3	45.2	44.0	1.01	28.7	N. A.	Shatter	1.25	1.48	N. A.	1298	18.6	2.7
45-5-1	46.3	44.9	0.98	26.3	N.A.	Major Fragment	1.15	1.42	N.A.	1218	16.0	2.5
45-5-2	47.4	46.0	0.93	23.5	N.A.	Major Fragment	1.05	1.18	N.A.	1115	13.1	1.7
45-5-3	44.6	43.9	1.01	23.7	0.5	Intact	1.65	1.96	0.02	1058	12.5	4.8
38-12.5-1	27.8	37.1	1.04	33.3	N. A.	Shatter	1.45	1.22	N. A.	926	15.4	1.8
38-12.5-2	28.6	38.0	1.00	39.9	N. A.	Shatter	1.55	1.80	N. A.	1142	22.8	4.0
38-12.5-3	28.4	38.4	0.96	41.2	N. A.	Shatter	1.55	1.89	N. A.	1169	24.1	4.5
38-7.5-1	26.3	37.4	0.96	32.8	N.A.	Major Fragment	0.60	0.64	N.A.	862	14.1	0.5
38-7.5-2	27.2	38.2	0.93	35.4	N. A.	Shatter	0.85	1.61	N. A.	963	17.0	3.2

*: The value in the bracket is the second measurement

**: The abnormal dent depths due to the human error during the tests

***: No dent was formed under a hailstone impact

G300_1.00 mm (cont'd)

Test ID	Mass (g)	Average Diameter (mm)	Density (g/cm^3)	Impact Velocity (m/s)	Rebound Velocity (m/s)	Hailstone Integrity	Dent Depth		Coefficient of Restitution	Impact Moment (g.m/s)	Impact Energy (Joule)	Energy of Plastic Deformation (Joule)
							Gauge (mm)	3D Scan (mm)				
38-7.5-3	26.6	37.2	0.99	30.0	N. A.	Shatter	0.70	0.70	N.A.	798	12.0	0.6
38-4-1	26.9	37.2	1.00	25.8	0.5	Minor Fragment	0.00	0.00	0.02	695	9.0	0.0
(38-4-2)**	26.3	36.9	1.00	20.5	2.3	Intact	0.70	0.83	0.11	539	5.5	0.9
38-4-3	28.5	38.6	0.94	27.3	2.0	Intact	1.15	1.43	0.07	779	10.6	2.5
33-3-1	18.2	32.9	0.98	26.4	N. A.	Shatter	0.00	0.00	N.A.	480	6.3	0.0
33-3-2	19.6	33.0	1.04	24.5	2.4	Minor Fragment	0.00	0.91	0.10	479	5.9	1.0
33-3-3	19.8	33.1	1.04	26.0	N. A.	Shatter	0.00	0.00	N.A.	515	6.7	0.0
33-6-1	17.8	32.3	1.01	33.1	N. A.	Shatter	0.85	1.15	N.A.	590	9.8	1.7
33-6-2	17.9	32.4	1.00	28.4	N. A	Major Fragment	0.45	0.79	N.A.	506	7.2	0.8
33-6-3	16.4	31.6	1.00	33.7	N. A.	Shatter	0.95	1.15	N.A.	552	9.3	1.7
33-11-1	18.4	32.4	1.03	39.3	1.2	Minor Fragment	1.35	1.53	0.03	725	14.3	2.9
33-11-2	16.5	31.5	1.01	35.7	N. A.	Shatter	0.85	1.41	N.A.	589	10.5	2.5
33-11-3	17.2	31.0	1.10	28.5	N. A.	Shatter	0.55	1.25	N.A.	492	7.0	1.9
25-10-1	8.5	24.9	1.05	41.1	N. A.	Shatter	0.35	0.38	N.A.	348	7.1	0.2
25-10-2	10.1	25.8	1.13	39.0	N. A.	Shatter	0.20	0.18	N.A.	393	7.7	0.0
25-10-3	9.4	26.7	0.95	38.6	N. A.	Shatter	0.00	0.00	N.A.	363	7.0	0.0
25-6-1	8.8	25.9	0.97	30.0	N. A.	Shatter	0.00	0.00	N.A.	264	4.0	0.0
25-6-2	9.4	25.7	1.05	30.6	N. A.	Shatter	0.00	0.00	N.A.	287	4.4	0.0
25-6-3	8.9	25.9	0.99	32.2	N. A.	Shatter	0.00	0.00	N.A.	287	4.6	0.0
25-3-1	9.9	26.1	1.06	27.1	N. A.	Shatter	0.00	0.00	N.A.	267	3.6	0.0
(25-3-2)***	8.5	25.1	1.03	14.8	1.3	Intact	0.00	0.00	0.09	125	0.9	0.0
25-3-3	9.5	26.0	1.04	20.8	N. A.	Shatter	0.00	0.00	N.A.	198	2.1	0.0

*: The value in the bracket is the second measurement

**: The abnormal dent depths due to the human error during the tests

***: No dent was formed under a hailstone impact

Appendix D: Relationship between the dent depth and the impact energy of artificial hailstones

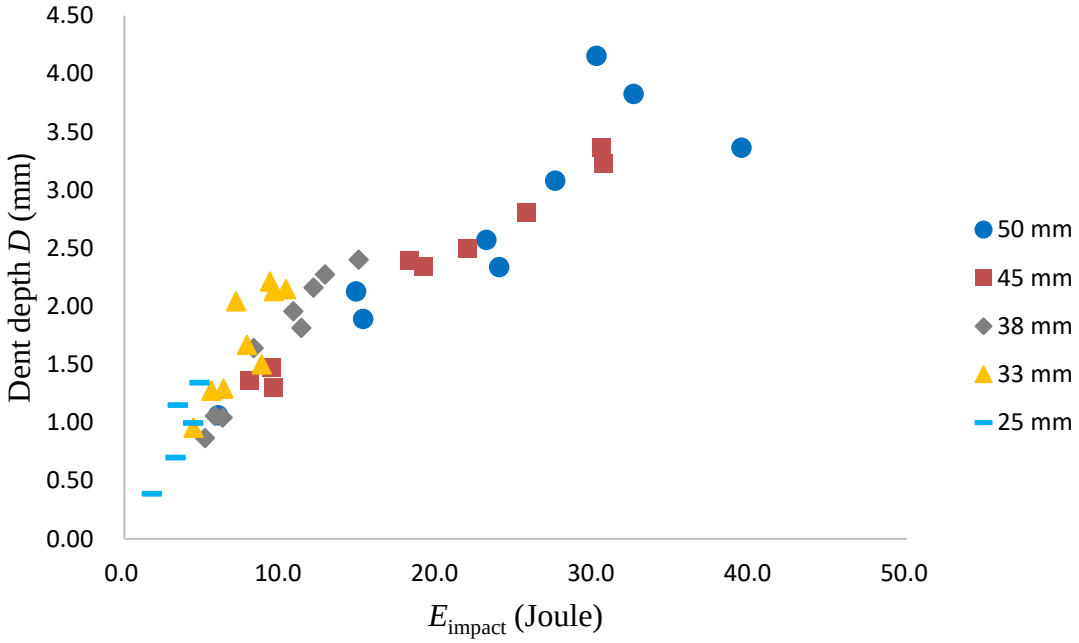

Figure D.1: 'Dent depth D' vs 'E_{impact}' for G550_0.35 mm steel sheets

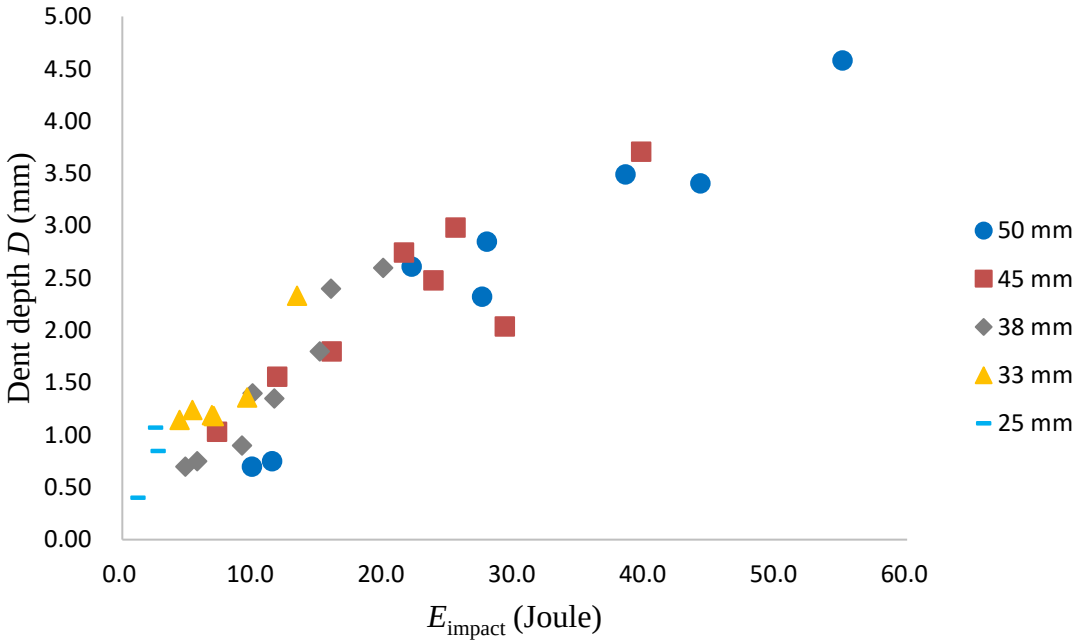

Figure D.2: 'Dent depth D' vs 'E_{impact}' for G550_0.42 mm steel sheets

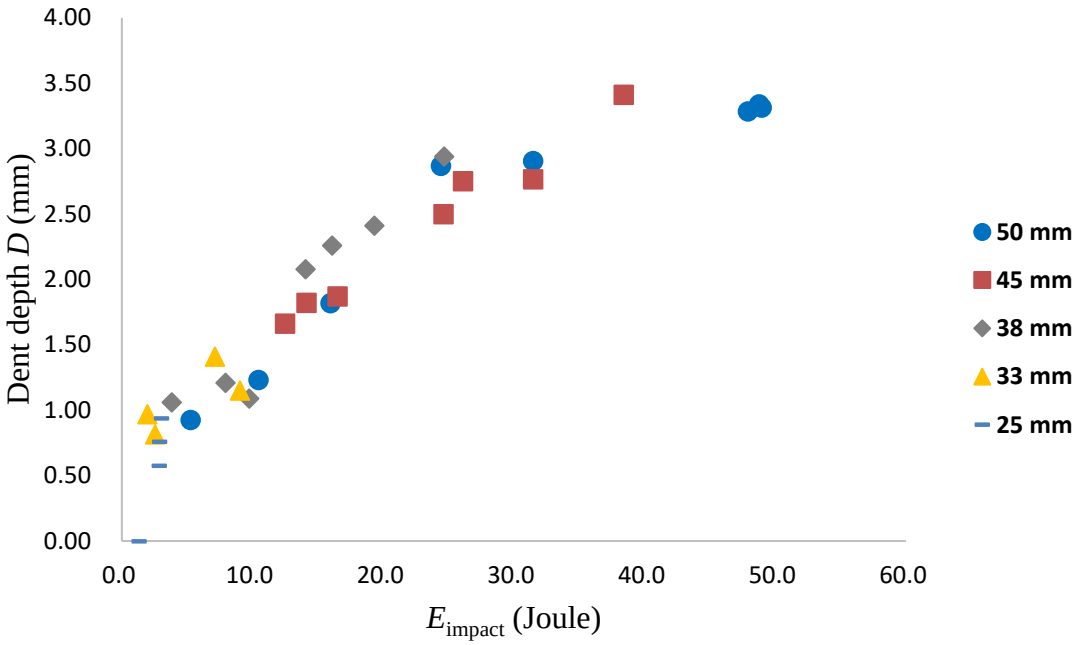

Figure D.3: 'Dent depth D' vs 'E_{impact}' for G550_0.55 mm steel sheets

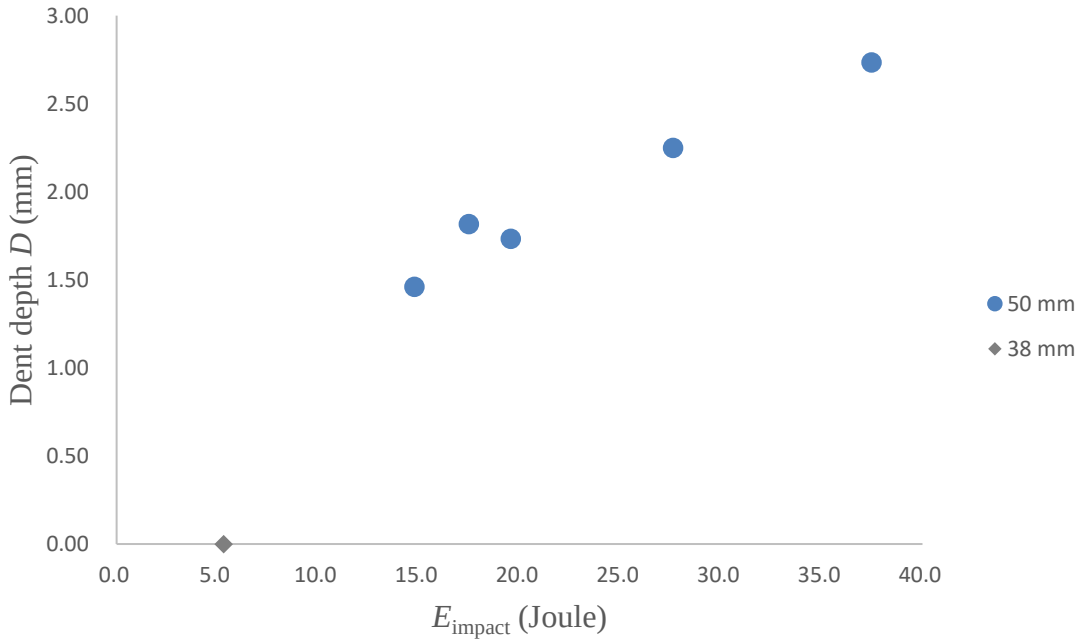

Figure D.4: 'Dent depth D' vs 'E_{impact}' for G550_1.00 mm steel sheets

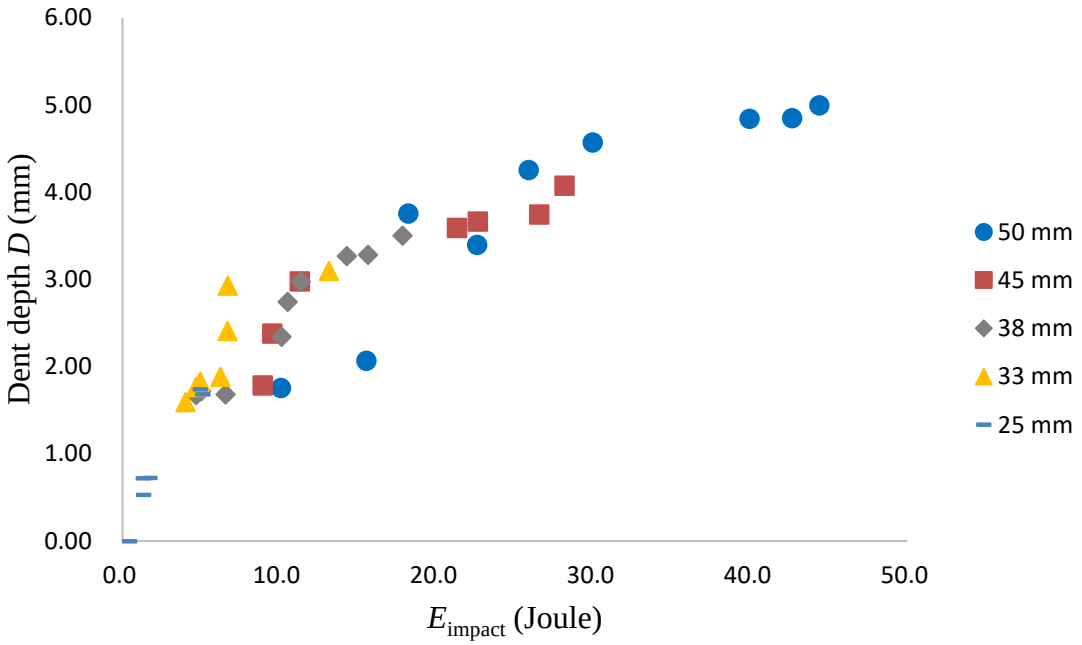

Figure D.5: 'Dent depth D' vs 'E_{impact}' for G300_0.55 mm steel sheets

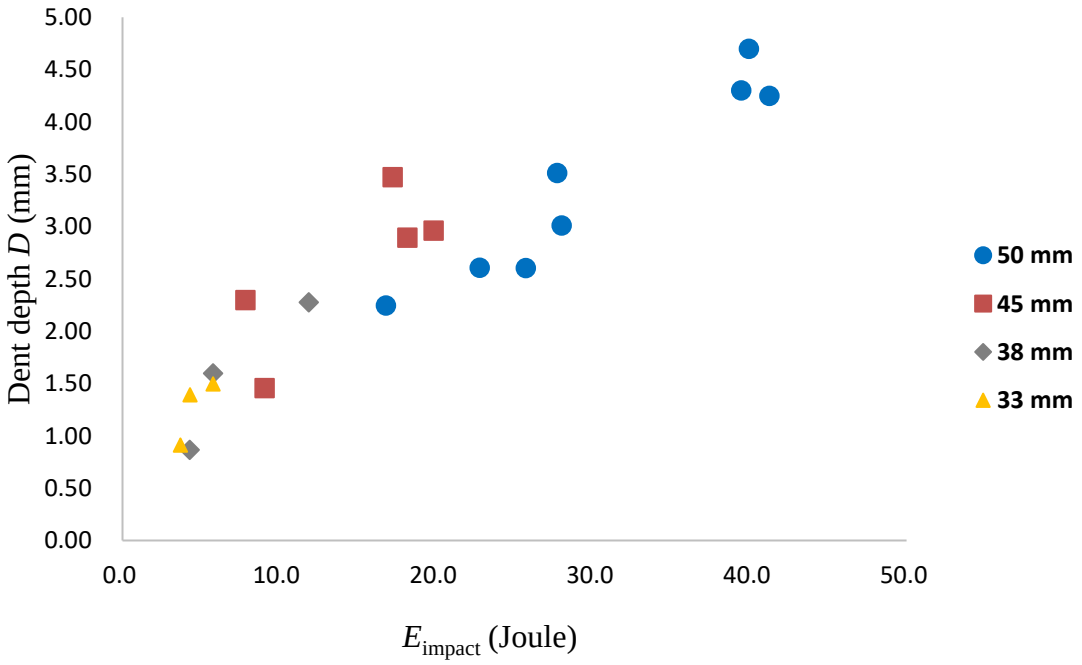

Figure D.6: 'Dent depth D' vs 'E_{impact}' for G300_0.75 mm steel sheets

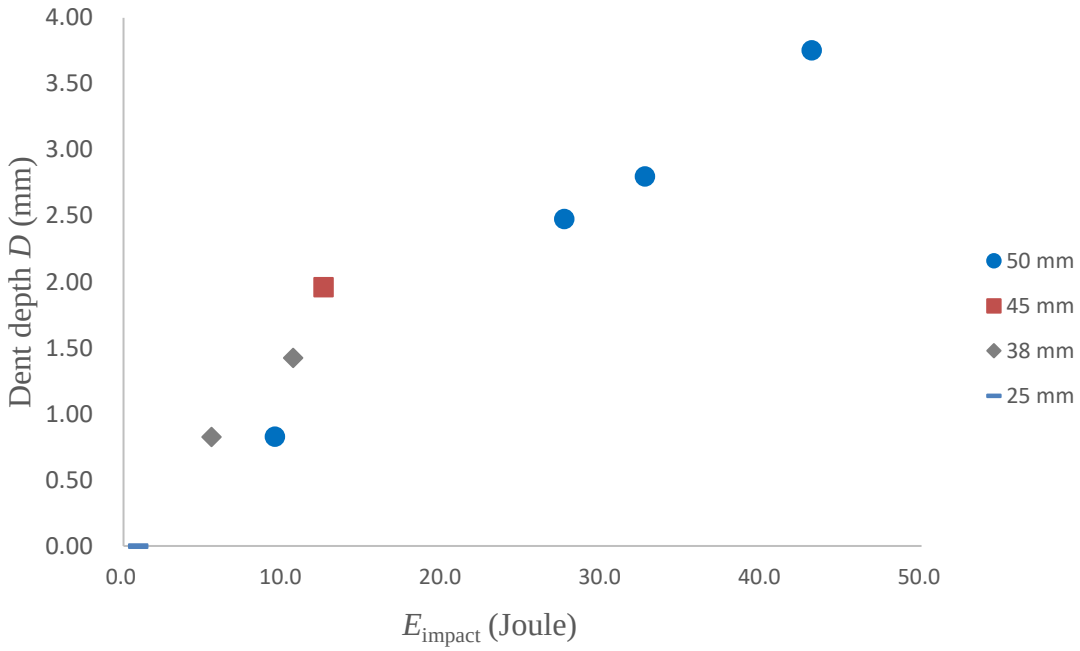

Figure D.7: 'Dent depth D' vs 'E_{impact}' for G300_1.00 mm steel sheets

Appendix E: Relationship between the energy of flexural vibration (E_v) and the impact energy of artificial hailstones (E_{impact})

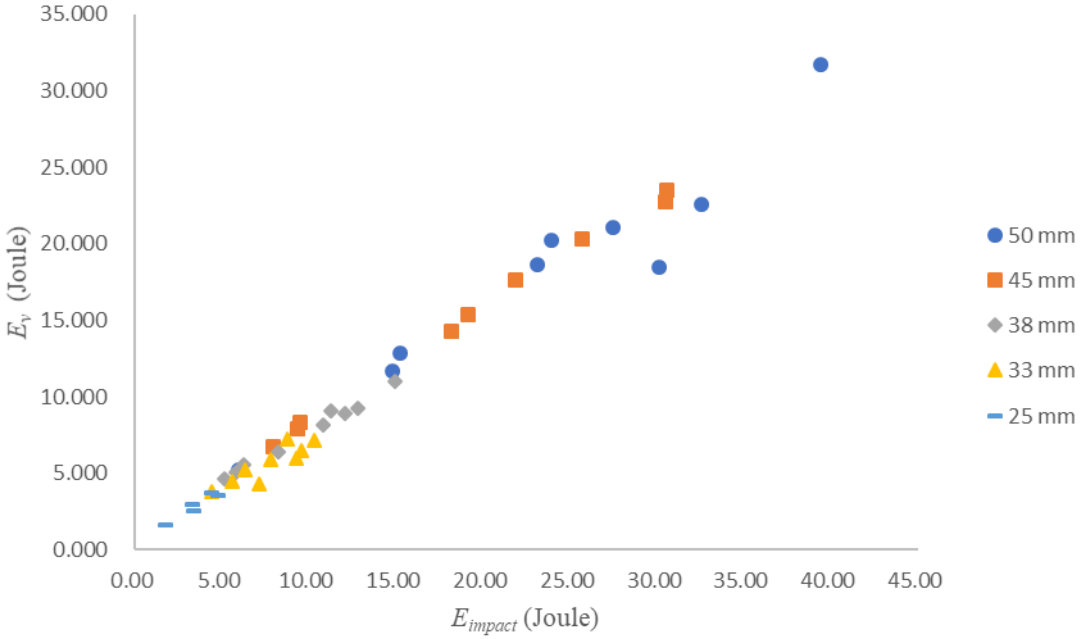

Figure E.1: 'E_v' vs 'E_{impact}' for G550_0.35 mm steel sheets

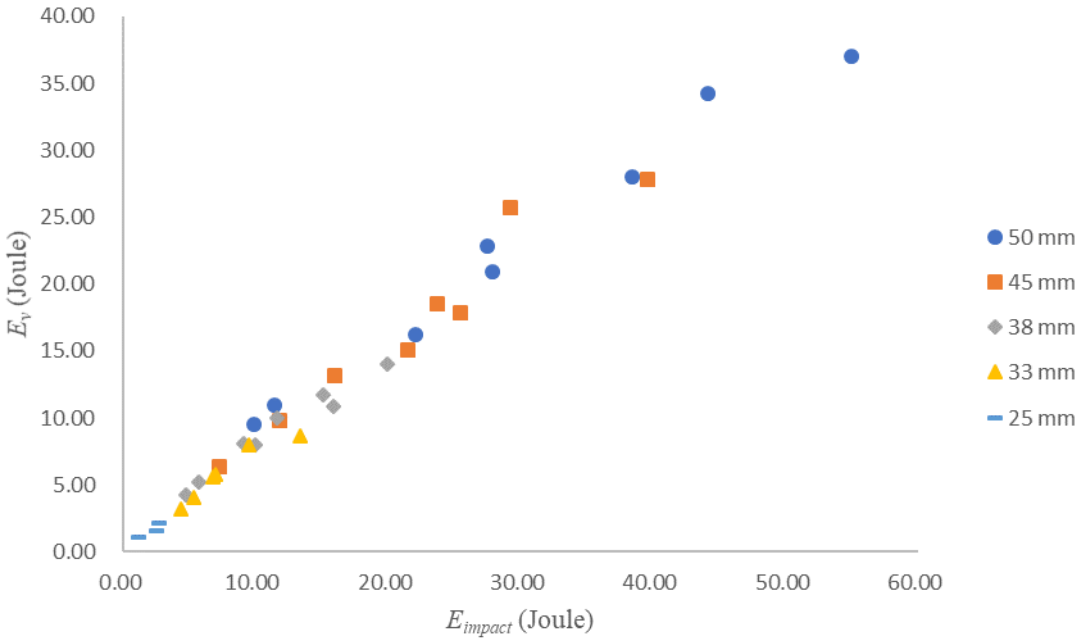

Figure E.2: 'E_v' vs 'E_{impact}' for G550_0.42 mm steel sheets

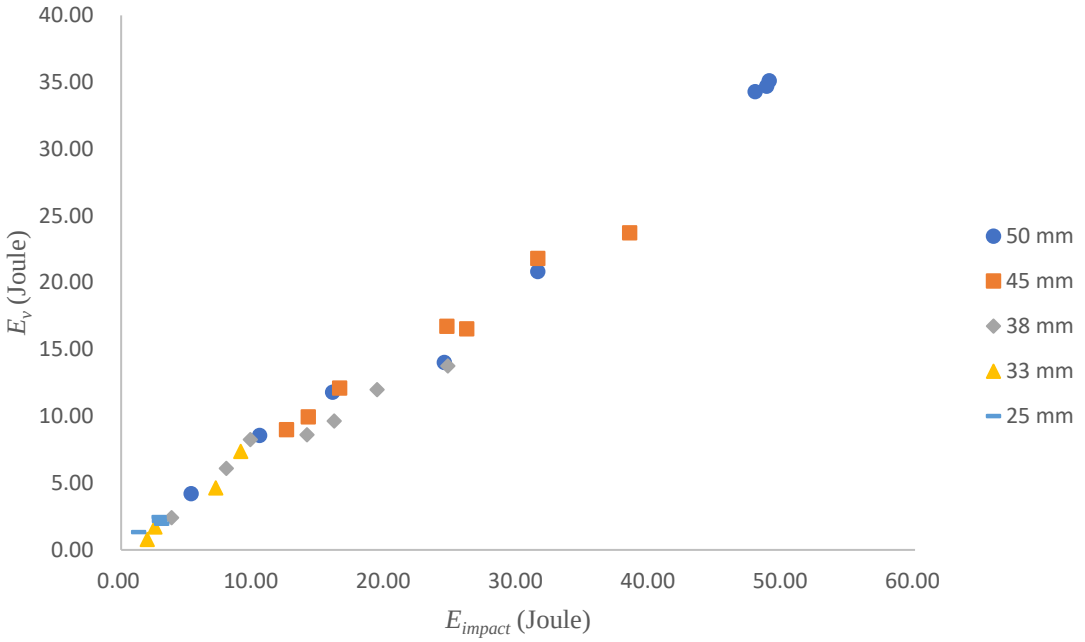

Figure E.3: 'E_v' vs 'E_{impact}' for G550_0.55 mm steel sheets

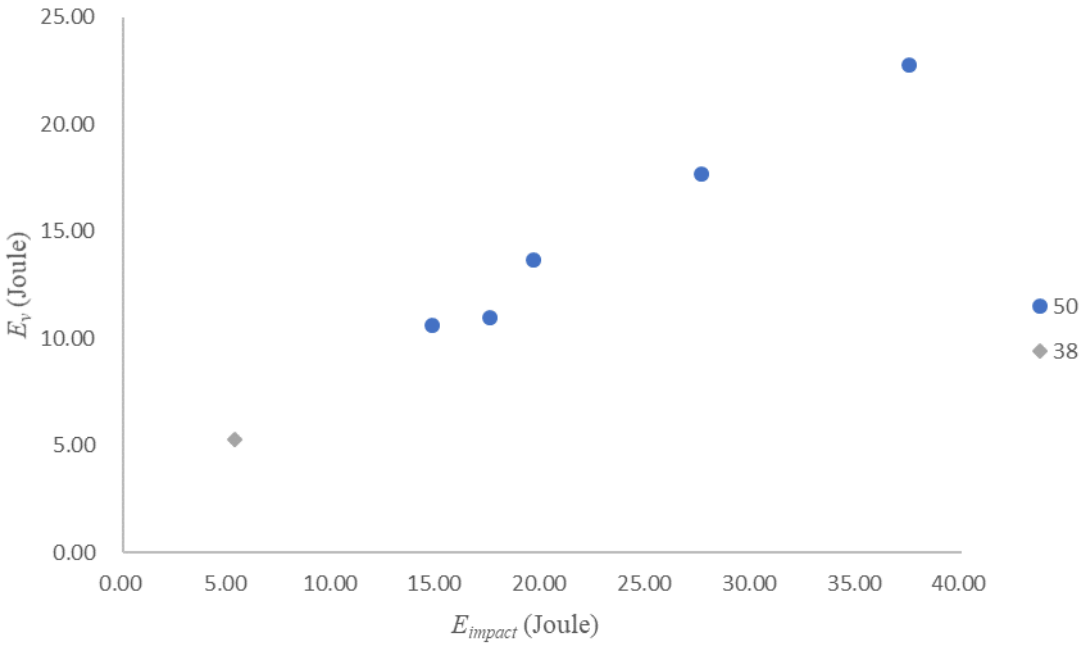

Figure E.4: 'E_v' vs 'E_{impact}' for G550_1.00 mm steel sheets

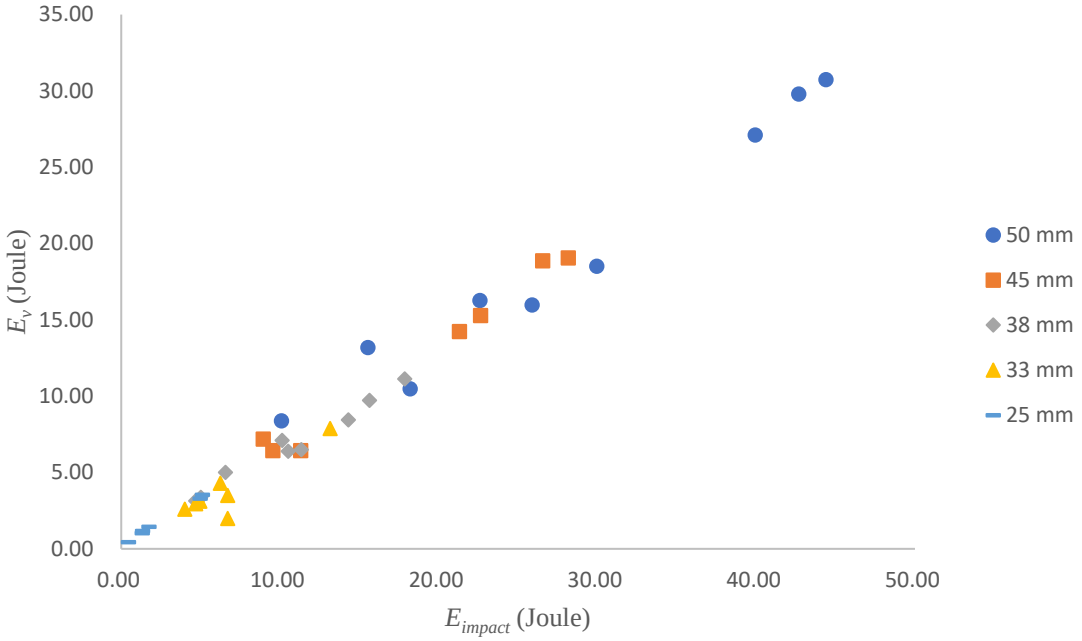

Figure E.5: 'E_v' vs 'E_{impact}' for G300_0.55 mm steel sheets

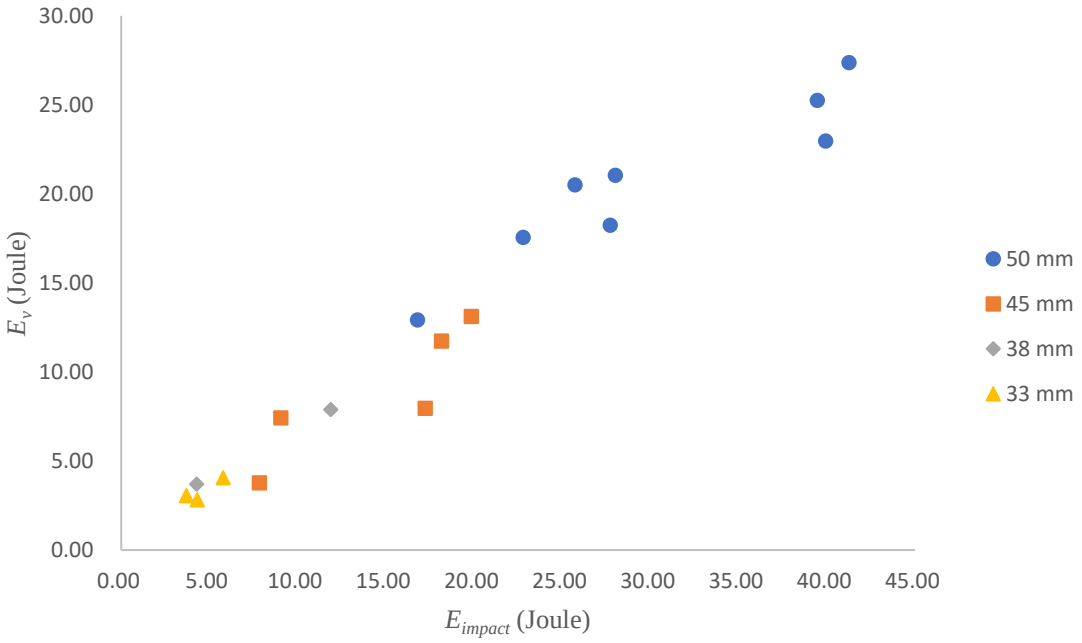

Figure E.6: 'E_v' vs 'E_{impact}' for G300_0.75 mm steel sheets

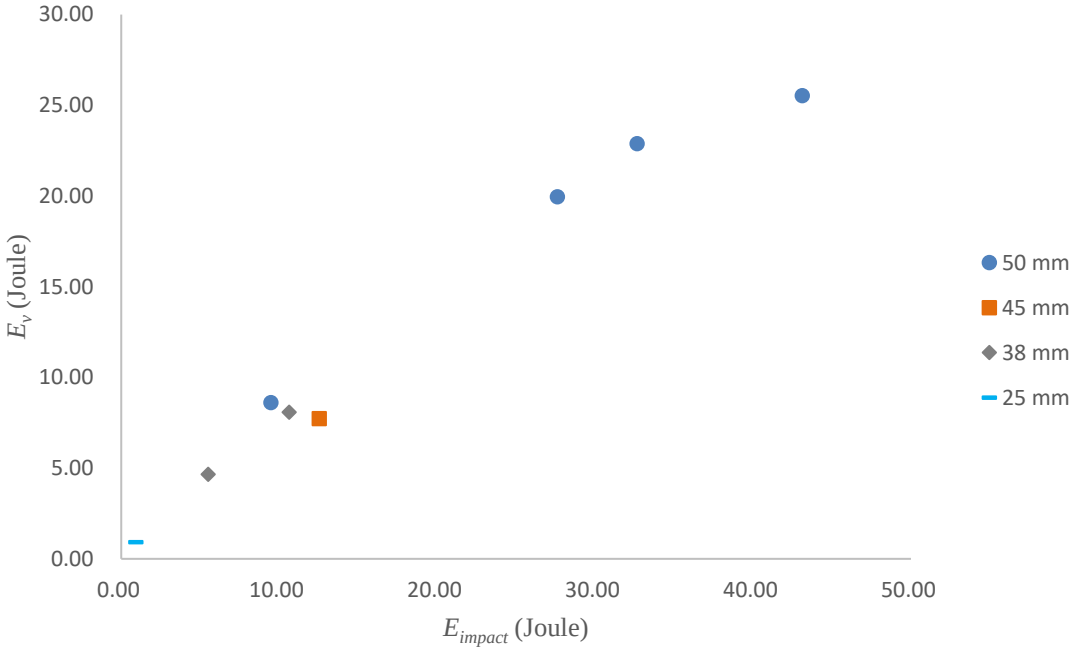

Figure E.7: 'E_v' vs 'E_{impact}' for G300_1.00 mm steel sheets

Appendix F: Material Properties of Steel Panels

The yield stress σ_y and the tensile strength σ_u of each type of sheet steels were determined through six 12.5-mm wide tension coupon tests. Half of the specimens weretested in the rolling direction of the steel sheet (denoted with prefix "L" in Tables G.1 and G.2), and the other half in the direction perpendicular to the rolling direction (denoted with prefix "T" in Tables G.1 and G.2). The stroke rate was constant at 1 mm/minute.

Table F.1: Measured yield stresses of G300 and G550 steel sheets

	σ_y-L1 (MPa)	σ_y-L2 (MPa)	σ_y-L3 (MPa)	σ_y-T1 (MPa)	σ_y-T2 (MPa)	σ_y-T3 (MPa)	Average (MPa)
G300_0.55 mm	328	268	314	362	281	341	316
G300_0.75 mm	380	369	277	325	302.5	302.5	326
G300_1.00 mm	380	405	390	415	390	403	397
G550_0.35 mm	568	652	588	623	654	623	618
G550_0.42 mm	652	647	619	654	706	620	650
G550_0.55 mm	692	693	714	765	765	756	731
G550_1.00 mm	589	544	650	631	655	689	626

Table F.2: Measured tensile strengths of G300 and G550 steel sheets

	σ_u-L1 (MPa)	σ_u-L2 (MPa)	σ_u-L3 ((MPa)	σ_u-T1 (MPa)	σ_u-T2 (MPa)	σ_u-T3 (MPa)	Average (MPa)
G300_0.55 mm	360	284	329	404	318	357	342
G300_0.75 mm	423	429	328	345	364	368	376
G300_1.00 mm	413	426	409	487	484	466	448
G550_0.35 mm	584	659	605	673	669	708	650
G550_0.42 mm	701	679	658	718	760	803	720
G550_0.55 mm	712	712	732	790	780	791	753
G550_1.00 mm	599	553	668	635	669	703	638

In Chapter 5, the average value between the yield stresses measured in the rolling direction and in the perpendicular direction of each sheet steel is used in the calculations. The average yield stresses σ_y, tensile strengths σ_u and elongations at fracture over 15 mm, 25 mm and 50 mm gauge lengths ε_{15}, ε_{25} and ε_{50}, and uniform elongation outside the fracture ε_{uo} of the steel materials as obtained from 12.5 mm wide tension coupons are shown in Tables F.3.

Table F.3: Average Material Properties of G550_0.55 mm and G300_1.00 mm steel sheets

Grade	Measured thickness, t (mm)	σ_y (MPa)	σ_u (MPa)	Ratio of σ_u/σ_y	ε_{15} (%)	ε_{25} (%)	ε_{50} (%)	ε_{uo} (%)
G550	0.55	731	753	1.03	9.22	5.80	2.97	1.85
G300	1.01	397	448	1.13	43.6	36.7	27.5	22.9

Appendix G: Rebound energy on corrugated sheets

Table G.1: Ratio of rebound energy to impact energy

Hailstone size (mm)	Impact velocity (m/s)	Rebound Velocity (m/s)	Ratio of rebound energy to impact energy	Hailstone Integrity
38	41.6	2.15	0.27%	Intact
38	37.5	N.A.	N.A.	Shattered
38	29.6	N.A.	N.A.	Shattered
38	33.4	N.A.	N.A.	Shattered
38	38.6	1.64	0.19%	Intact

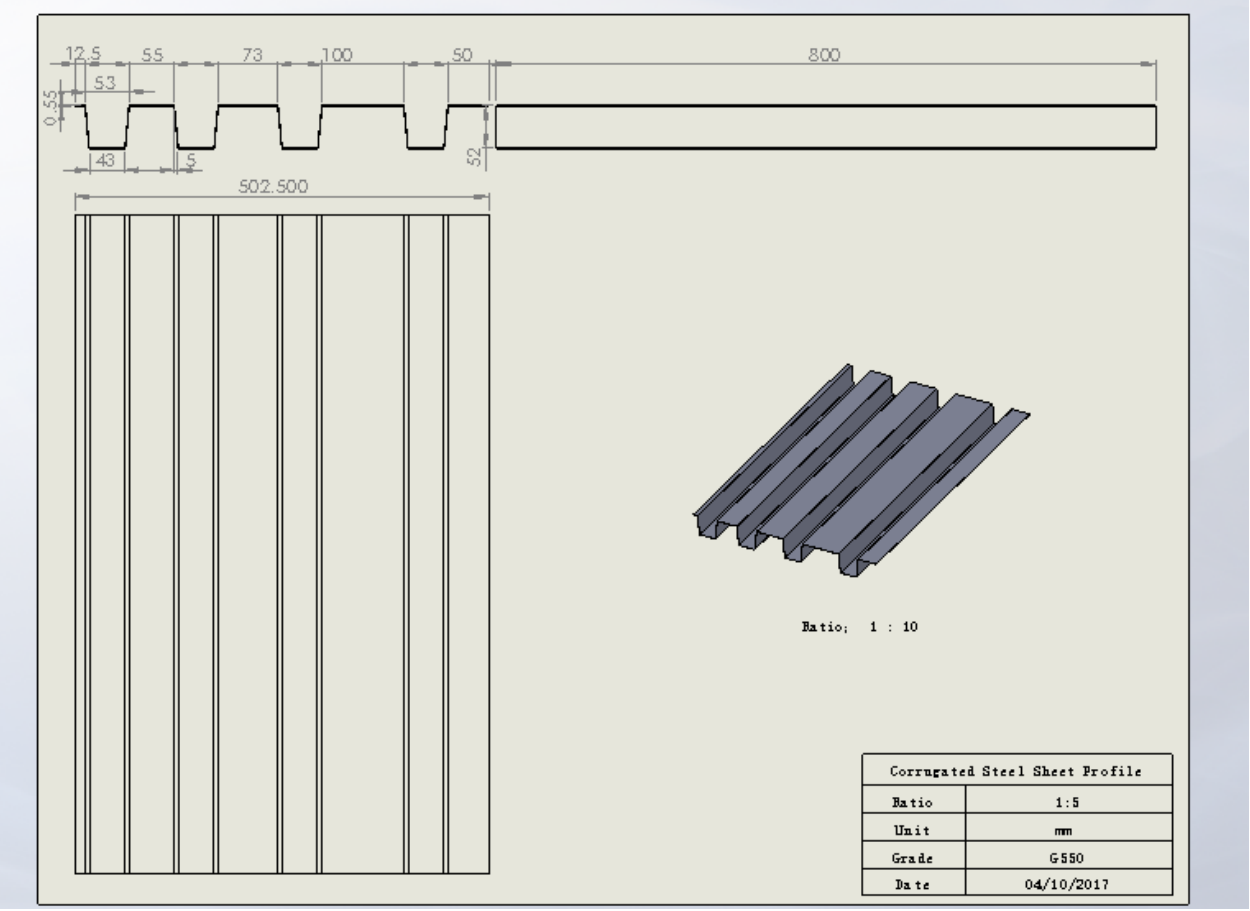

Figure G.1: Drawing of the corrugated sheet profile

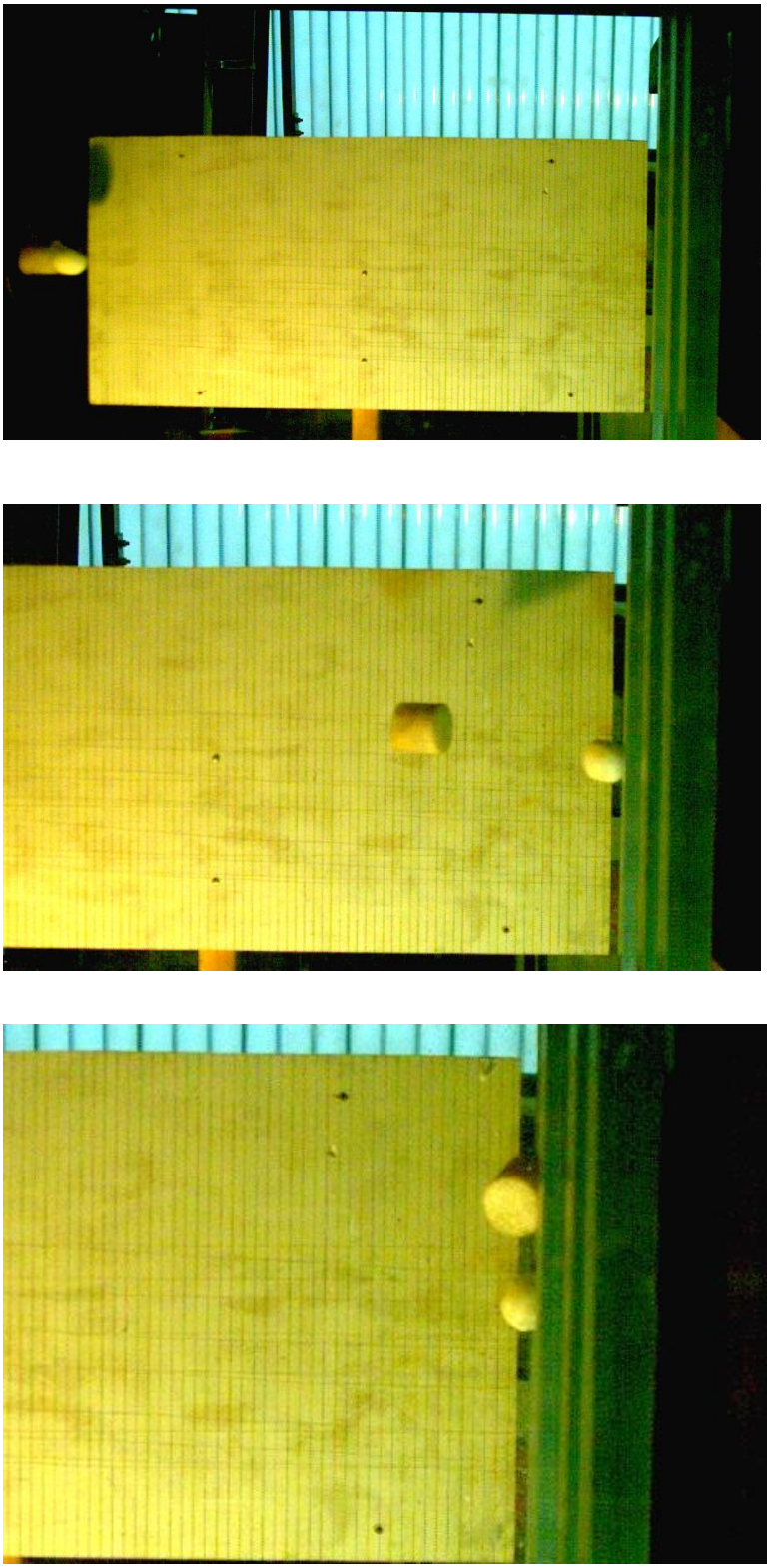

Figure G.2: Pictures of the impact on corrugated steel sheet